

DTIC FILE COPY

2

AD-A199 963

NAVAL POSTGRADUATE SCHOOL

Monterey, California



THESIS

DTIC
ELECTE
OCT 31 1988
S D
E

PASSIVE RANGE ESTIMATION
USING OVER SEA MULTIPATH

by

Avner Gal

June 1988

Thesis Advisor:

Jeffrey B. Knorr

Approved for public release; distribution is unlimited

UNCLASSIFIED

SECURITY CLASSIFICATION OF THIS PAGE

REPORT DOCUMENTATION PAGE

APR 1988 962

1a. REPORT SECURITY CLASSIFICATION UNCLASSIFIED			1b. RESTRICTIVE MARKINGS	
2a. SECURITY CLASSIFICATION AUTHORITY			3. DISTRIBUTION/AVAILABILITY OF REPORT Approved for public release; distribution is unlimited	
2b. DECLASSIFICATION/DOWNGRADING SCHEDULE				
4. PERFORMING ORGANIZATION REPORT NUMBER(S)			5. MONITORING ORGANIZATION REPORT NUMBER(S)	
3a. NAME OF PERFORMING ORGANIZATION Naval Postgraduate School		6b. OFFICE SYMBOL (If applicable) 62	7a. NAME OF MONITORING ORGANIZATION Naval Postgraduate School	
6c. ADDRESS (City, State, and ZIP Code) Monterey, California 93943-5000			7b. ADDRESS (City, State, and ZIP Code) Monterey, California 93943-5000	
8a. NAME OF FUNDING / SPONSORING ORGANIZATION		8b. OFFICE SYMBOL (If applicable)	9. PROCUREMENT INSTRUMENT IDENTIFICATION NUMBER	
3c. ADDRESS (City, State, and ZIP Code)			10. SOURCE OF FUNDING NUMBERS	
			PROGRAM ELEMENT NO.	PROJECT NO.
			TASK NO.	WORK UNIT ACCESSION NO.
11. TITLE (Include Security Classification) PASSIVE RANGE ESTIMATION USING OVER SEA MULTIPATH(U)				
12. PERSONAL AUTHOR(S) GAL, Avner				
13a. TYPE OF REPORT Master's Thesis		13b. TIME COVERED FROM TO	14. DATE OF REPORT (Year, Month, Day) June 1988	15. PAGE COUNT 126
16. SUPPLEMENTARY NOTATION The views expressed in this thesis are those of the author and do not reflect the official policy or position of the Department of Defense or the U.S. Government.				
17. COSATI CODES			18. SUBJECT TERMS (Continue on reverse if necessary and identify by block number)	
FIELD	GROUP	SUB-GROUP	multipath; smooth sea; rough sea; Ament model; sea state; estimation, range, height	
19. ABSTRACT (Continue on reverse if necessary and identify by block number) This thesis suggests an unconventional, unique method for passive range and height estimation of a cruising missile, or other microwave transmitter. Based on multipath propagation, the method uses 5 receiving antennas in a ladder configuration. Ratios of received signal powers are compared with values from lookup tables to determine the correct location of the transmitter. Computer simulation results are presented, to verify the suggested method.				
20. DISTRIBUTION/AVAILABILITY OF ABSTRACT <input checked="" type="checkbox"/> UNCLASSIFIED/UNLIMITED <input type="checkbox"/> SAME AS RPT <input type="checkbox"/> DTIC USERS			21. ABSTRACT SECURITY CLASSIFICATION UNCLASSIFIED	
22a. NAME OF RESPONSIBLE INDIVIDUAL Jeffrey B. Knorr			22b. TELEPHONE (Include Area Code) 408-646-2815	22c. OFFICE SYMBOL 62Ko

DO FORM 1473, 84 MAR

83 APR edition may be used until exhausted
All other editions are obsolete

SECURITY CLASSIFICATION OF THIS PAGE

U.S. Government Printing Office: 1986-606-24.

Approved for public release; distribution is unlimited

Passive Range Estimation Using Over Sea Multipath

by

Avner Gal
Lt., Israeli Navy
B.Sc. in Electrical Engineering, Technion-Israel
Institute of Technology, Haifa, Israel, 1982

Submitted in partial fulfillment of the
requirements for the degree of

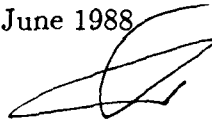
MASTER OF SCIENCE
IN ELECTRICAL ENGINEERING

from the

NAVAL POSTGRADUATE SCHOOL

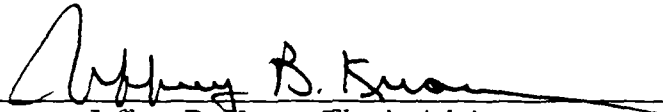
June 1988

Author:



Avner Gal

Approved by:



Jeffrey R. Knorr, Thesis Advisor



Michael A. Morgan, Second Reader



John P. Powers, Chairman
Department of Electrical and Computer Engineering



Gordon E. Schacher
Dean of Science and Engineering

ABSTRACT

This thesis suggests an unconventional, unique method for passive range and height estimation of a cruising missile, or other microwave transmitter. Based on multipath propagation, the method uses five receiving antennas in a ladder configuration. Ratios of received signal powers are compared with values from lookup tables to determine the correct location of the transmitter. Computer simulation results are presented, to verify the suggested method.

Accession For	
NTIS GRA&I	<input checked="" type="checkbox"/>
DTIC TAB	<input type="checkbox"/>
Unannounced	<input type="checkbox"/>
Justification	
By	
Distribution/	
Availability Codes	
Dist	Avail and/or Special
A-1	



TABLE OF CONTENTS

I.	INTRODUCTION	1
II.	NATURE OF THE PROBLEM	3
	A. GENERAL	3
	1. Triangulation	3
	2. Auto-Triangulation	4
III.	THEORY OF MULTIPATH PROPAGATION OF ELECTROMAGNETIC WAVES	6
	A. GENERAL	6
	B. SMOOTH SEA	10
	C. ROUGH SEA	14
	1. Reflection Types	15
	a. Specular Reflection	15
	b. Diffuse Reflection (scattering)	15
	2. Profile Types	19
	a. Sawtooth Profile	19
	b. Sinewave Profile	19
	c. Random Profile	20
	D. AMENT MODEL FOR IRREGULAR TERRAIN	21
IV.	THEORY OF RANGE ESTIMATION USING MULTIPATH EFFECT	27

A.	THEORETICAL SOLUTION	27
B.	PRACTICAL SOLUTION (OVER SMOOTH SEA)	32
C.	PRACTICAL SOLUTION (OVER ROUGH SEA)	33
V.	EXPERIMENTAL PROCEDURE AND RESULTS	40
A.	ASSUMPTIONS	40
B.	ESTIMATION PROCESS	41
1.	General Discussion	41
a.	Frequency Measurement	41
b.	Off Line Tables	41
c.	Attenuation Coefficient Ratio Tables	41
d.	Amplitude Measurement	41
e.	Comparison	42
f.	Validation	42
g.	Output	42
2.	Detailed Discussion	43
a.	Frequency Measurement	43
b.	Off Line Tables	43
c.	Attenuation Coefficient Ratio Tables (η_i^2/η_j^2)	47
d.	Amplitude Measurement	47
e.	Comparison	47

f. Validation	49
g. Output	50
C. FINAL RESULTS	51
VI. ADDITIONAL PARAMETERS CONSIDERATION	66
A. VERTICAL POLARIZATION	66
B. RECEIVER HEIGHT	68
C. SHIP TILTING	68
D. RECEIVER NOISE	73
E. ATMOSPHERIC ATTENUATION	73
F. OTHER MODELS	75
G. EARTH CURVATURE	76
VII. COMPUTER PROGRAM	79
VIII. SUMMARY AND CONCLUSIONS	84
APPENDIX A: REFLECTION COEFFICIENT MODELS	86
A. BULLINGTON MODEL	86
1. Sawtooth Profile	86
2. Sinusoidal Profile	87
3. Triangular Profile	87
4. Sine Square Profile	88
B. DAVIES MODEL	89
C. ISAKOVICH MODEL	90

APPENDIX B: COMPUTER PROGRAM LISTING	96
LIST OF REFERENCES	104
BIBLIOGRAPHY	106
INITIAL DISTRIBUTION LIST	107

LIST OF TABLES

3.1 WAVE HEIGHT PARAMETERS AND CRITICAL ANGLES FOR SPECULAR REFLECTION, VERSUS SEA STATE	23
--	----

LIST OF FIGURES

2.1 Triangulation Geometry	4
3.1 Simplified Multipath Geometry Over Smooth Terrain and Flat Earth	7
3.2 Geometry of Irregular Surface and Path Difference	7
3.3 Multipath Propagation	9
3.4 Reflection Coefficient in Vertical Polarization	11
3.5 Phase Difference in Vertical Polarization	12
3.6 Reflection Coefficient in Horizontal Polarization	13
3.7 First Fresnel Zone	13
3.8 Illustration of Diffuse and Specular Reflections	16
3.9 Reflection Areas in Different Roughness and Observation Angle	18
3.10 Reflection coefficients of Common Models for Irregular Terrain	20
3.11 Shadowing Effect Geometry	22
3.12 Shadowing Effect on Wave Height Standard Deviation	22
3.13 Rough Surface Reflection Coefficient According to Ament Model	23
3.14 Scattering Regions Versus Roughness	24
3.15 Scattering Regions Envelopes at 2 GHz	25
3.16 Scattering Regions Envelopes	26
4.1 Multipath Propagation Over a Calm Sea	29
4.2 Multipath Propagation Over a Very High Sea	30

4.3 Range Estimation Basic Geometry	31
4.4 Variation of Signal Strength with Range, for Different Transmitter Heights.	35
4.5 Variation of Signal Strength with Range, for Different Frequencies.	36
4.6 Variation of Signal Strength with Range, for Different Receiver Heights (Small Separation).	37
4.7 Variation of Signal Strength with Range, for Different Receiver Heights (High Separation).	38
4.8 Variation of Signal Strength with Range, for Very High Sea and Different Receiver Antenna Heights.	39
5.1 Flat Earth Multipath Geometry	45
5.2 Attenuation Coefficient Ratio	48
5.3 Comparison Process with 2.5% Window	52
5.3 (continued): Comparison Process with 2.5% Window	53
5.4 Comparison Process with 12% Window	54
5.4 (continued): Comparison Process with 12% Window	55
5.5 Validation Process	56
5.6 Ambiguity Level vs. Number of Receiving Antennas; Sea State 0 and 2.5% Window	57
5.7 Ambiguity Level vs. Number of Receiving Antennas; Sea State 0 and 12% Window	58
5.8 Ambiguity Level vs. Number of Receiving Antennas; Sea State 3 and 12% Window	59
5.9 Ambiguity Level vs. Number of Receiving Antennas; Sea State 3 and 5% Window	60

LIST OF FIGURES

2.1 Triangulation Geometry	4
3.1 Simplified Multipath Geometry Over Smooth Terrain and Flat Earth	7
3.2 Geometry of Irregular Surface and Path Difference	7
3.3 Multipath Propagation	9
3.4 Reflection Coefficient in Vertical Polarization	11
3.5 Phase Difference in Vertical Polarization	12
3.6 Reflection Coefficient in Horizontal Polarization	13
3.7 First Fresnel Zone	13
3.8 Illustration of Diffuse and Specular Reflections	16
3.9 Reflection Areas in Different Roughness and Observation Angle	18
3.10 Reflection coefficients of Common Models for Irregular Terrain	20
3.11 Shadowing Effect Geometry	22
3.12 Shadowing Effect on Wave Height Standard Deviation	22
3.13 Rough Surface Reflection Coefficient According to Ament Model	23
3.14 Scattering Regions Versus Roughness	24
3.15 Scattering Regions Envelopes at 2 GHz	25
3.16 Scattering Regions Envelopes	26
4.1 Multipath Propagation Over a Calm Sea	29
4.2 Multipath Propagation Over a Very High Sea	30

A.4 Bullington Model – Triangular Profile (expanded)	90
A.5 Bullington Model – Sine Square Profile	91
A.6 Davies Model	92
A.7 Isakovich Model with Zero Observation Angle, $\frac{m}{\sigma} = 10$	93
A.8 Isakovich Model with Zero Observation Angle, $\frac{m}{\sigma} = 20$	94
A.9 Isakovich Model with Observation Angle of -30° , $\frac{m}{\sigma} = 20$	95

LIST OF SYMBOLS

D	Earth Curvature Divergence Factor
E_t	Observation Angle (from Transmitter to Receiver)
h_r	Receiving Antenna Height
h_t	Transmitter Height
k	Propagation Factor ($2\pi/\lambda$)
l	Sea Wave Length
R	Transmitter to Receiver Range
R_d	Direct Range Between Transmitting Antenna to Receiving Antenna
R_n	Surface Roughness
S_d	Received Power of Direct Signal
S_r	Received Signal Power
T	Sea Wave Period
α	Tilting Angle
ϕ	Reflected Wave Phase
$\Delta\phi$	Phase Difference Between Direct and Indirect Waves
Δr	Path Difference Between Direct and Indirect Waves
ψ	Grazing Angle
θ_B	Beam Width
λ	Transmitter Wavelength
δ	Range Distance Between Direct and Indirect Paths
η^2	Multipath Effect Attenuation Coefficient
ρ	Reflection Coefficient

ρ_0	Smooth Terrain Reflection Coefficient
ρ_d	Diffuse Reflection Coefficient
ρ_s	Specular Reflection Coefficient
Δh	Sea Wave Height
σ_h	Sea Wave Height RMS Deviation
σ_a	RMS Sea Wave Slope

LIST OF ABBREVIATIONS

Amp.	Amplitude
Ant.	Antenna
ERP	Effective Radiated Power
EW	Electronic Warfare
IDF	Instantaneous Direction Finder
M.E.	Multipath Effect
NM	Nautical Mile
RCS	Radar Cross Section
RMS	Root Mean Square
RX.	Receiver
S.S.	Sea State
TX.	Transmitter

ACKNOWLEDGMENTS

Many thanks to Professor Jeffrey B. Knorr, for his good suggestions and support. I also want to thank Professor Michael A. Morgan for his practical comments. Captain Amnon Shefi, Israeli Navy, helped me with the "start up," and for this I thank him. I am also grateful to Mrs. Robert Limes for her excellent typing and patience.

And last, but certainly not least, I wish to thank my wife, [REDACTED] for her understanding and forbearance, and especially for taking care of our children, when I spent long hours working on the computer.

I. INTRODUCTION

The improved characteristics of a modern missile make the interception process difficult: the reduced Radar Cross Section (RCS) makes it hard to detect by using a radar, while late emission leaves little time for intercepting and initiating any necessary defense and Electronic Counter Measures (ECM) activities.

Conventional interception methods give only direction, and rough estimated range, and require a relatively long period of time.

This work suggests a unique, non-conventional method for passive range and height estimation of a cruising missile, as well as any other microwave transmitter. The method is based on over sea multipath propagation, and uses five receiving antennas in a ladder configuration. For each receiving antenna there is a particular multipath behavior, different than the other antennas. Comparing theoretical ratios of antenna pairs with actual received power ratios leads to an estimated location (range and height) of the transmitter.

The motivation for the need of such a method is given in Chapter II. Chapter III describes the theory behind multipath propagation of electromagnetic waves, over different kinds of sea surface. It also explains in detail the model for rough sea which we used in this work.

Chapter IV gives the basic theory of how the multipath propagation can be used for range estimation, and the conceptual estimation sequence. The detailed process, the assumptions being used during the research, and simulation results are given in Chapter V.

Additional parameters that were not taken into account in the process, as well as those only mentioned, are considered in Chapter VI, along with their influence on the experiment. The results are analyzed.

Chapter VII explains the computer program, and shows the concept behind the software process.

Chapter VIII summarizes and concludes the whole work, and gives some suggestions for future steps.

The rough sea model which we used in this work is the "Ament Model." Other familiar models are described in Appendix A. Listing of the computer program used is given in Appendix B.

II. NATURE OF THE PROBLEM

A. GENERAL

In the modern battlefield, where the electromagnetic complexity and density, as well as a missile's speed are very high, the probability of intercept is low, so detecting and intercepting missions became hard to achieve. The policy is to start the transmission as close to the target as possible, and to transmit for a minimum amount of time in order to be less "visible."

On the other hand, the radar cross section (RCS) of ships and especially missiles is being reduced, making it difficult for a radar to detect them.

Therefore, we see that intercepting a missile, especially an ultrasonic one, is a tough mission and might be achieved only during the last seconds, which might be too late.

By using a conventional interceptor, even if it is a fast one (monopulse receiver), only a direction can be found. Using the ship's radar for range finding can be worthless, because of the small RCS of the missile, and at the same time will help the other side to detect the source.

For these reasons, we prefer to find a missile (as well as other ships') location (direction and range) by using high speed passive equipment.

Two common methods for solving this problem are being used, and are listed below:

1. Triangulation

This method requires two independent interceptors on two different platforms sharing the information of the target direction. The location of the target

can be found on a map, as shown in Figure 2.1. Since each receiving antenna has its beamwidth, the position estimate is actually within a rhombus, and may not be as accurate as desired. The direction errors of the interceptors also add a particular level of inaccuracy to the estimation process.

Other disadvantages of this method are the need for two ships to be involved, with all the logistics and synchronization, and obviously the time frame needed for this process, which make it a poor choice for missile defense.

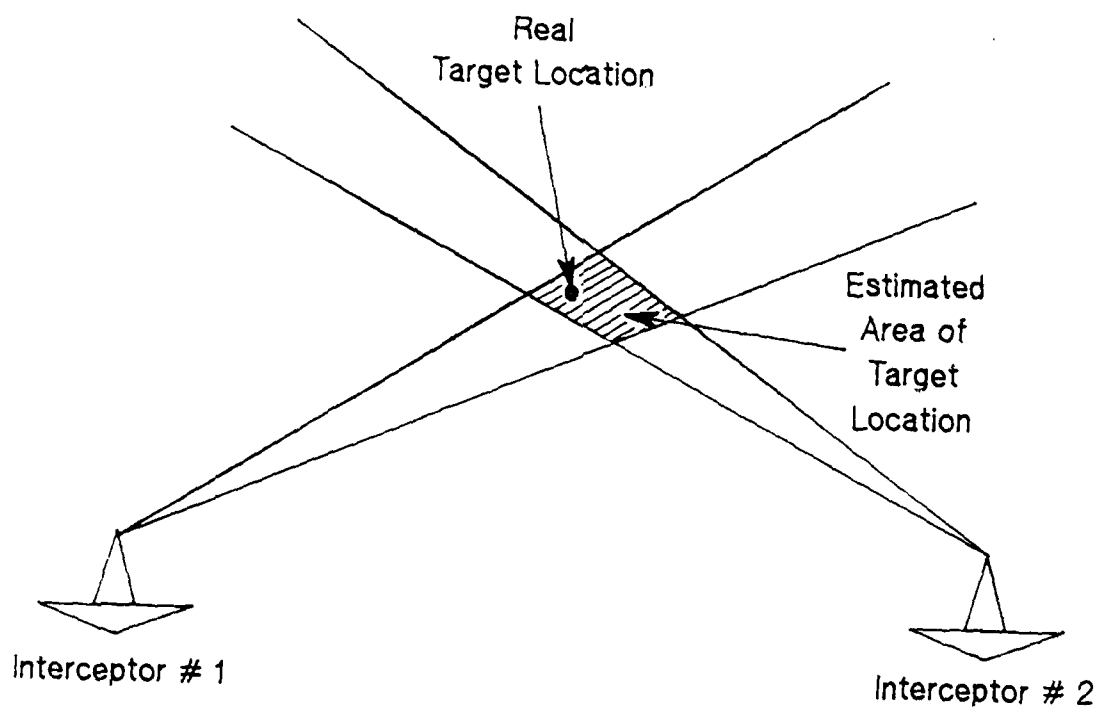


Figure 2.1: Triangulation Geometry.

2. Auto-triangulation

In order to estimate the location by using a single interceptor (single ship), we can make the triangulation by making sequential measurements, using the fact

that the interceptor itself is moving and changing its place. Obviously, this method takes a long time for processing, and therefore is good only for stable targets (shore radar, for example).

Actually, we cannot find the range of a moving target, especially a cruising missile, by using conventional methods, and so we need to have a special way for estimating the transmitter location.

The method suggested in this work uses the multipath propagation of a transmitted electromagnetic signal in order to estimate the transmitter range from the receiver, while the direction is still being found using any common method such as rotating antenna, Instantaneous Direction Finder, etc.

The theory of a general multipath propagation over smooth and rough sea is described in the next chapter.

III. THEORY OF MULTIPATH PROPAGATION OF ELECTROMAGNETIC WAVES

In a usual radar case, the multipath propagation generally causes tracking difficulties, especially over a smooth sea, which causes specular reflections.

In this chapter we will review the multipath propagation theory, divided into smooth and rough terrains.

A. GENERAL

A transmitted signal from a radar antenna spreads as it is leaving the antenna surface. A direct path exists between the transmitter (radar) antenna and the target (receiver antenna in our case), as well as an indirect path along which the signal transmitted from the transmitter antenna hits the sea surface and is reflected to the receiver antenna.

The signals arriving from these two paths create interference in the receiver, and the relative phase difference dictates if it is a creative or destructive interference. The path difference depends on the direct range R , transmitter antenna height h_t , and receiver antenna height h_r . Other factors have some influence as well, and will be discussed later in the next sections. Figure 3.1 shows the geometry of the multipath propagation over a smooth sea, assuming a flat earth.

Since the sea state has significant contribution to the interference, a basic question that can be asked is how to distinguish between a smooth and rough surface (sea in our case). The answer for this question is not a straight-forward one, and, as a matter of fact, there is neither a single answer nor a defined border

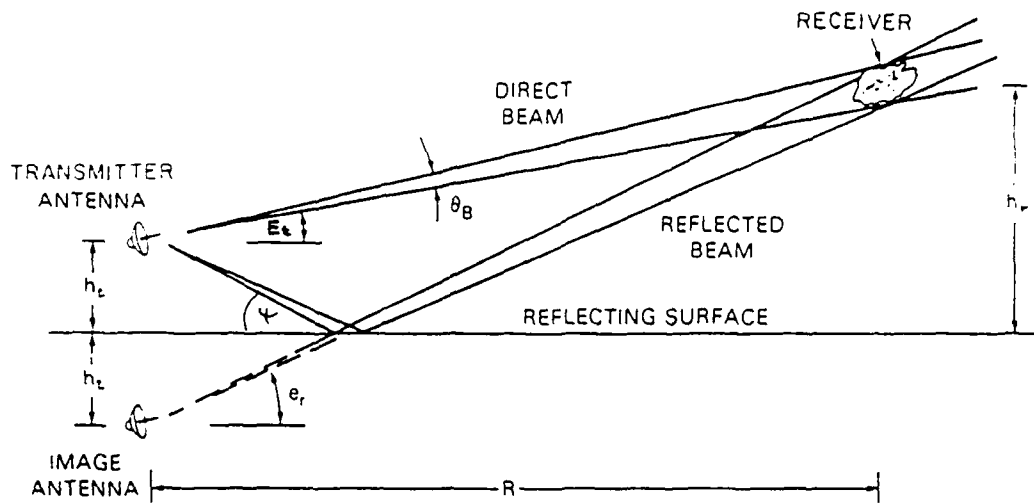


Figure 3.1: Simplified Multipath Geometry Over Smooth Terrain and Flat Earth Assumption [From Ref. 1].

between the two cases. A method for having a quantitative solution for this problem was suggested by Lord Rayleigh, and is described herein [after Ref. 2].

Before starting the detailed analysis, we will give some definitions which are relevant to our discussion, referring to Figure 3.2:

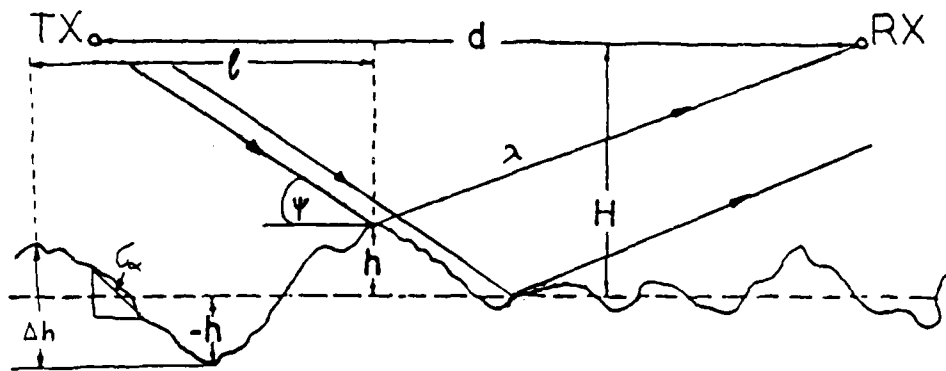


Figure 3.2: Geometry of Irregular Surface and Path Difference [From Ref. 3].

- Wave Height Δh : The vertical distance between the wave's trough and its crest.
- Wavelength λ : The horizontal distance between two adjacent crests (measured in the direction of wave propagation).
- Wave Period T : Time interval between two adjacent crests passing the same fixed point relative to the ground.

Consider an irregular surface with irregularities of height Δh . If two parallel rays of the same wavelength λ hit the surface with a grazing angle ψ , as illustrated in Figure 3.2, the path difference between them will be Δr , where:

$$\Delta r = 2\Delta h \sin \psi. \quad (3.1)$$

Translating this into phase difference, we obtain:

$$\Delta \phi = k\Delta r = \frac{2\pi}{\lambda} \Delta r,$$

and substituting (3.1) we have:

$$\Delta \phi = \frac{4\pi\Delta h}{\lambda} \sin \psi. \quad (3.2)$$

The phase difference $\Delta \phi$ can vary between 0 and π , where a totally smooth surface will occur when $\Delta \phi = 0$. Zero phase can be achieved when there are no irregularities, i.e., $\Delta h = 0$, or when the grazing angle is zero. From the above, we can assume a smooth surface when:

$$\frac{\Delta h}{\lambda} \rightarrow 0 \quad \text{or} \quad \psi \rightarrow 0. \quad (3.3)$$

When the phase difference between the direct and reflected signal components is equal to π , there will be a destructive interference, and no received energy at all if there is a perfect reflection ($|\rho| = 1$).

In order to choose a point where the surface becomes rough, we can arbitrarily choose any value between $\Delta\phi = 0$ and $\Delta\phi = \pi$. The most popular value is half the way ($\Delta\phi = \pi/2$), as was chosen by Rayleigh, and hence, the "Rayleigh criterion" for a smooth surface is:

$$\Delta h < \frac{\lambda}{8 \sin \psi}. \quad (3.4)$$

Other values have been chosen as well [Ref. 2,3,4,5,6].

From observing Equation (3.2), we can learn that the phase behavior is a periodic one, hence the interference will have maxima and minima in sequence.

A typical received signal in the presence of multipath propagation over a smooth sea is shown in Figure 3.3. The amplitude decay is due to the spherical spreading of the received signal ($1/R^2$).

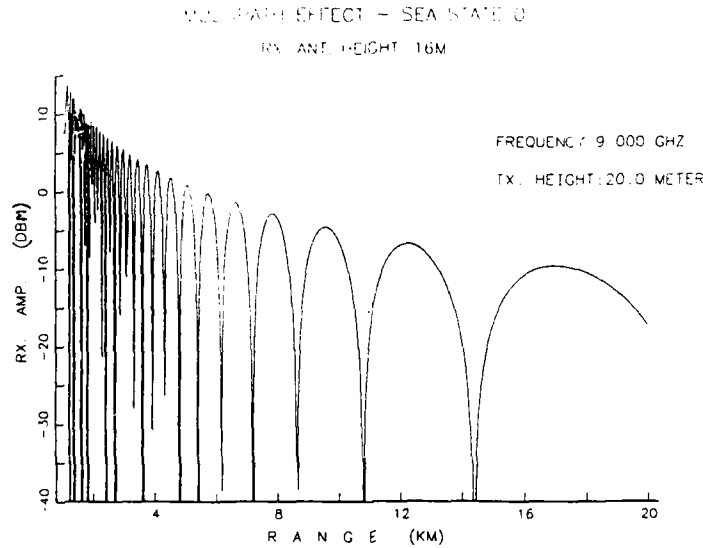


Figure 3.3: Multipath Propagation.

B. SMOOTH SEA

Looking at the multipath propagation more carefully, we should notice that there are additional phase and amplitude changes in the reflected wave due to the reflection itself, as well as amplitude difference between the reflected wave and the direct one, since the propagation path lengths are not the same.

The amplitude difference due to the difference in path lengths is very small, and hence can be neglected, since the paths differ only by a short distance compared to the total path length. [Ref. 7]

The phase and the amplitude changes due to the reflection itself depend on the grazing angle, frequency, and polarization.

Figures 3.4 and 3.5 illustrate the magnitude and phase (respectively) for vertical polarization, while Figure 3.6 shows the magnitude of the reflection coefficient for horizontal polarization.

Note the small changes in the value of the reflection coefficient for horizontal polarization, which means that amplitude changes due to reflection can be neglected for small grazing angles (assuming reflection coefficient magnitude = 1). The phase difference in horizontal polarization can be considered as 180°, since for grazing angles of 0° to 90° it changes only up to 4°. [Ref. 7]

Assuming a flat earth and a smooth terrain (reflection coefficient = -1), the ratio between the received power in the receiving antenna in the presence of multipath, compared to a free space (for small grazing angles) is η^2 [Ref. 3,9], where:

$$\eta^2 = 4 \sin^2 \frac{2\pi h_t(h_t + h_r)}{\lambda \cdot R} \quad (\psi \rightarrow 0), \quad (3.5)$$

using the same notation as in Figure 3.1. The shape of η^2 is shown in Figure 3.3 for a typical case.

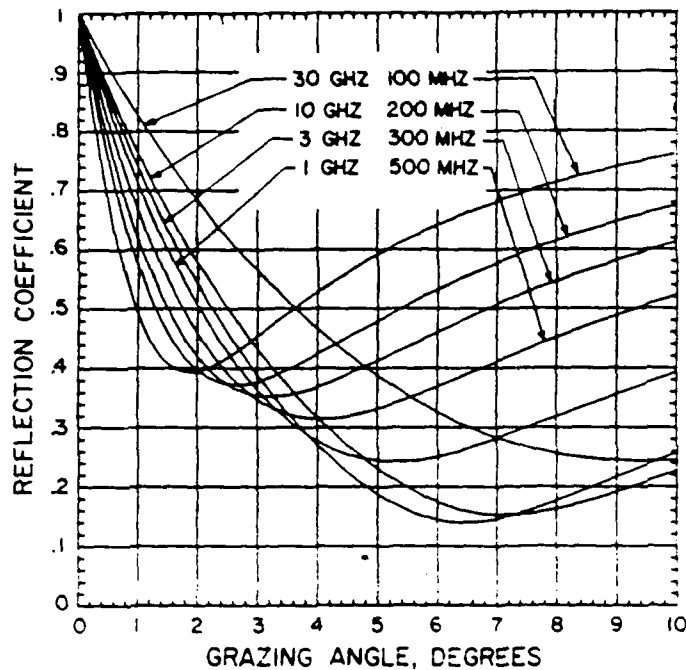


Figure 3.4: Reflection Coefficient in Vertical Polarization
[From Ref. 7].

In order to be more precise, we need to take into account the fact that the earth is not flat. This fact will cause some changes in the geometry, and hence will influence the signal amplitude.

Actually, the reflection coefficient depends on three main parameters:

- 1) Plane smooth surface reflection coefficient ρ .
- 2) Earth curvature, D , which reduces the reflection (in some cases, depending on the geometry).
- 3) Surface roughness R_n .

The actual reflection coefficient, hence, is [Ref. 6]:

$$\rho' = \rho \cdot D \cdot R_n. \quad (3.6)$$

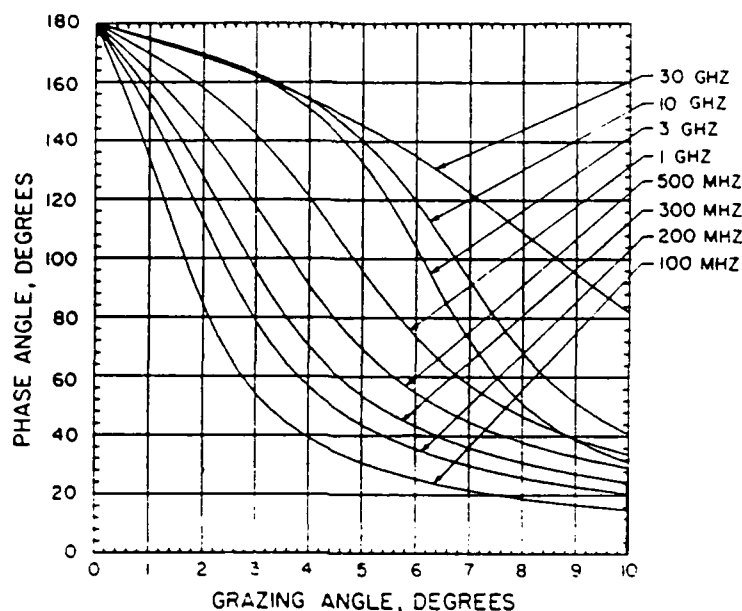


Figure 3.5: Phase Difference in Vertical Polarization [From Ref. 7].

The value of R_n is between 0 and 1, depending on the terrain, and it will be discussed in detail in the next section.

The earth curvature factor D (Divergence factor) has also values between 0 and 1, where in the flat earth case it will be unity.

Practically, in the scope of this work, we can use the flat earth assumption, since the geometry of the problem (transmitter height less than about 100 meter, receiver antenna height at about the same and both heights are much smaller than the distance in between) leads to small grazing angle and allows the assumption of parallel direct and reflected rays [Ref. 7].

Even though the transmitter is considered a point source, the reflections from the sea come from a particular zone, rather than in a single point. We shall look for all the points (loci), from which the reflected signal will reach the receiving

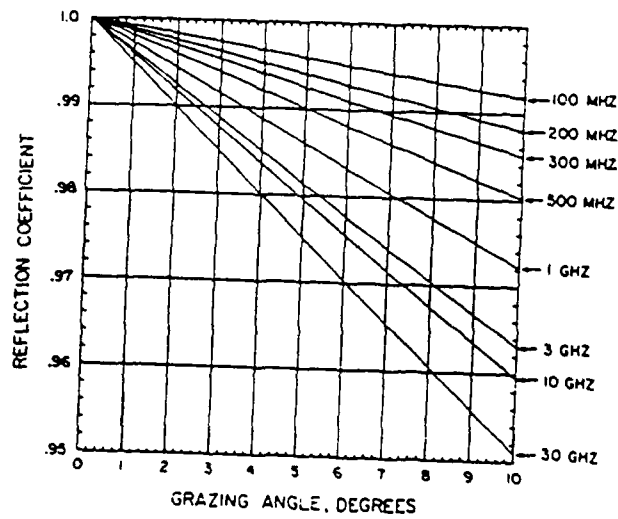


Figure 3.6: Reflection Coefficient in Horizontal Polarization [From Ref. 8].

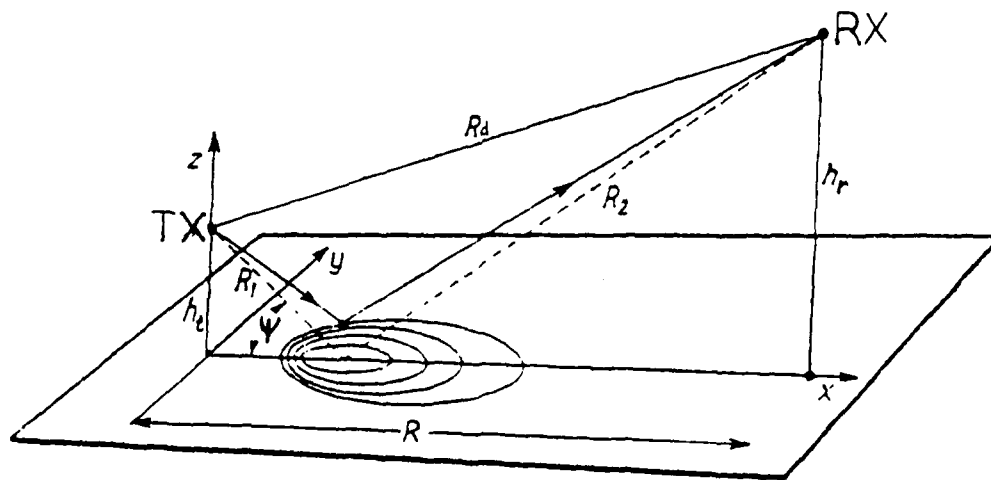


Figure 3.7: First Fresnel Zone [From Ref. 2].

antenna with the same phase shift, relative to the direct radiation, as illustrated in Figure 3.7. The loci obey Equation (3.7).

$$R_1 + R_2 - R_d = \delta, \quad (3.7)$$

or after arranging:

$$R_1 + R_2 = R_d + \delta = \text{Constant}. \quad (3.8)$$

Equation (3.8) describes ellipsoids, so that the reflection zones are actually ellipsoids which form the Fresnel zones (Fresnel ellipsoids). Near the wavelength that has the most interest to us, 3 cm, (or frequencies around 10 GHz), the area of the first Fresnel zone is about 2000 square meters [Ref. 2,3,6]. It is common to take the whole first Fresnel zone as the reflection area.

C. ROUGH SEA

The smooth sea case is generally rare, while some kind of roughness is more common, producing complications to the problem by adding more parameters, some of them arbitrary. Due to these facts, the rough sea case is difficult to analyze and predict.

A more accurate solution leads to more complications and difficulties, so in practice we try to simplify and make assumptions in order to get a solvable case. Still we need to be very careful so that the result will approximate reality even after using these assumptions.

In general, we can say that the first problem is to find a correct compromise between excess rigor which may yield no practical result, and too many simplifications which may lead to incorrect results and hence wrong conclusions [Ref. 3].

In practice, the common general assumptions which take place in the rough sea case are:

- Scattering elements are much larger than the propagated wavelength,

- Only the far field is calculated,
- Diffraction and reflections between waves are neglected,
- A particular model for the roughness shape is assumed (depending on the case), and average wave height is assumed, and,
- Constant sea state (roughness) is assumed for the whole area of interest.

1. Reflection types

At this point we will distinguish between two kinds of reflections:

a. **Specular reflection**

Similar to the smooth surface (as in a mirror case), specular reflection can be characterized as obeying the classical optics rules, as well as having a coherent phase. The direct source for this kind of reflection is the first Fresnel zone (Fresnel ellipse) radiated points. The phases of the different points (from the receiver point of view) are approximately equal, hence the reflection is coherent, as mentioned previously. The specular reflection fluctuations are relatively small in amplitude.

b. **Diffuse reflection (scattering)**

Caused due to irregularities in the surface, scattering cannot be predicted from the phase and directivity points of view. This scattering will occur over larger areas than the specular reflection (first Fresnel zone) and is incoherent in phase. The diffuse scattering has large amplitude fluctuations. We can also say that the smooth sea analysis is deterministic, while the rough sea analysis (both specular and diffuse reflections) is stochastic in nature [Ref. 5].

In general, there will be both reflection components, since a surface is neither totally smooth, nor extremely rough. The two components are illustrated in Figure 3.8 [Ref. 2,7,10].

The specular and diffuse reflection coefficient components will be denoted as ρ_s and ρ_d , respectively. The effective reflection coefficient will be a multiplication of the smooth terrain coefficient ρ_0 , and the relevant specular or diffuse coefficient. Hence, for the specular component, ρ_s , the reflection coefficient will be:

$$\rho = \rho_0 \cdot \rho_s, \quad (3.9)$$

and obviously will be smaller than that of a smooth sea ρ_0 (since each coefficient is less than unity).

The diffuse reflection will have a coefficient of

$$\rho = \rho_0 \cdot \rho_d, \quad (3.10)$$

again, smaller than ρ_0 .

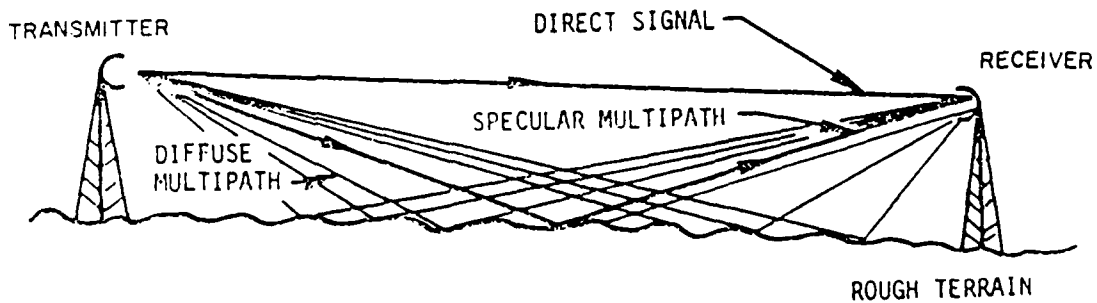


Figure 3.8: Illustration of Diffuse and Specular Reflections
[From Ref. 10].

The diffuse reflection coefficient, due to its random nature, is found to have a Rayleigh distribution probability function for the amplitude, as given in Equation (3.11), while the phase has a uniform distribution between 0 and 2π .

The diffuse reflection coefficient amplitude has the form:

$$\rho_d = \sqrt{2} \cdot \Gamma \cdot \exp(j\sigma_\alpha), \quad (3.11)$$

where:

σ_α is the RMS wave slope (unitless), as shown in Figure 3.2,

$$\Gamma = 0.77 \cdot [1 - \exp(-4\pi\delta)] \cdot \exp(-4.73 \cdot \delta), \text{ and,} \quad (3.12)$$

$$\delta = \frac{\sigma_h \cdot \sin \psi}{\lambda}, \quad (3.13)$$

where σ_h is the standard deviation of the wave height, related to the peak to trough height. [Ref. 5]

Assuming a smooth terrain, there will be a center point of reflection. The diffused reflection comes from the whole area surrounding this point, the glistening surface [Ref. 2,11], which depends on the observation angle from the transmitter to the receiver (E_t in Figure 3.1), and on the RMS wave slope (σ_α).

A typical RMS slope, σ_α , is about 0.2 radians, and it depends on the wind velocity. The amplitude of the reflection coefficient ρ_d has an extreme of 0.4, which rarely occurs, while a typical value is 0.35. [Ref. 11]

We should notice that for a flat earth assumption, the grazing angle ψ is the same as the observation angle E_t from the transmitter to the receiver (see Figure 3.1). The idea of the different reflection areas due to observation angle E_t , and sea state (roughness) is demonstrated in Figure 3.9. In this Figure, σ_α represents the rough surface RMS slope.

The specular reflection coefficient has been analyzed by many, and there are quite a few models for this component. Each model uses different assumptions for the computations, and therefore there are (in some cases) different results. The conclusion from this is that the results are highly dependent on the roughness type which is assumed.

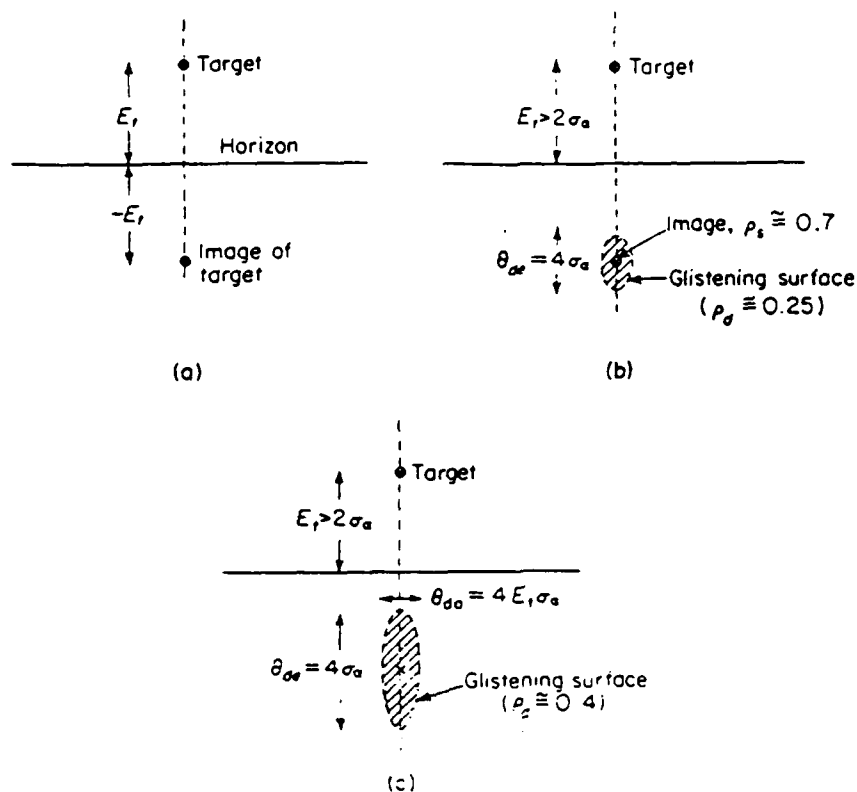


Figure 3.9: Reflection Areas in Different Roughness and Observation Angle, E_t : (a) Specular reflection, $\rho_s \approx 1, \rho = \rho_0$, (b) Slight roughness, $(\sigma_h/\lambda) \cdot \sin E_t \approx 0.06$, (c) Rough Surface [From Ref. 11].

In order to be as close to the experimental data with a generic formulation as possible, we can, in general, define the reflection coefficient, ρ , as [Ref. 12]:

$$\rho = \int_{-\infty}^{\infty} p(\phi) \cos \phi d\phi, \quad (3.14)$$

where:

ϕ is the phase of each particular element of the reflected wave in relation to a median plane surface, and,

$p(\phi)$ is the probability distribution of all the phases ϕ along the path.

2. Profile Types

Using Equation (3.14), we find that the common profile models for rough terrain are [Ref. 2,12]:

a. Sawtooth profile

The phase ϕ varies uniformly between maximum values of $\pm\phi_m$, and the probability distribution therefore is:

$$p(\phi) = \frac{1}{2\phi_m}, \quad (3.15)$$

while the reflection coefficient is:

$$\rho = \frac{\sin \phi_m}{\phi_m} = \text{sinc} \phi_m. \quad (3.16)$$

The idea here is that the wave height is uniform, but wave slopes are arbitrary.

b. Sinewave profile

The phase ϕ behaves like a sine wave with maximum amplitude of $\pm\phi_m$. In this case, the probability distribution is:

$$p(\phi) = \frac{1}{2\pi\phi_m \cos \nu}, \quad (3.17)$$

where ν is an arbitrary parameter, and:

$$\rho = J_0(\phi_m),$$

where J_0 is the Bessel function of zero order.

c. Random profile

The phase ϕ has normal (gaussian) probability distribution with standard deviation of σ . Here,

$$p(\phi) = \frac{\exp -(\phi^2/2\sigma^2)}{\sqrt{2\pi} \cdot \sigma}, \quad (3.18)$$

and the reflection coefficient in this case is

$$\rho = \exp -(\sigma^2/2). \quad (3.19)$$

The latter profile is similar, in a sense, to the Ament model, which will be discussed later in this chapter. The three profiles are drawn in Figure 3.10 [Ref. 12].

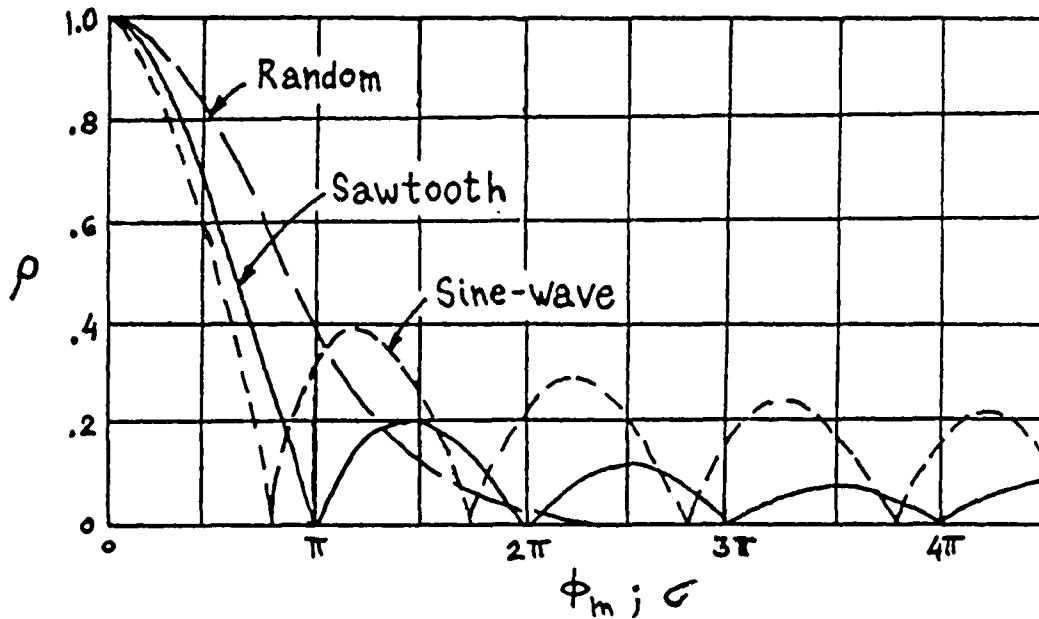


Figure 3.10: Reflection Coefficients of Common Models for Irregular Terrain [From Ref. 12].

A further discussion on other models is given in Appendix A.

The most general and the most popular model is the one by W. S. Ament.* This model assumes a normal (gaussian) distribution, and it is popular since it does not include any discontinuities as other distributions do, but still meets the actual (experimental) data. For these reasons it seems to be the most realistic model [Ref. 2].

The Ament model is discussed and analyzed in many books and articles, and from now on we will concentrate especially on it [Ref. 2, 3, 5, 6, 7, 9, 11, 13, 14, 15].

D. AMENT MODEL FOR IRREGULAR TERRAIN

The Ament model assumes that the wave height is normally (gaussian) distributed, and it does not take into account the shadowing effect, where parts of the surface which are hidden by higher parts are not being illuminated by the incident wave. The shadowing effect takes place at very small grazing angles, while for higher angles it has no effect. The geometry is shown in Figure 3.11. [Ref. 13]

Figure 3.12 shows the influence of the shadowing effect on the wave height standard deviation, related to the grazing angle [Ref. 13].

The specular component of the reflection coefficient in this model is:

$$\rho_s = \exp -2 \left(\frac{2\pi\sigma_h \sin \psi}{\lambda} \right)^2, \quad (3.20)$$

where:

σ_h is the RMS deviation of the waves height,

ψ is the grazing angle (refer to Figure 3.1), and,

* W. S. Ament, "Toward a Theory of Reflection by a Rough Surface," Proc. I.R.E., vol. 41, p. 142, January 1953.

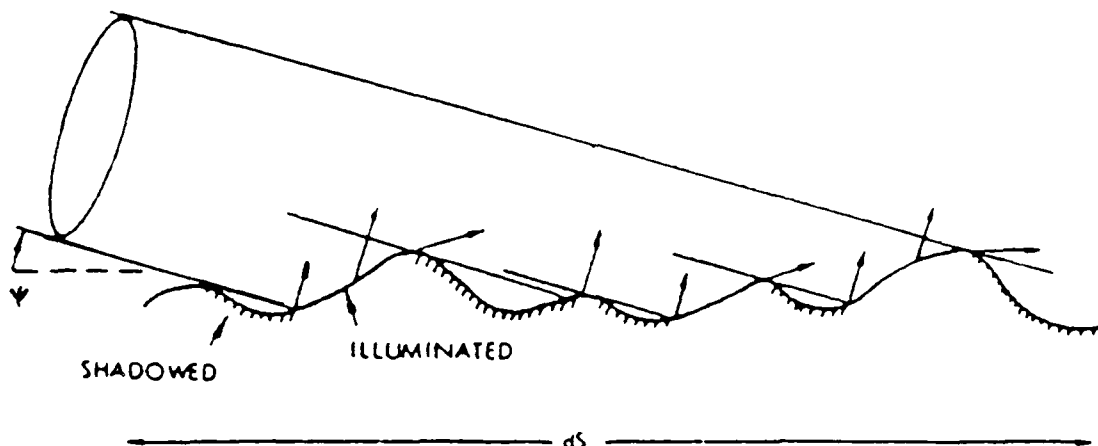


Figure 3.11: Shadowing Effect Geometry [From Ref. 13].

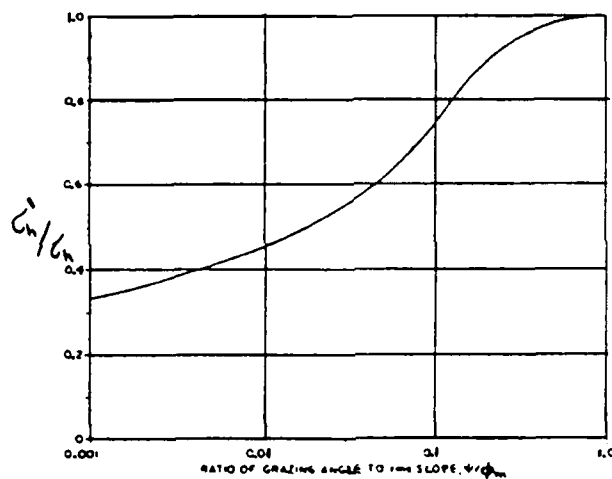


Figure 3.12: Shadowing Effect on Wave Height Standard Deviation [From Ref. 13].

λ is the incident wavelength.

Figure 3.13 shows the specular reflection coefficient component according to Ament model [Ref. 7].

The parameter σ_h is proportional to the sea state, and is given with other relevant parameters in Table 3.1 [after Ref. 2,11].

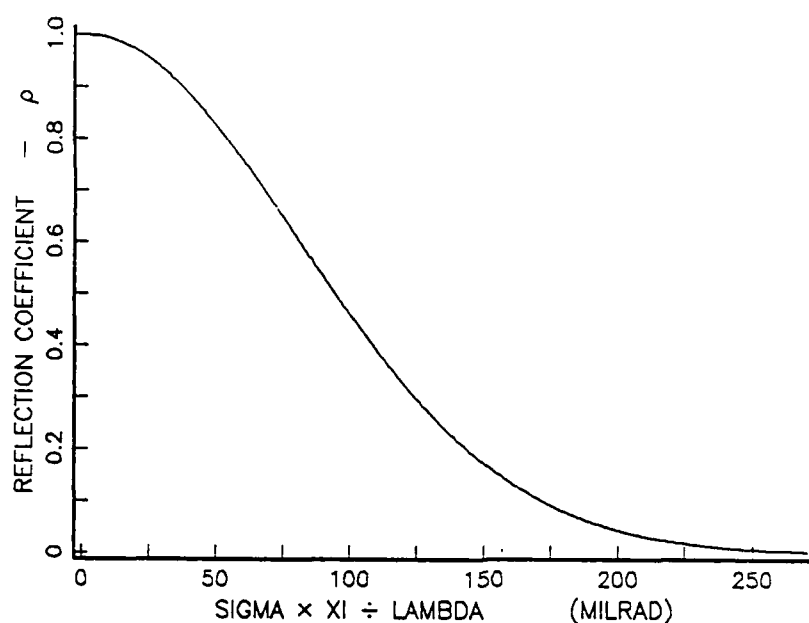


Figure 3.13: Rough Surface Reflection Coefficient According to Ament Model.

TABLE 3.1: WAVE HEIGHT PARAMETERS AND CRITICAL ANGLES FOR SPECULAR REFLECTION, VERSUS SEA STATE.

sea state number	description of sea	wave height (m)	RMS height σ_h (m)	critical angle ($^\circ$), ψ_{\max}	
				3 GHz	10 GHz
0	calm	0	0		
1	smooth	0-0.3	0-0.065	> 6	> 1.8
2	slight	0.3-1	0.065-0.21	1.8-6	0.5-1.8
3	moderate	1-1.5	0.21-0.32	1.2-1.8	0.3-0.5
4	rough	1.5-2.5	0.32-0.54	0.7-1.2	0.2-0.3
5	very rough	2.5-4	0.54-0.86	0.4-0.7	0.12-0.2
6	high	4-6	0.86-1.3	0.3-0.4	0.09-0.12
7	very high	> 6	> 1.3	< 0.3	< 0.09

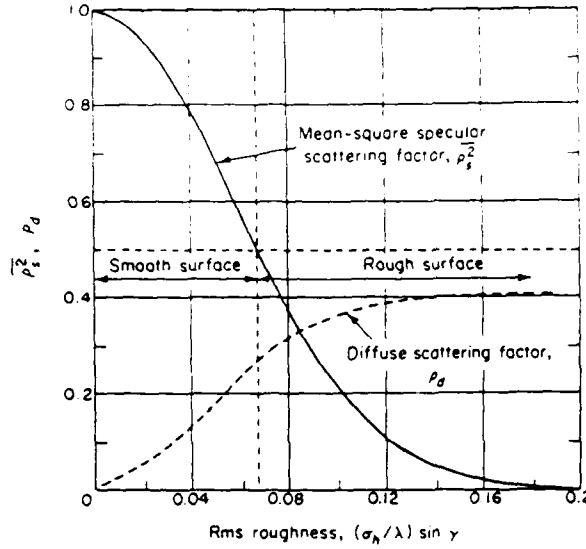


Figure 3.14: Scattering Regions Versus Roughness [From Ref. 11].

Using the Ament model, we can distinguish more carefully between rough and smooth sea, and check the conditions for diffuse and specular reflection. Recall (3.20) for convenience:

$$\rho_s = \exp -2 \left(\frac{2\pi\sigma_h \sin \psi}{\lambda} \right)^2.$$

We can consider the terrain as a rough one if $\rho_s \leq 0.5$, which is equivalent to:

$$\frac{\sigma_h}{\lambda} \sin \psi_{\max} \geq 0.0665. \quad (3.21)$$

For a particular wavelength at a given sea state, there is a critical grazing angle ψ_{\max} , calculated from (3.21), above for which the sea surface is taken as rough. This angle is shown in Table 3.1.

The specular reflection coefficient component is significant until the grazing angle exceeds twice the critical angle. Beyond that point, the diffuse component becomes the significant one. The different regions of roughness type are illustrated in Figure 3.14. [Ref. 2,11,14]

Another way of looking at the specular (coherent) and diffuse (incoherent) scattering regions is given in Figure 3.15. Here we can see the boundaries between the scattering regions for different grazing angles. The graph in Figure 3.15 is given for 2 GHz. For higher frequencies, the graph will become more compressed, by the reciprocal of the frequency. [Ref. 15]

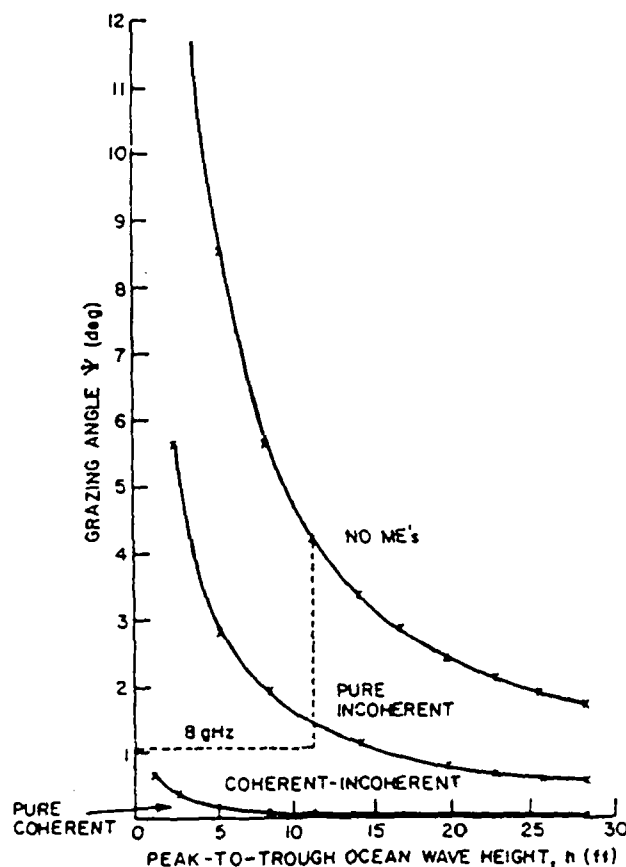


Figure 3.15: Scattering Regions Envelopes at 2 GHz [From Ref. 15].

A similar graph for a constant wave height of 0.92 meter and different frequencies is given in Figure 3.16. Here again, for higher wave heights, the envelopes will be compressed by the same factor by which the height is increased. [Ref. 15]

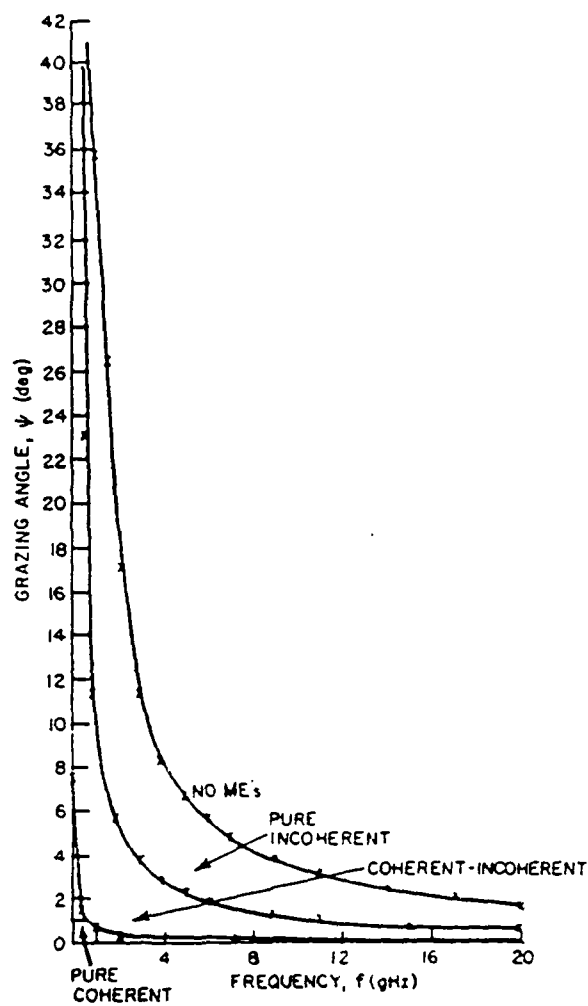


Figure 3.16: Scattering Regions Envelopes at Peak to Through Wave Height of 0.92 meter [From Ref. 15].

IV. THEORY OF RANGE ESTIMATION

USING MULTIPATH EFFECT

A. THEORETICAL SOLUTION

The multipath effect attenuation, as a function of range over a smooth sea, is well known, if both the transmitter and receiver height, as well as the frequency of the signal are given. This was described in the previous chapter.

For a rough sea, the overall shape remains similar, except that the curve has more fluctuations. Still, by using a particular model, such as the Ament model in our case, we can deal with the multipath propagation as a known factor.

Figures 4.1 and 4.2 show typical multipath propagation over a calm sea (state 0) and over a very high sea (state 7), respectively. We can notice that in the rough sea case, the attenuation coefficient decreases arbitrarily in the short ranges, and has an arbitrary ripple over the whole range.

From the above, the multipath attenuation η^2 can be written as a function of the range between the transmitter and the receiver R and of the transmitter height h_t , for a given receiver height h_r :

$$\eta^2 = f(R, h_t) \Big|_{h_r = \text{const.}} \quad (4.1)$$

The received signal is attenuated relative to free space. It is a combination of both the direct and indirect components. Hence, the received signal can be written as:

$$S_r = S_d \cdot \eta^2, \quad (4.2)$$

where:

S_r is the received signal power,

S_d is the direct component of the signal power, and,

η^2 is the multipath power attenuation factor, given by Equation (3.5).

Since, as mentioned before, we cannot specify the direct component S_d , we need to eliminate it in order to solve the problem. A simple way for doing that is by using a pair of receiving antennas, one above the other, so that the range R will remain the same, while their heights have no practical influence on the direct signal amplitude. We should also remember that the transmitter height, h_t , is constant for both receiving antennas.

If we use the ratio of the output powers from the two antennas,

$$\frac{(S_r)_1}{(S_r)_2} = \frac{S_d \cdot \eta_1^2}{S_d \cdot \eta_2^2} = \frac{\eta_1^2}{\eta_2^2}, \quad (4.3)$$

we will be dependent only on the geometry of the receiver and the transmitter, without caring about the direct signals' amplitude.

Referring to Equation (4.1), we notice that we still have two unknowns, R and h_t . Using the fact that we have two receiving antennas, while the range R and the transmitter height h_t are the same, we need to find the correct ratio η_1^2/η_2^2 which will give the right combination of range and height (R and h_t). Figure 4.3 shows the geometry of the problem. A more detailed explanation of the sequence is given below.

Let us assume, for simplicity, that the multipath propagation curve is a linear function (we shall return to the actual case later on), hence it behaves like an isomorphic function.

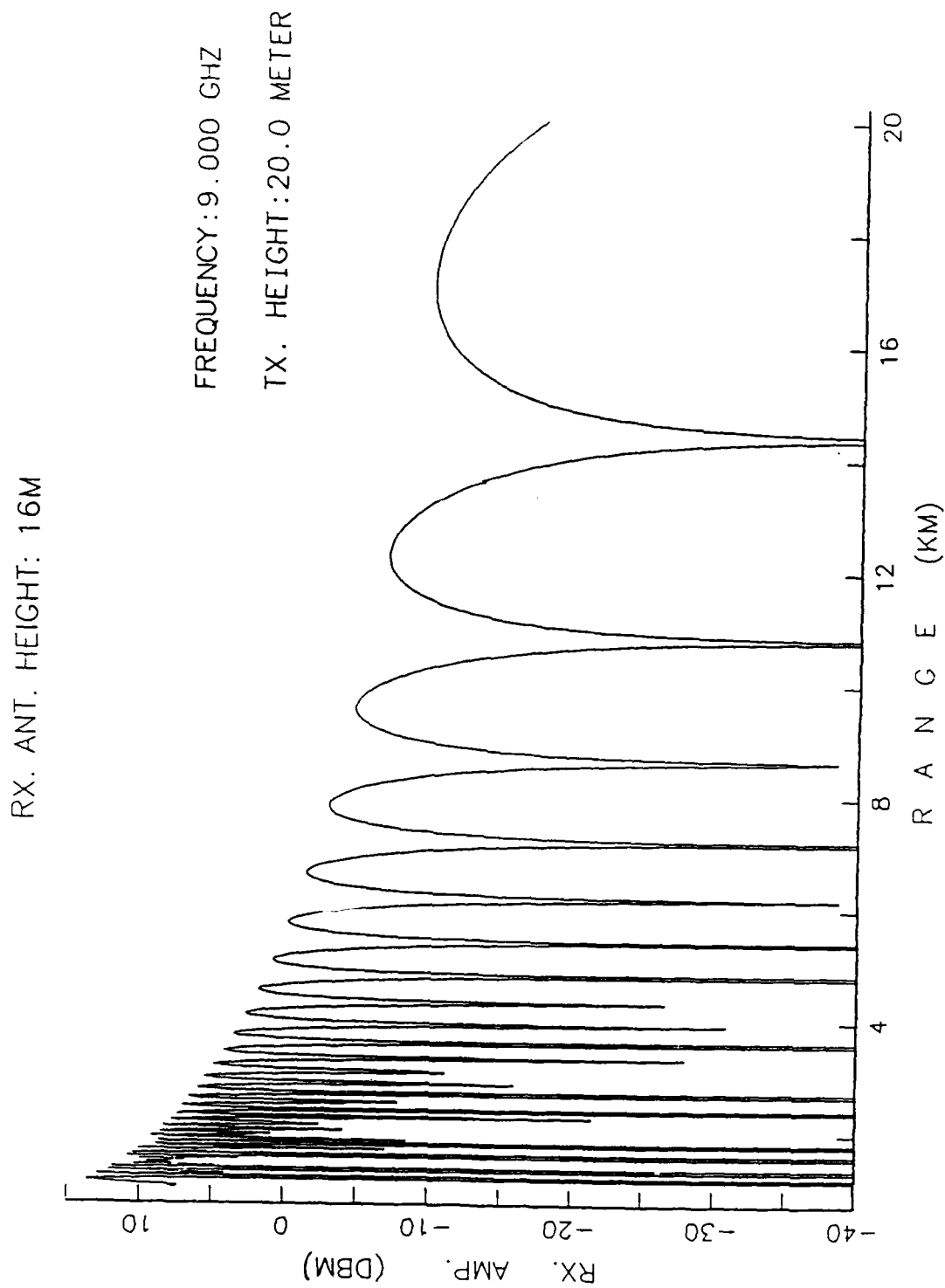


Figure 4.1: Multipath Propagation Over a Calm Sea.

MULTIPATH EFFECT - SEA STATE 7

RX. ANT. HEIGHT: 16M

FREQUENCY: 9.000 GHZ
TX. HEIGHT: 20.0 METER

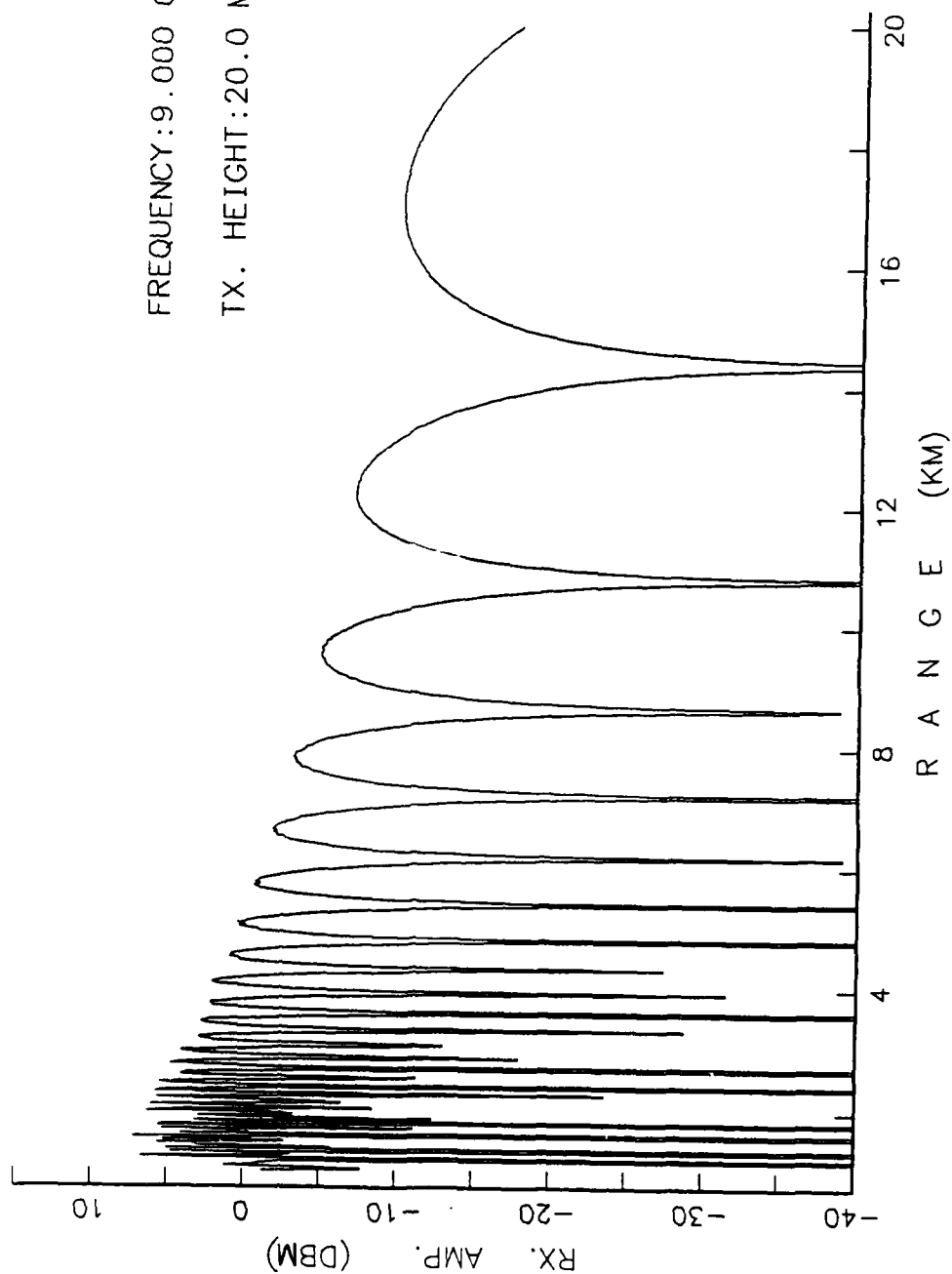


Figure 4.2: Multipath Propagation Over a Very High Sea.

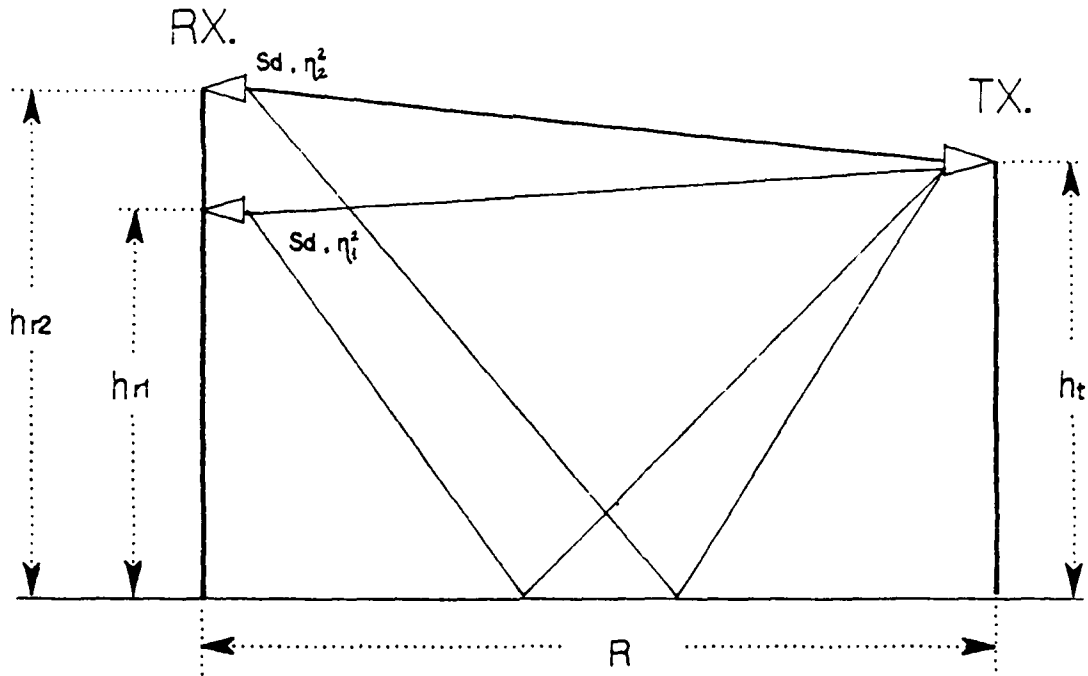


Figure 4.3: Range Estimation Basic Geometry.

The power ratio of the outputs of the two receiving antennas can be written as:

$$\frac{(S_r)_1}{(S_r)_2} = \frac{\eta_1^2}{\eta_2^2} = \frac{f(R, h_t)|_{h_{r1}}}{f(R, h_t)|_{h_{r2}}} = g\left(\frac{h_{r1}}{h_{r2}}\right), \quad (4.4)$$

so it actually depends on the receiving antenna heights, which are known.

Since we assumed that the problem has an isomorphic characteristic, a given ratio has only a single combination of range and transmitter height which fits this ratio.

Keeping in mind those conclusions, the range estimation process will require:

- 1) receiving a signal and analyzing its frequency and direction.
- 2) using Equation (3.5), creating two (off line) tables (matrices) at that particular frequency, for which the coordinates are range and transmitter height, while

the contents are the attenuation coefficients for each R and h_t combination, while the parameter is the receiver height (hence there are two tables).

- 3) calculating an (off line) look-up table for the same frequency, ranges and transmitter heights, which has the values of the ratio between the two tables created in step 2.
- 4) calculating the ratio between the two received signals, which is similar (see Equation 4.3) to the ratio of the attenuation coefficients.

Now, all we have to do is to search in the look up table from step 3, and find the range and the transmitter height, so the last step will be:

- 5) searching for the right combination of range and height.

B. PRACTICAL SOLUTION (OVER SMOOTH SEA)

Practically, the multipath propagation leads to a multi-valued curve, hence the problem is not isomorphic any more, but has an ambiguous solution. Since the function is not linear any more, and involved with two unknown variables, we cannot use any analytical solution (like we could have used in the theoretical case), but only a numerical solution can take place. The idea is similar to the one described in the theoretical case with a pair of antennas.

We saw before that two receiving antennas give a single ratio, hence we cannot solve the ambiguity problem (because of the periodic behavior of the multipath effect).

Adding a third antenna will give a second relation, so we can now use the process described previously for the two pairs, with a few candidate combinations (R and h_t), and by comparing their locations between the two lists of candidates, choosing that one which appears in both of the lists; all the other locations are false ones.

If the solution still is not a single one, we can add another antenna(s), until the comparison between all of the ratios leads to a single location. An important condition is that all of the receiving antennas be installed one above the other.

A trade-off between the number of antennas and accuracy should be done: on one hand we want minimum ambiguous points (different points with the same ratios group) which dictates many antennas, but on the other hand we should use a realistic number of antennas.

The influence of the different parameters on the multipath behavior can be seen in Figures 4.4 to 4.6.

From observing these figures, we can conclude that:

- 1) as the frequency increases, the curves become more complex (signal strength varies more rapidly with range),
- 2) complexity increases with transmitter height, and,
- 3) for increased receiving antenna height, the curves become more complex. This fact suggests keeping the antennas at lower height, but on the other hand, we should separate them enough to reduce the ambiguity. The receiving antennas in Figure 4.6 are 0.2 meters apart, so the curves are very similar to each other. In Figure 4.7, the antennas are separated by 3 meters, and the curves are well distinguished.

Note that for short range we have very high complexity, which will be treated later on.

C. PRACTICAL SOLUTION (OVER ROUGH SEA)

In the case of rough sea, the main idea remains the same, although the signal exhibits fading as a function of the sea state. As the receiving antenna is raised, the influence of the roughness becomes more important. Figure 4.8 shows the multipath propagation curves over sea state 7, for different antenna heights. It

is obvious from these graphs that the higher the antenna is, the more rapid the fading.

The look-up tables should take in account also the sea roughness parameter, where in our case we choose the Ament model, as described in Chapter III.

After considering the facts mentioned above, the estimation process remains the same as described in the previous sections.

MULTIPATH EFFECT - SEA STATE 0

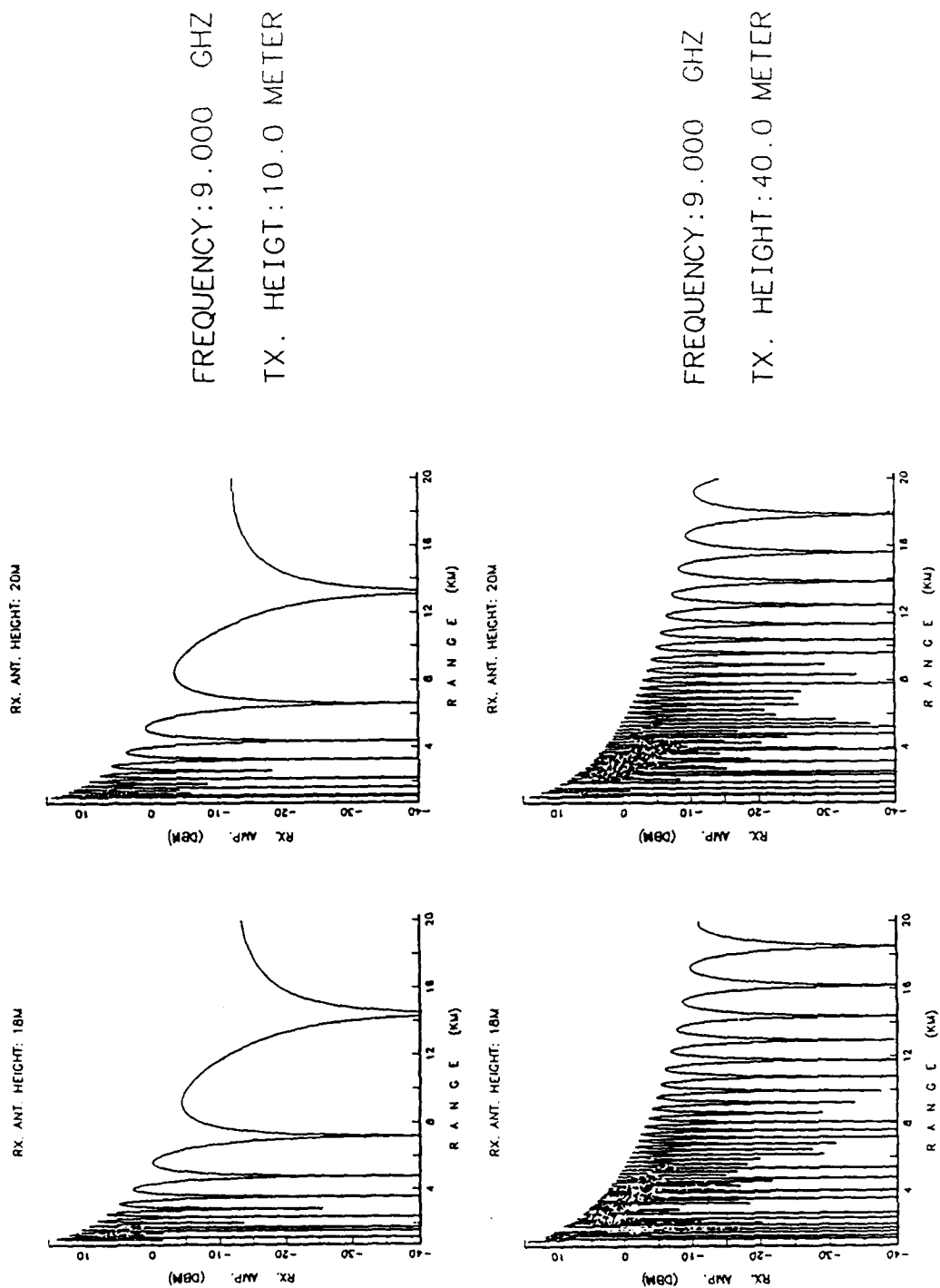


Figure 4.4: Variation of Signal Strength with Range, for Different Transmitter Heights.

MULTIPATH EFFECT - SEA STATE 0

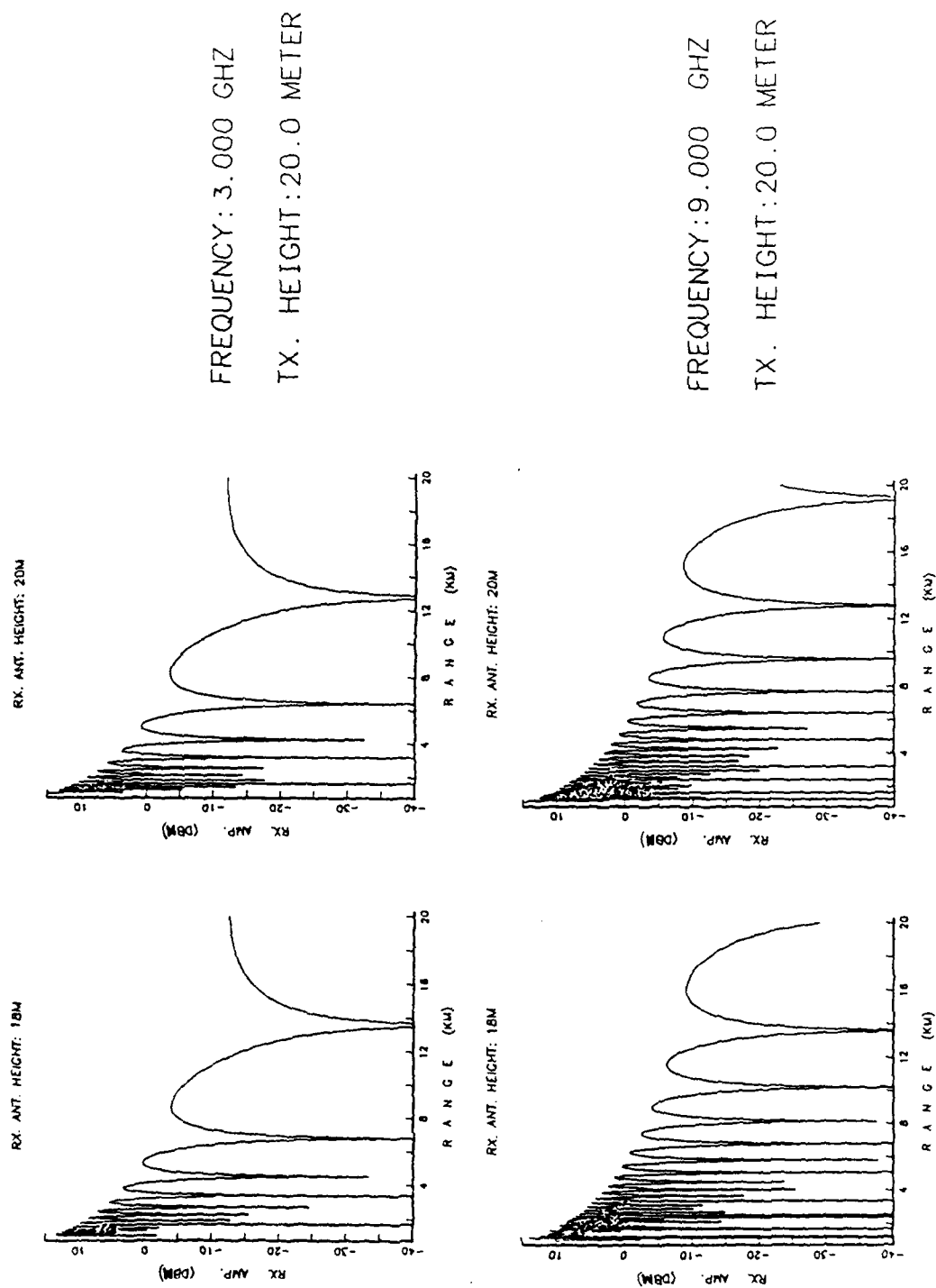


Figure 4.5: Variation of Signal Strength with Range, for Different Frequencies.

MULTIPATH EFFECT - SEA STATE 0

RX. ANT. HEIGHT: 16; 16.2 METER

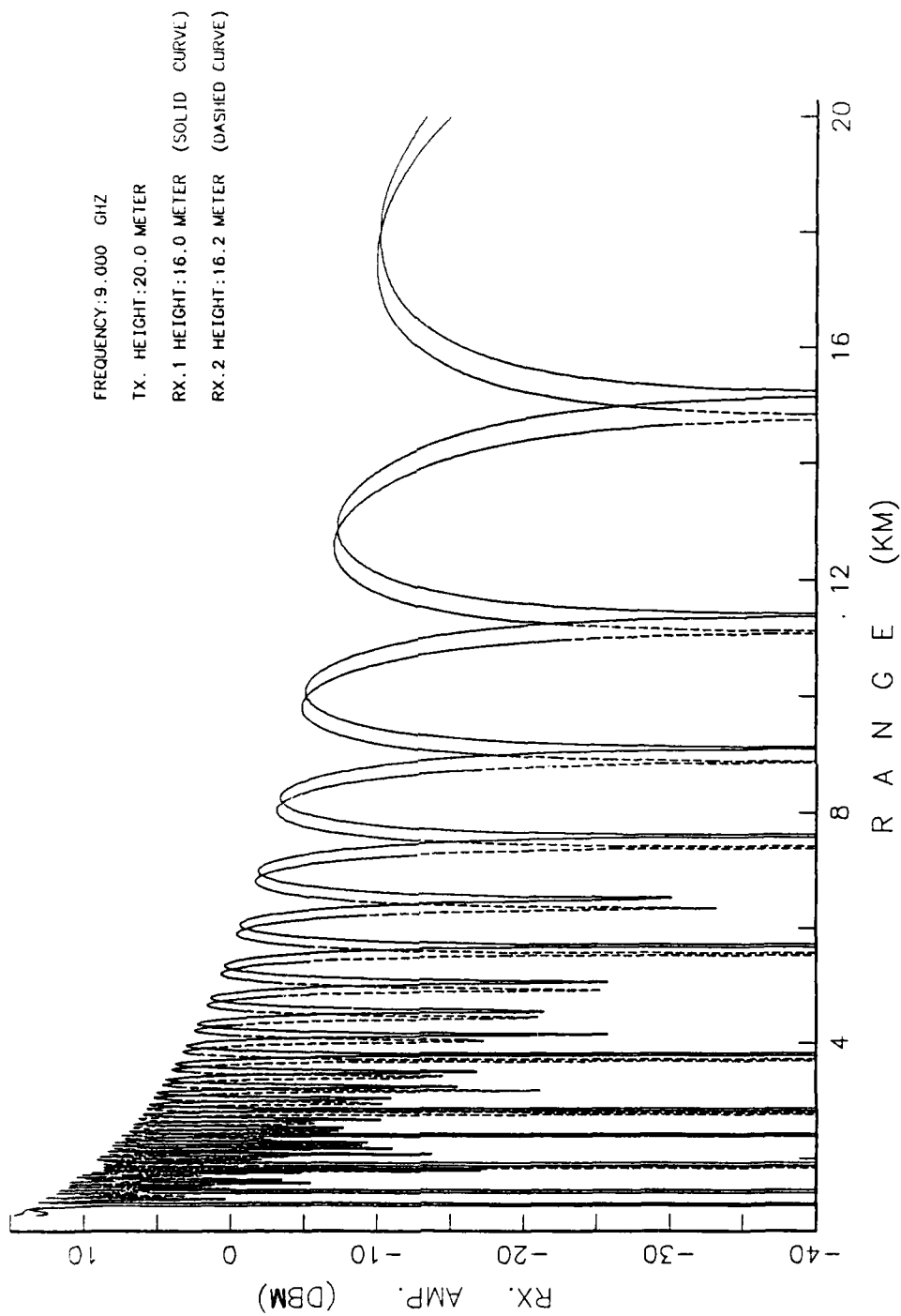


Figure 4.6: Variation of Signal Strength with Range, for Different Receiver Heights (Small Separation).

MULTIPATH EFFECT - SEA STATE 0
RX. ANT. HEIGHT: 16; 19 METER

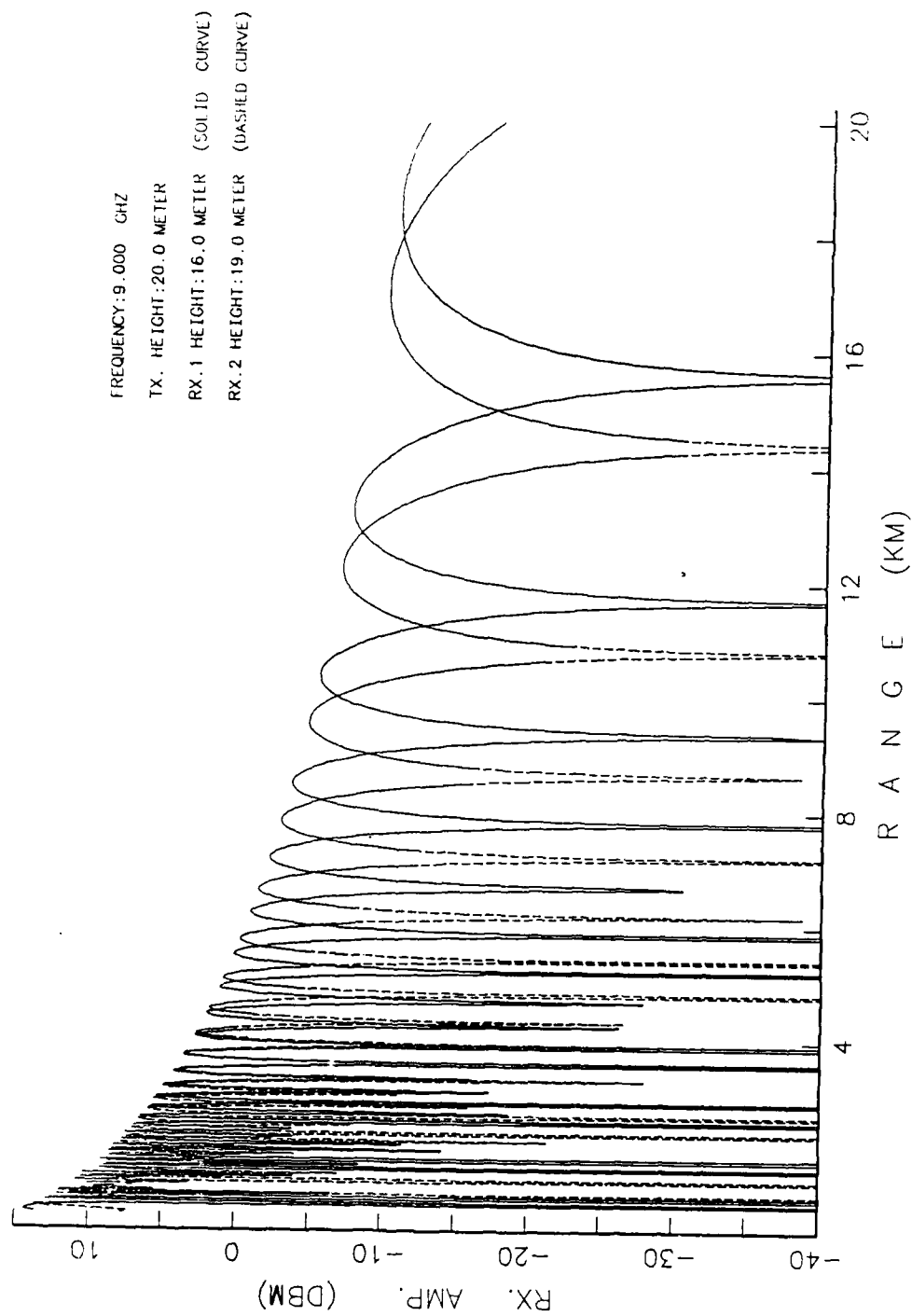


Figure 4.7: Variation of Signal Strength with Range, for Different Receiver Heights (High Separation).

MULTIPATH EFFECT - SEA STATE 7

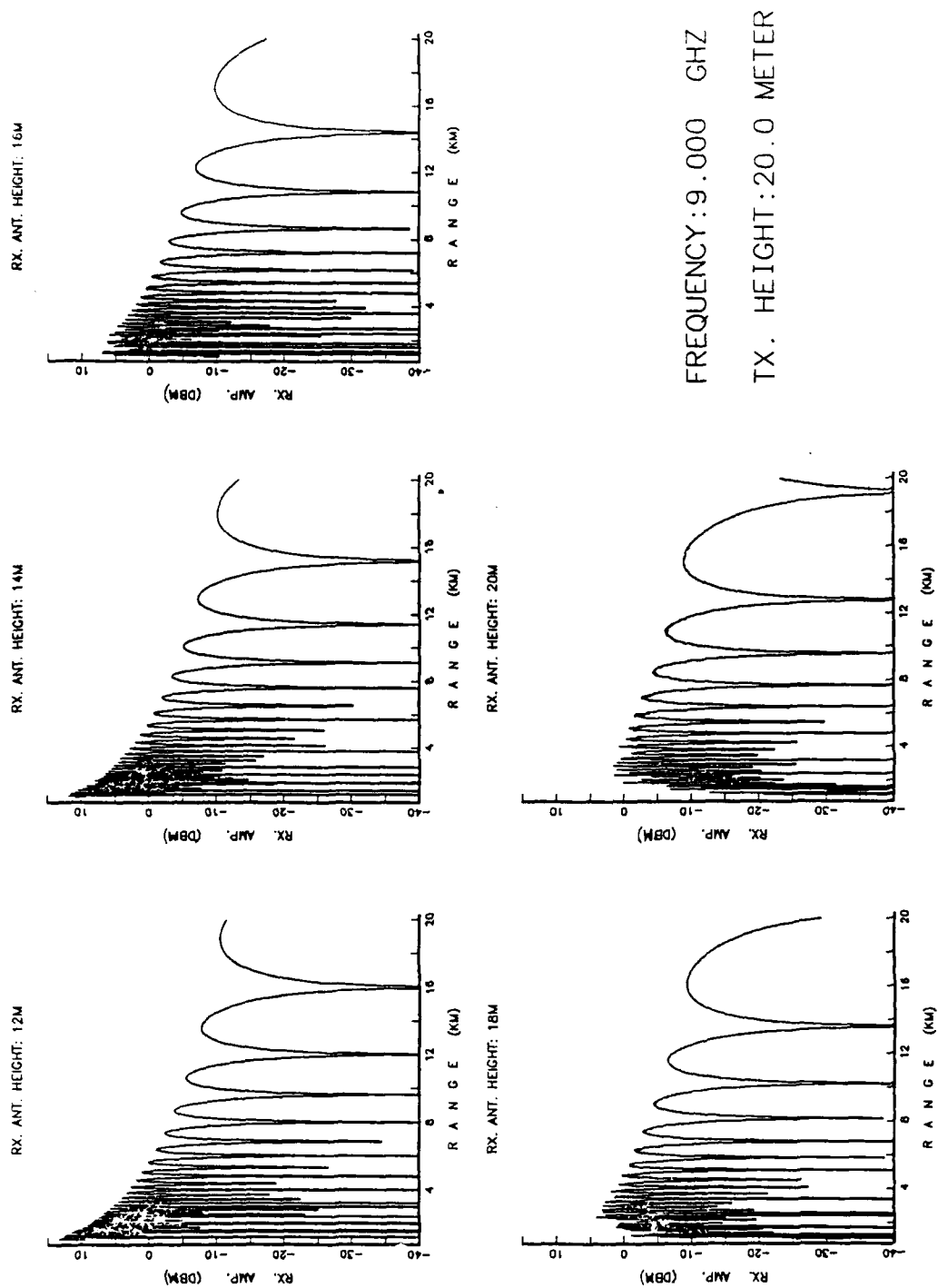


Figure 4.8: Variation of Signal Strength with Range, for Very High Sea and Different Receiver Antenna Heights.

V. EXPERIMENTAL PROCEDURE AND RESULTS

Now that we have presented the theory of how to use the multipath effect for estimating range, we can discuss how we applied that for solving the problem in our research. The assumptions, practical difficulties, and then some simulation results will be presented.

A. ASSUMPTIONS

Since the actual problem is a very complicated one, due to many surface parameters, where some of them are unknowns and/or very difficult to predict, we made some logical assumptions in order to obtain a solution.

- Polarization: the seeker was assumed to have horizontal polarization, hence the reflection coefficient was taken as unity in amplitude, with a 180° phase shift. The differences for vertical polarization will be discussed in Chapter VI.
- Sea state: the whole area of interest, i.e., the whole range between the transmitter and the receiver was assumed to have the same sea state condition.
- Earth curvature: a plane earth was assumed. A spherical earth case is discussed in Chapter VI.
- Atmosphere: a homogeneous atmosphere was assumed.
- Movement: the suggested method considers relative movement between the transmitter and the receiver. For homing missile, this is obvious. In other cases, such as estimating range between own ship and a stable transmitter (shore based radar, for example), we shall assume that the ship is moving relative to the radar. If there is no relative movement at all, the result can be incorrect.
- Geometry: It was assumed that the antenna separation, from the point of reflection, was much larger than the signal wavelength [Ref. 2]. Since we are dealing with microwave signals (from 2 GHz at least), this assumption is valid. (If this condition is not true, the reflection coefficients have some more complexity.)

- Range interval: almost any range interval can be assumed, but note that for the long ranges we should check the geometry and see if the plane earth assumption is still applicable. Since we concentrated in this work on homing missiles, the seeker transmitting range is the one of importance, and hence a maximum range of 20 Km (about 11 NM) is considered, while a minimum of 1 Km (about half a NM) assumed.

B. ESTIMATION PROCESS

With the assumptions of the previous section in mind, let us repeat briefly the range estimation process. We shall look more closely at the details shortly.

1. General Discussion:

A general solution requires the following steps:

a. Frequency Measurement:

Since the whole process is frequency dependent, this will be the very first step made by any EW receiver.

b. Off Line Tables:

In this step we build the theoretical tables for all ranges and heights of interest (i.e., the possible locations of the transmitter), for each receiving antenna height. The inputs for creating those tables are frequency, receiving antenna height, and sea state, which dictates the attenuation factor to be placed in the table.

c. Attenuation Coefficient Ratio Tables:

After we have the theoretical receiving values (from the previous step), we calculate (for each range and height combination) the ratios of the output signals for each receiving antenna pair.

d. Amplitude Measurement:

We must measure the received signal amplitude of each receiving antenna (we will discuss later the number of receiving antennas), and make a table of amplitude ratios. For example: suppose we have three receiving antennas, where

each one receives a signal with amplitude s_1, s_2 , and s_3 , respectively. The ratio table will have two elements: s_2/s_1 and s_3/s_1 .

e. Comparison:

Now, that we have the measured signal ratio (from step d), and the theoretical one (step b), we need to compare – for each receiving antenna pair, the actual value with the off line (theoretical) value, and record range-height combinations for which they are equal. These range-height combinations represent possible transmitter locations.

Since, as we mentioned in Chapter IV, the problem has an ambiguous solution, there will be several possible locations, even though only one of them is the correct one. The next step is to determine the correct location.

f. Validation:

In order to choose the correct location from all the candidate locations determined in step e, we will compare all the locations determined for the first pair of receiving antennas, and the second pair of receiving antennas. There is, ideally, only a single location, which should appear common to all the pairs.

Practically, because of the high ambiguity level (especially for the relatively short ranges), and also because of approximations in the implementation, there will still be more than a single location. In order to resolve this problem, we shall use more receiving antennas, which provides more ratios. This allows the ambiguity to be reduced to an acceptable minimum.

g. Output:

The matrix location is translated into an estimate of transmitter range and height. This is accomplished by using the coordinates of the look up table.

2. Detailed Discussion

The following section explains in detail every step listed before.

a. Frequency Measurement:

Since this requires an external system, we will not discuss it. Any EW receiver on board can be used for frequency measurement and direction finding. The frequency data is provided as an input to the range estimation process.

b. Off Line Tables:

This step uses the theoretical equations for calculating the multipath attenuation factor η^2 . For each receiving antenna we have a particular table, where the coordinates are transmitter height, h_t (vertical axis), and range, R (horizontal axis).

The height axis is divided into 36 "slices" with a 1 meter resolution, starting at a minimum height of 5 meters, and ending at a maximum of 40 meters. (These numbers are parameters, which can be changed easily.)

The range axis runs from 1 Km to 20.5 Km, and was originally divided into 130 equal steps of 50 meters each. Since the ambiguity for short ranges is very high, this partition caused some problems in finding the correct location for short ranges. This suggested the need for higher resolution at short range. The chosen partition is 130 steps of 50 meters each, up to the range of 7.5 Km, and then reduced resolution of 125 steps, 100 meter each, until the maximum range. (Again, all these numbers are parameters which can be changed.)

The multipath attenuation factor is calculated by using the following formulae:

The basic attenuation, η^2 , for a smooth sea case is [Ref. 3,9]:

$$\eta^2 = 4 \sin^2 \frac{2\pi h_t(h_t + h_r)}{\lambda \cdot R} \quad (\psi \rightarrow 0), \quad (5.1)$$

where: h_t is the transmitting antenna height,

h_r is the receiver antenna height,

λ is the signal wavelength,

R is the range between transmitter and receiver, and,

ψ is the grazing angle.

In the case of a rough sea, we have to multiply η^2 by the reflection coefficient, ρ , which is different in various models. In our case we used, as described in Chapter III, the Ament model:

$$\rho = \exp -2 \left(\frac{2\pi\sigma_h \sin \psi}{\lambda} \right)^2, \quad (5.2)$$

where: σ_h is the RMS deviation of the waves' height,

ψ is the grazing angle, and,

λ is the signal wavelength.

Therefore, in a rough sea case, the multipath attenuation factor will be:

$$\eta_{\text{rough sea}}^2 = \eta_{\text{smooth sea}}^2 \cdot \rho. \quad (5.3)$$

The grazing angle ψ in equation (5.2) is a derivative of the geometry. It depends on transmitter height, receiver height and range. Figure 5.1 shows the geometry from which we calculate ψ .

We shall now derive the grazing angle ψ [According to Ref. 7]. From Figure 5.1 we see that

$$R_d = \sqrt{(h_t - h_r)^2 + R^2}. \quad (5.4)$$

We define the range difference between the indirect path and the direct path as δ , where:

$$\delta = R_1 + R_2 - R_d. \quad (5.5)$$

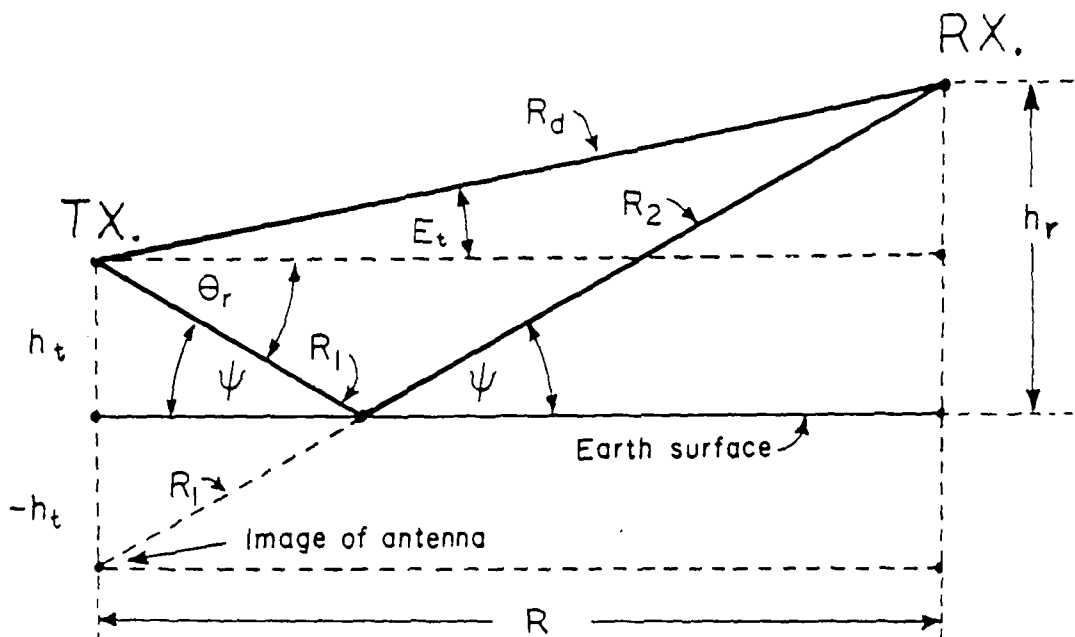


Figure 5.1: Flat Earth Multipath Geometry [From Ref. 7].

Looking at the image of the transmit antenna, we see that

$$R_1 + R_2 = \sqrt{(h_t + h_r)^2 + R^2}. \quad (5.6)$$

Substituting Equations (5.4) and (5.6) into Equation (5.5), we obtain:

$$\delta = \sqrt{(h_t + h_r)^2 + R^2} - \sqrt{(h_t - h_r)^2 + R^2}. \quad (5.7)$$

Let us assume that the range R is much greater than the antenna heights, and also $R^2 \gg (h_t + h_r)^2$. In this case, we can approximate Equations (5.4) and (5.6) as:

$$R_d = \sqrt{(h_t - h_r)^2 + R^2} \approx R \left[1 + \frac{(h_t + h_r)^2}{2R^2} \right], \quad (5.8)$$

and,

$$R_1 + R_2 = \sqrt{(h_r + h_t)^2} \approx R \left[1 + \frac{(h_t - h_r)^2}{2R^2} \right], \quad (5.9)$$

respectively.

Substituting Equations (5.8) and (5.9) into Equation (5.5), we obtain, after arranging:

$$\delta \approx \frac{(h_t + h_r)^2 - (h_t - h_r)^2}{2R} = \frac{2h_t h_r}{R}. \quad (5.10)$$

Observing again the imaged antenna, the angle θ_r is given by

$$\theta_r = \sin^{-1} \frac{h_t + h_r}{R_1 + R_2}, \quad (5.11)$$

and we notice that it equals (interchangeable angles) the grazing angle, ψ . Using Equation (5.5), we finally find the grazing angle to be:

$$\psi = \sin^{-1} \frac{h_t + h_r}{R_d + \delta}. \quad (5.12)$$

Since we know all the parameters from solving previous equations, we can now find ψ . (Actually, we do not know the range R , but we should remember that in this step we are building tables, so the range is being used as a parameter.)

The only variable still missing for solving Equation (5.2), (the reflection coefficient), is the wave height RMS deviation σ_h . This value depends on the sea state, and is given in tables in the literature. Table 3.1 shows this parameter (as well as some others), as a function of sea state.

The propagation attenuation factor ($\frac{1}{4\pi R^2}$ in the one way case) also has its impact on the received signal. Since we deal with ratios, this factor cancels itself, and therefore had not been taken into account during the calculations.

c. Attenuation Coefficient Ratio Tables (η_i^2/η_j^2):

Having created the different tables for each antenna, we now create a new set of tables, which contain the ratios of the received signal amplitudes for the antenna pairs. For three receiving antennas we get two tables, while for N receiving antennas there will be $N - 1$ tables.

Figure 5.2 shows graphs of the ratio table data for sea state zero, at 9 GHz and a transmitter height of 20 meters. Note that for clarity only one “slice” is shown, referred to the particular transmitter height. The table is actually three-dimensional (range, transmitter height, and amplitude ratio).

d. Amplitude Measurement:

The first and major assumption is that all the receiving channels are calibrated. In this case, two similar signal amplitudes at the input to different channels will create the same amplitude at the outputs of those channels.

Actually, there is no need for single channel amplitude measurements, since we deal with ratios. For this reason, we measure the individual signal amplitudes and immediately divide between pairs to form the desired ratios.

e. Comparison:

We now have in hand all the details needed to find the correct location of the transmitter, assuming of course, that the model is accurate.

A comparison is made among the ratio levels from steps c and d. Every place that both levels are the same, is “marked down” by a “candidate location flag.” Figure 5.3 shows the received signal ratios (constant level line) and the corresponding candidate location flags, for four antenna pairs.

Again, we should remember that the real comparison is being made between many more points, since there is a third dimension (height). For simplicity, we show here only one of 36 height slices.

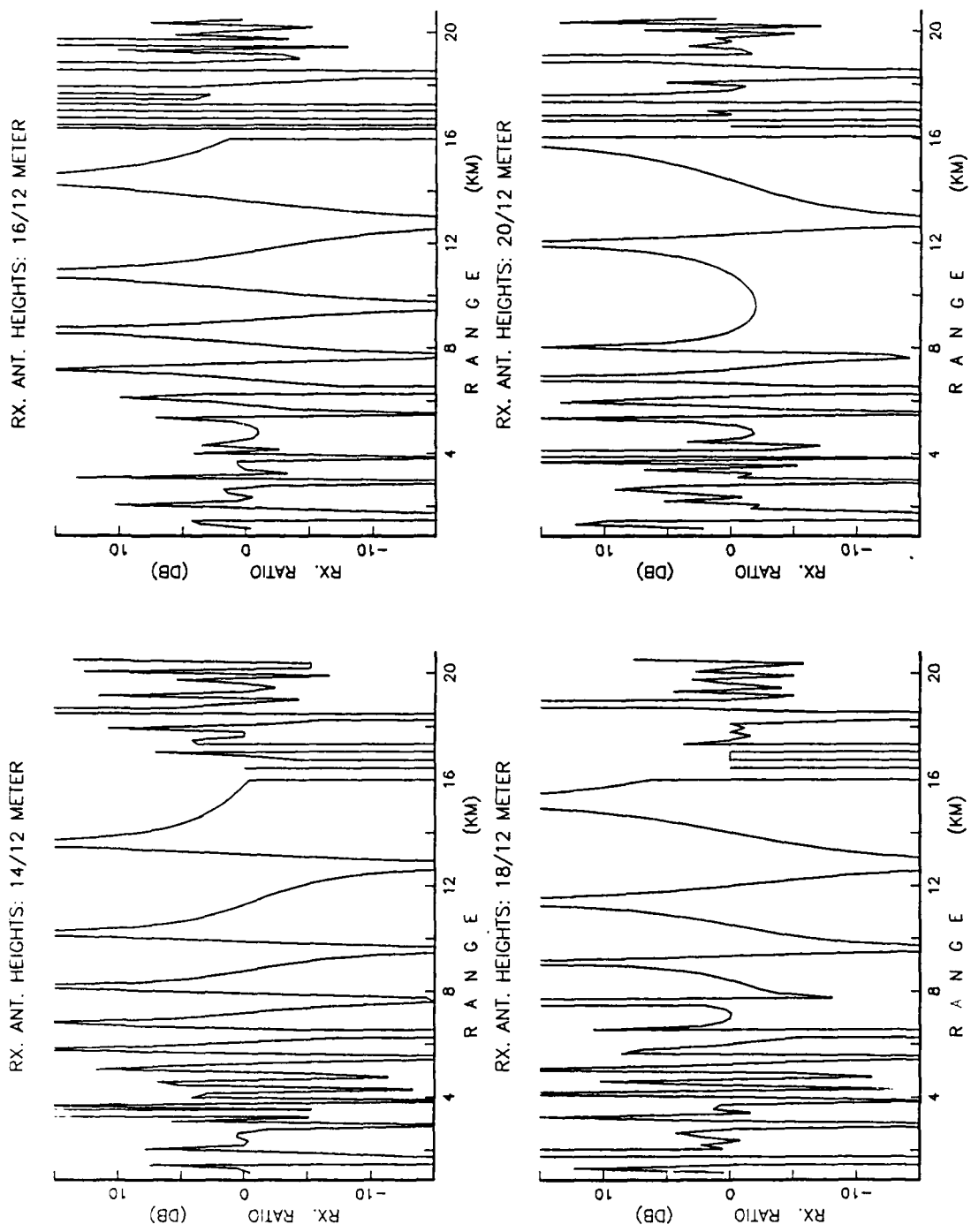


Figure 5.2: Attenuation Coefficient Ratio.

The dots in Figure 5.3 (upper portion) represent the real calculated values, while the connecting curves are made by extrapolation. Therefore, a candidate location flag is set only when the measured signal ratio is within a specified distance from the calculated signal ratio. This distance is determined by the width of a comparison window which is a software parameter. The wider the window, the more candidate location flags we will set. On the other hand, we cannot allow too narrow a window, since there is a risk of losing correct locations. It is obvious that as we use higher resolution in the lookup table, we can also narrow the comparison window.

Figure 5.4 shows the candidate location flags for the same scenario as in Figure 5.3, but with a wider comparison window. Notice that more flags appear in this case.

For a higher sea state, there are random fluctuations in signal level, and the comparison becomes harder. We must open the window wider, but at the same time more incorrect locations are flagged. A practical compromise is required.

f. Validation:

After we have all of the candidate location flags, we need to decide which location is correct. The method of doing this is by doing a cross location: comparing between all the flags, and checking which one repeats in all of the ratios.

If after this process there is more than a single location (more than only one cross location), the measurement cannot give a correct location, so we discard it, and start a new session.

Practically, using three receiving antennas (two ratios) gives no single location in most cases, and therefore we need to add more antennas in order to have more ratios. During the experiments we tried using different numbers of antennas, and the final sufficient result uses five receiving antennas.

Figure 5.5 shows the candidate location flags for each antenna pair and the crossing between them, giving a single valid location marked by a diamond. The sea state is zero, and the window width is 2.5%. Here, we can see not only a single "slice", but the whole combination of range and height. From this it is obvious that a single pair of antennas gives no information at all (too many candidate location flags).

For the case of three antennas, (see Figure 5.6), the ambiguity is reduced significantly (only two flags overlapping), while adding a fourth antenna, reduces the location to a single, correct one. In this particular case, four receiving antennas give the correct location. In many cases, though, four antennas will still leave some order of ambiguity, but the fifth one will, in most cases, give a correct, single location.

The ambiguity level reduction as a function of number of receiving antennas is well illustrated in Figure 5.6, for sea state zero.

For a wider window there will be more flags, as shown in Figure 5.7, and here we can see that only the fifth antenna solves the ambiguity.

When the sea state is higher, a wide window will lead to a large level of ambiguity. Figure 5.8 shows a 12% window in sea state 3, where there are four locations. Reducing the width to 5% will reduce the number of locations to two, as shown in Figure 5.9, while the ambiguity will totally disappear for a 2.5% window, as in Figure 5.10.

g. Output:

The previous step brought up a single location flag, which shows the correct location of the transmitter in the range-height table. The output step translates the table location into the real coordinates of range and height, and types it as an output result.

C. FINAL RESULTS

As mentioned earlier in this chapter, the final resolution used here, is 130 steps of 50 meters each, from the minimum range up to 7.5 Km, and then 125 steps of 100 meters each to the maximum range. The comparison window width is 2.5%.

With these parameters, estimation results are given in Figures 5.11 and 5.12, for sea states 0 and 3, respectively. It should be mentioned that the estimated range sometimes deviates from the actual range by a few tens of meters, which cannot be seen in the graph, due to resolution.

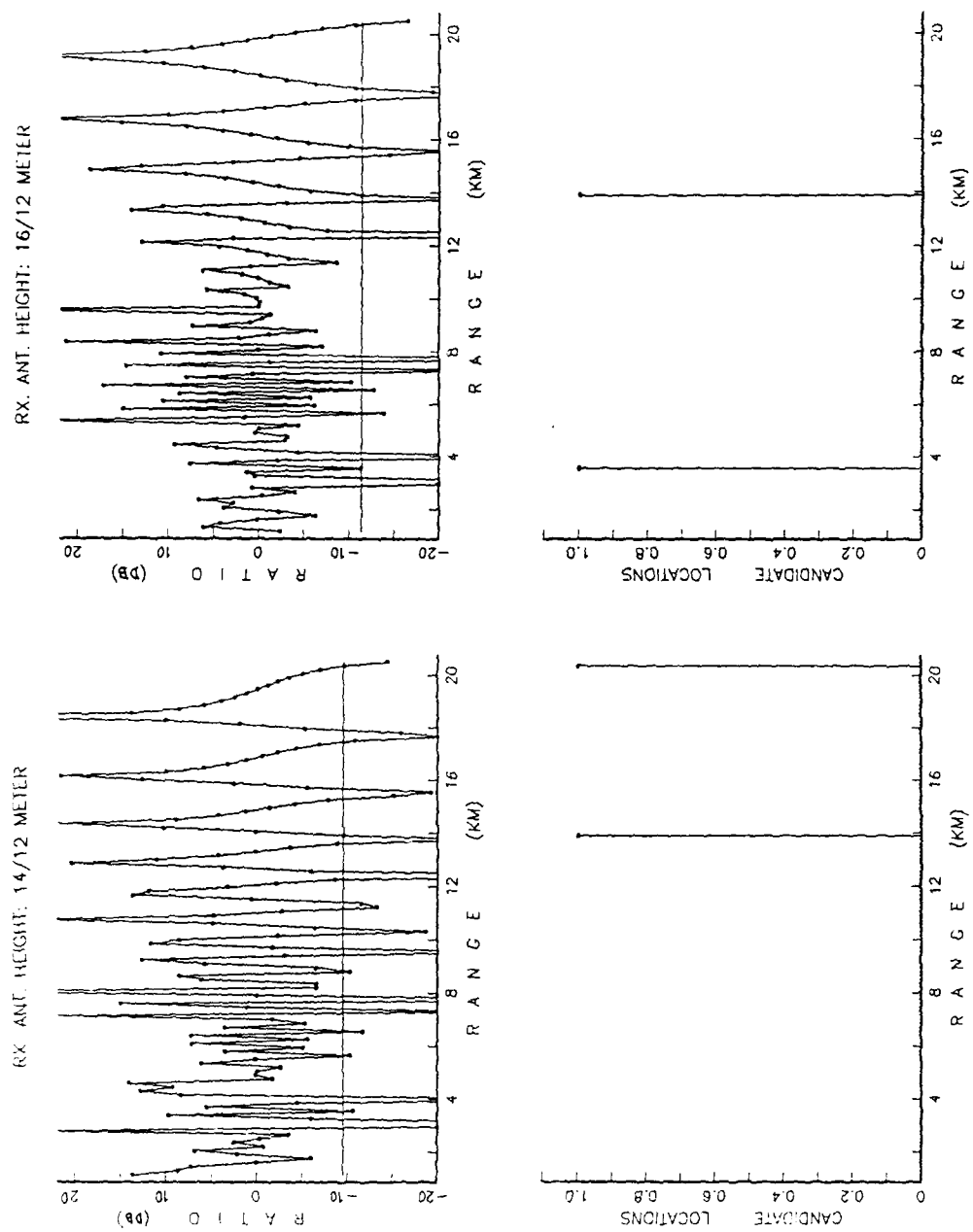


Figure 5.3: Comparison Process with 2.5% Window.

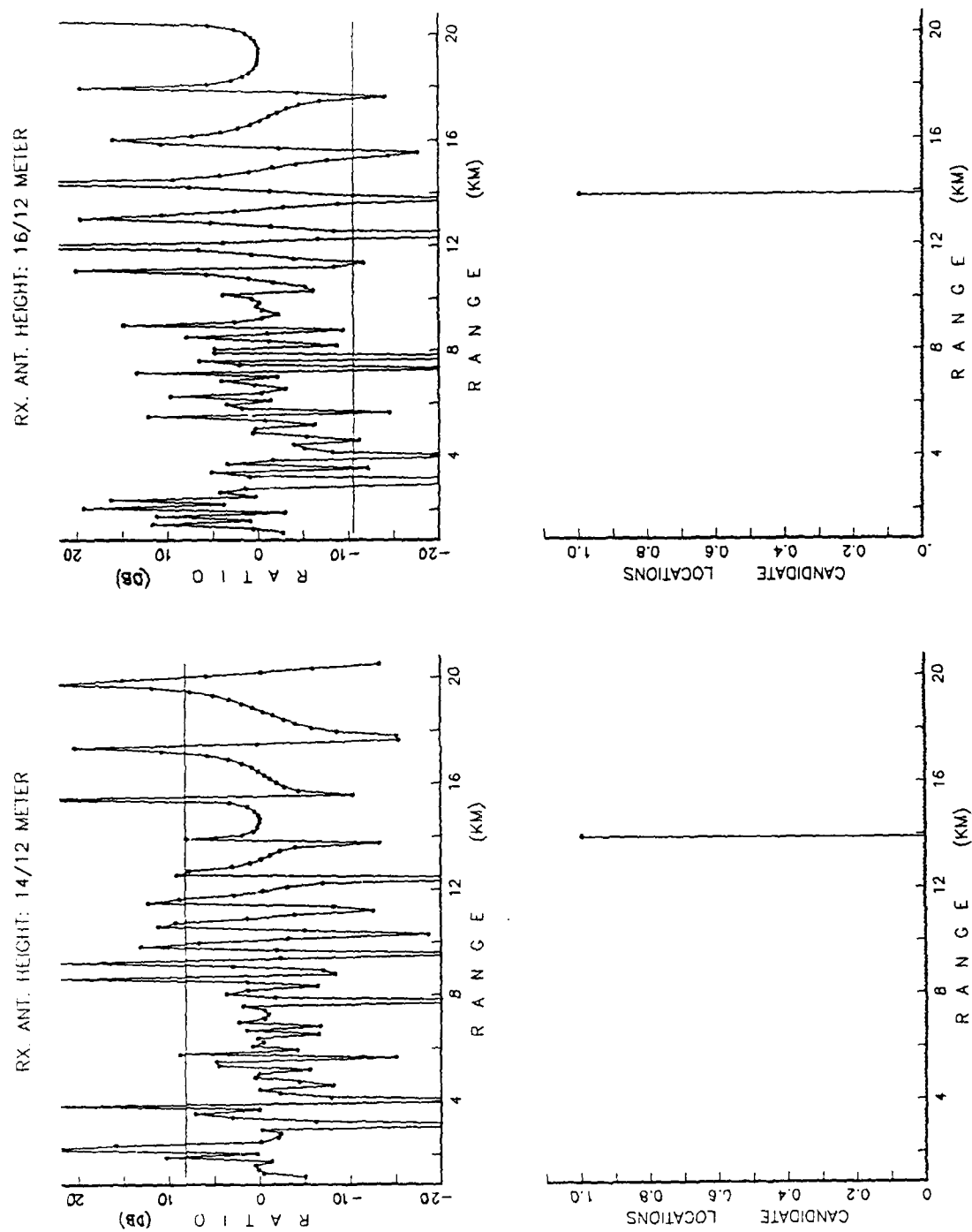


Figure 5.3 (continued): Comparison Process with 2.5% Window.

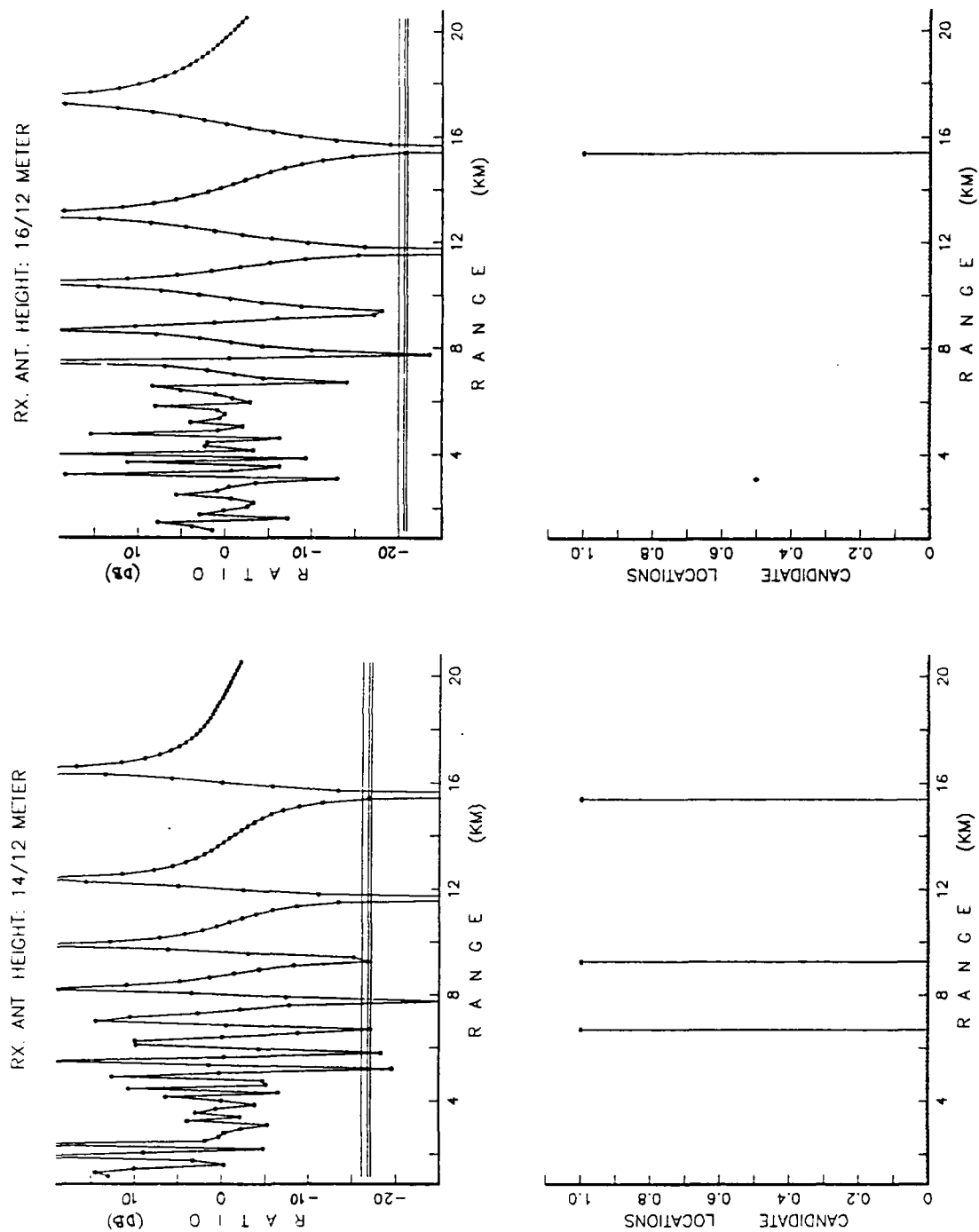


Figure 5.4: Comparison Process with 12% Window.

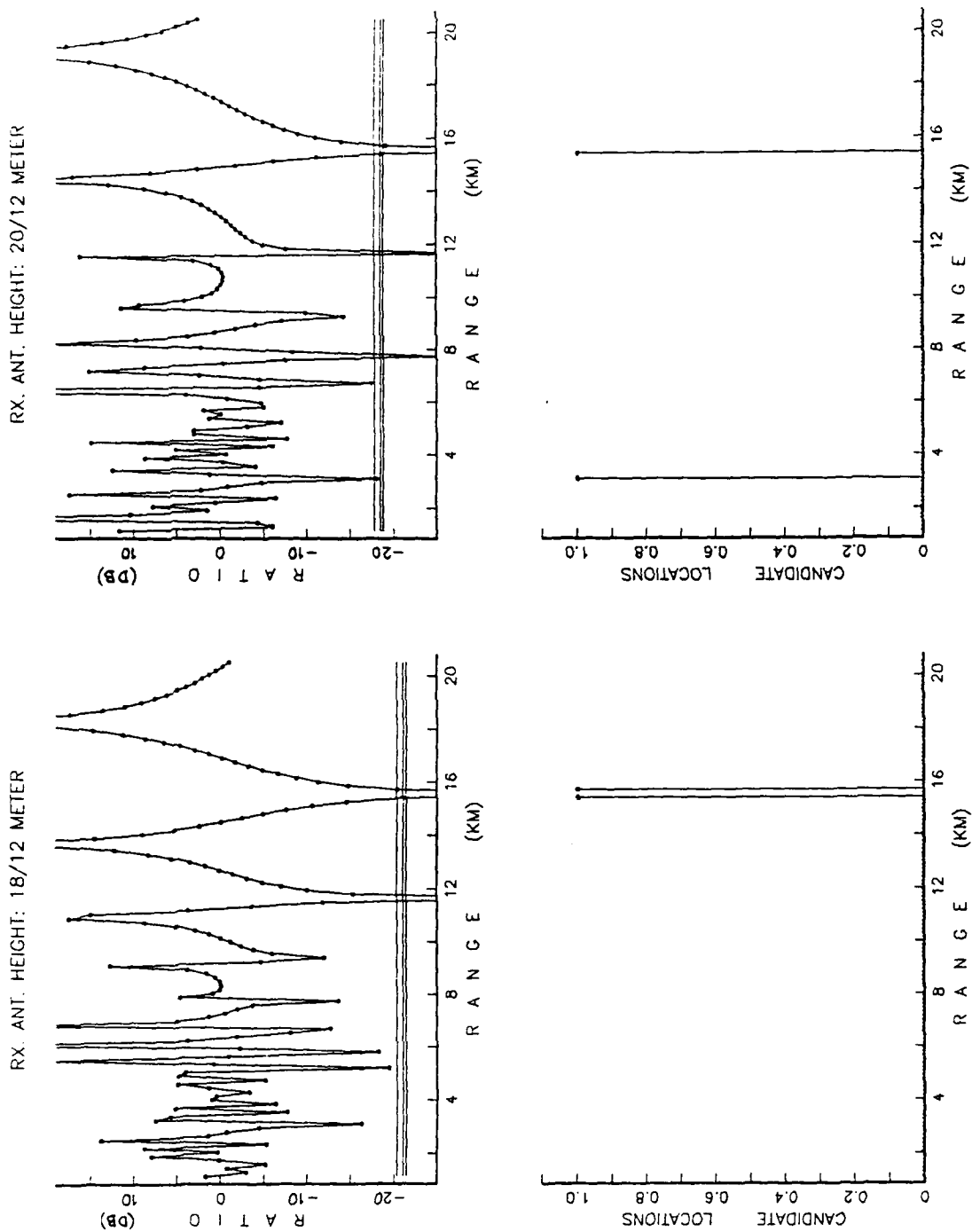


Figure 5.4 (continued): Comparison Process with 12% Window.

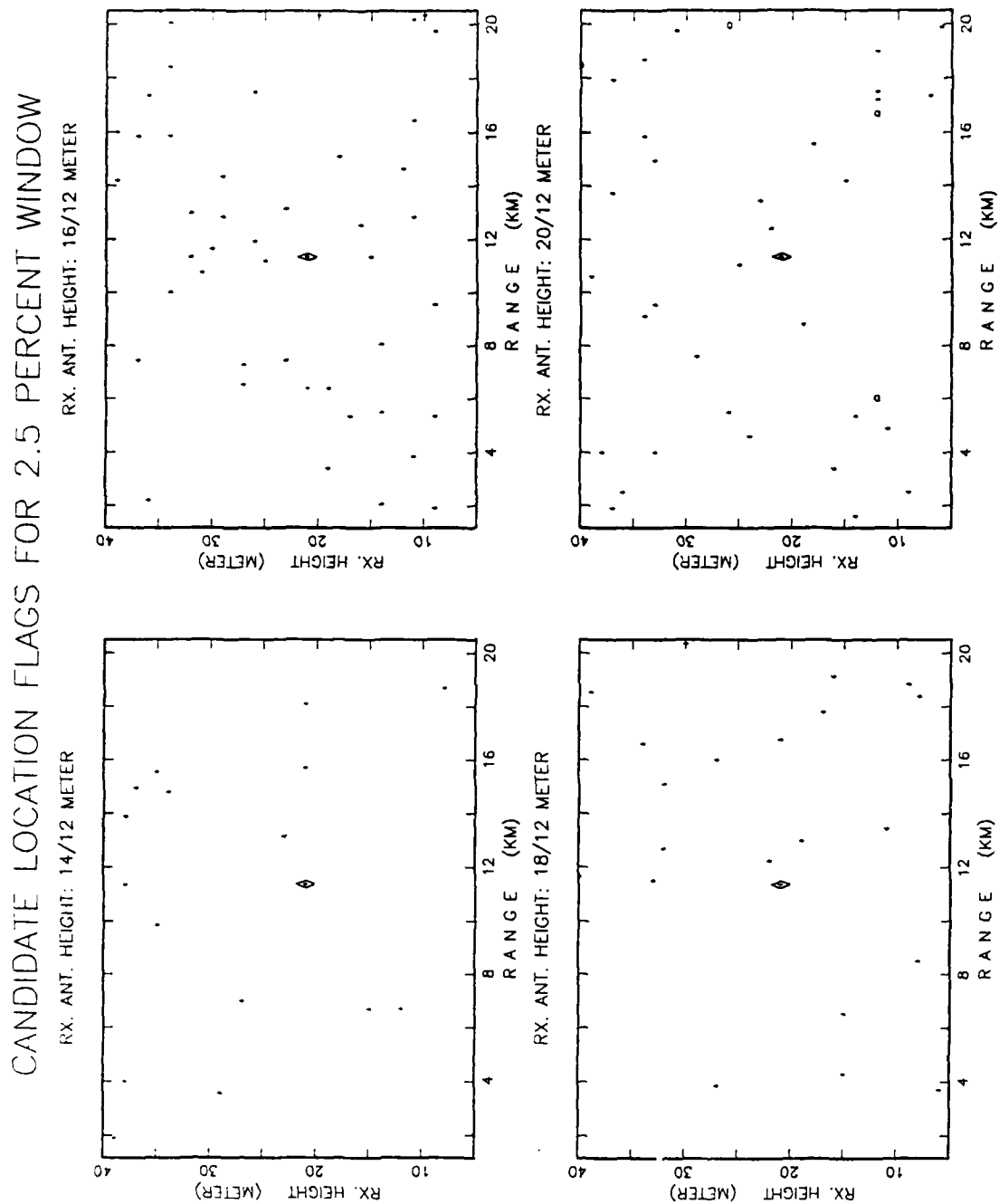


Figure 5.5: Validation Process. Correct Location Marked by a Diamond.

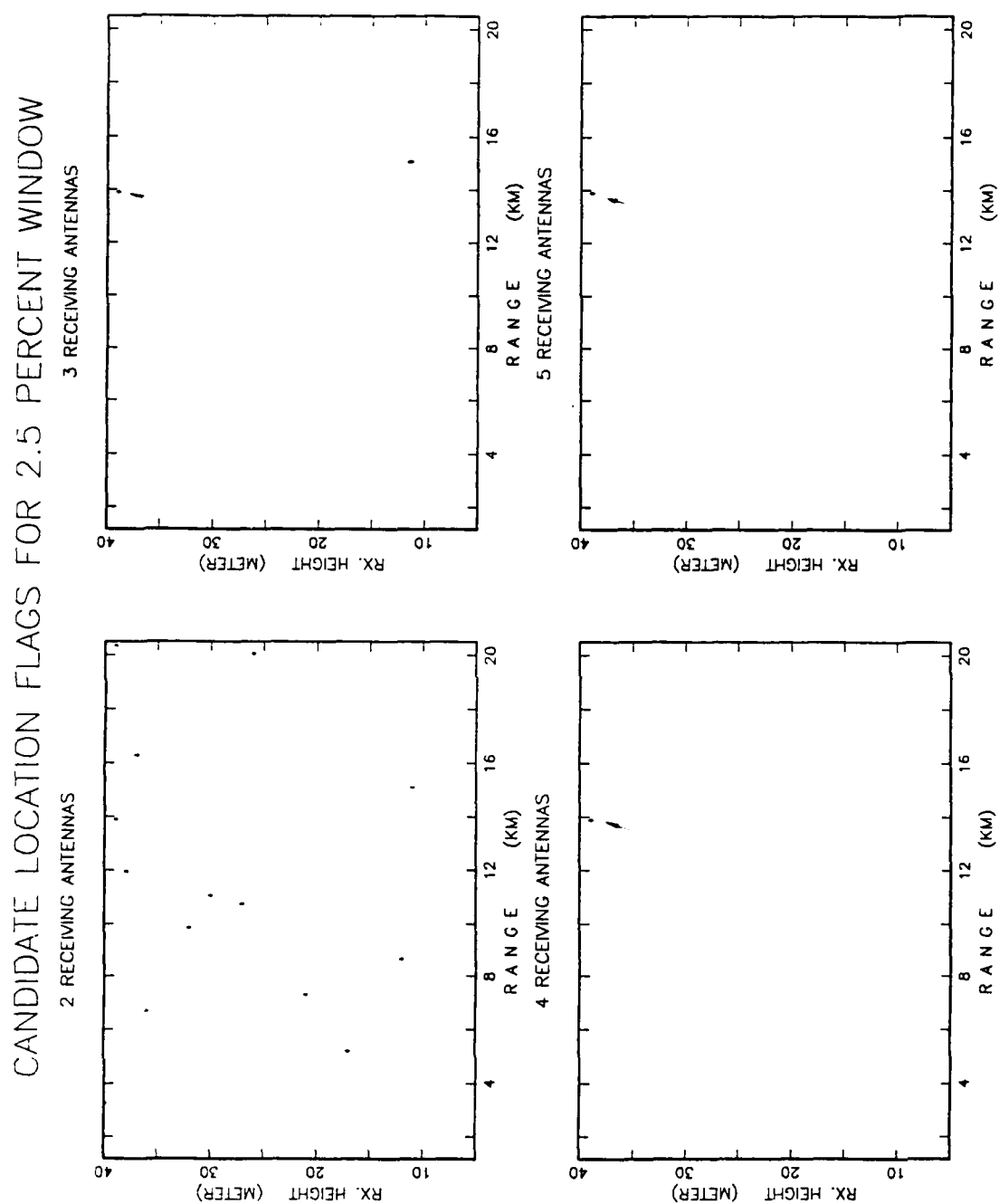


Figure 5.6: Ambiguity Level vs. Number of Receiving Antennas; Sea State 0 and 2.5% Window.

VALIDATED LOCATION FLAGS FOR 12 PERCENT WINDOW

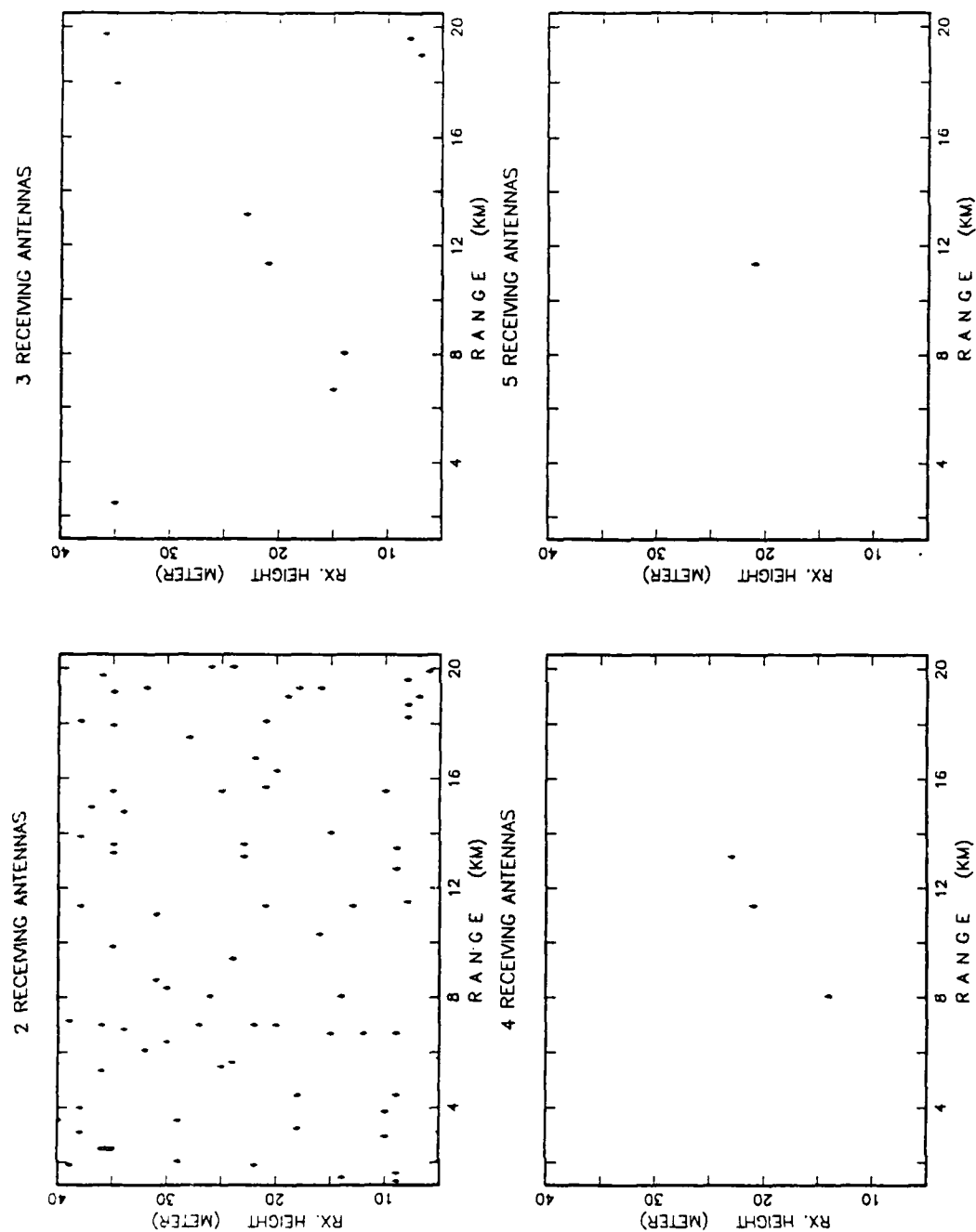


Figure 5.7: Ambiguity Level vs. Number of Receiving Antennas; Sea State 0 and 12% Window.

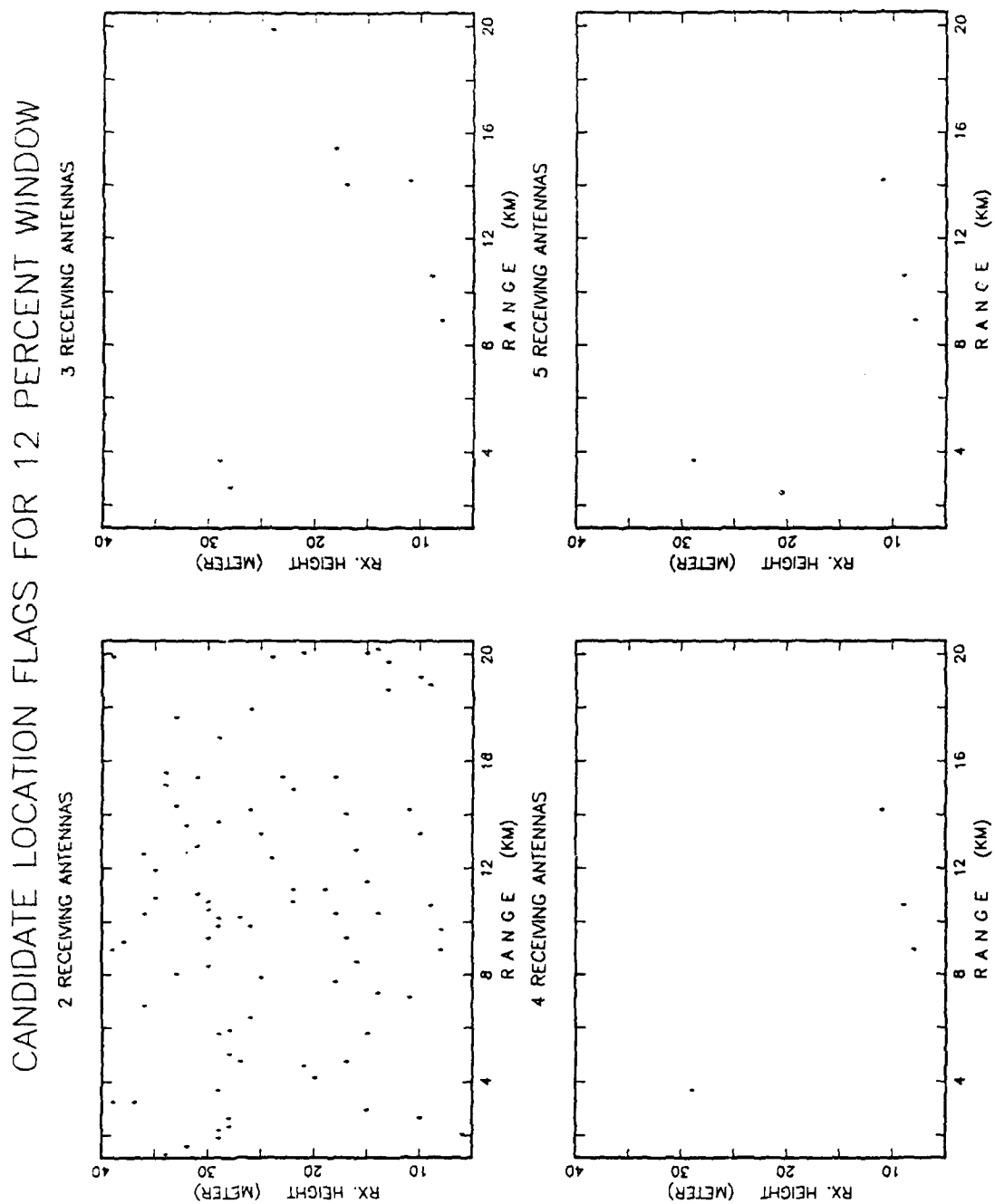


Figure 5.8: Ambiguity Level vs. Number of Receiving Antennas; Sea State 3 and 12% Window.

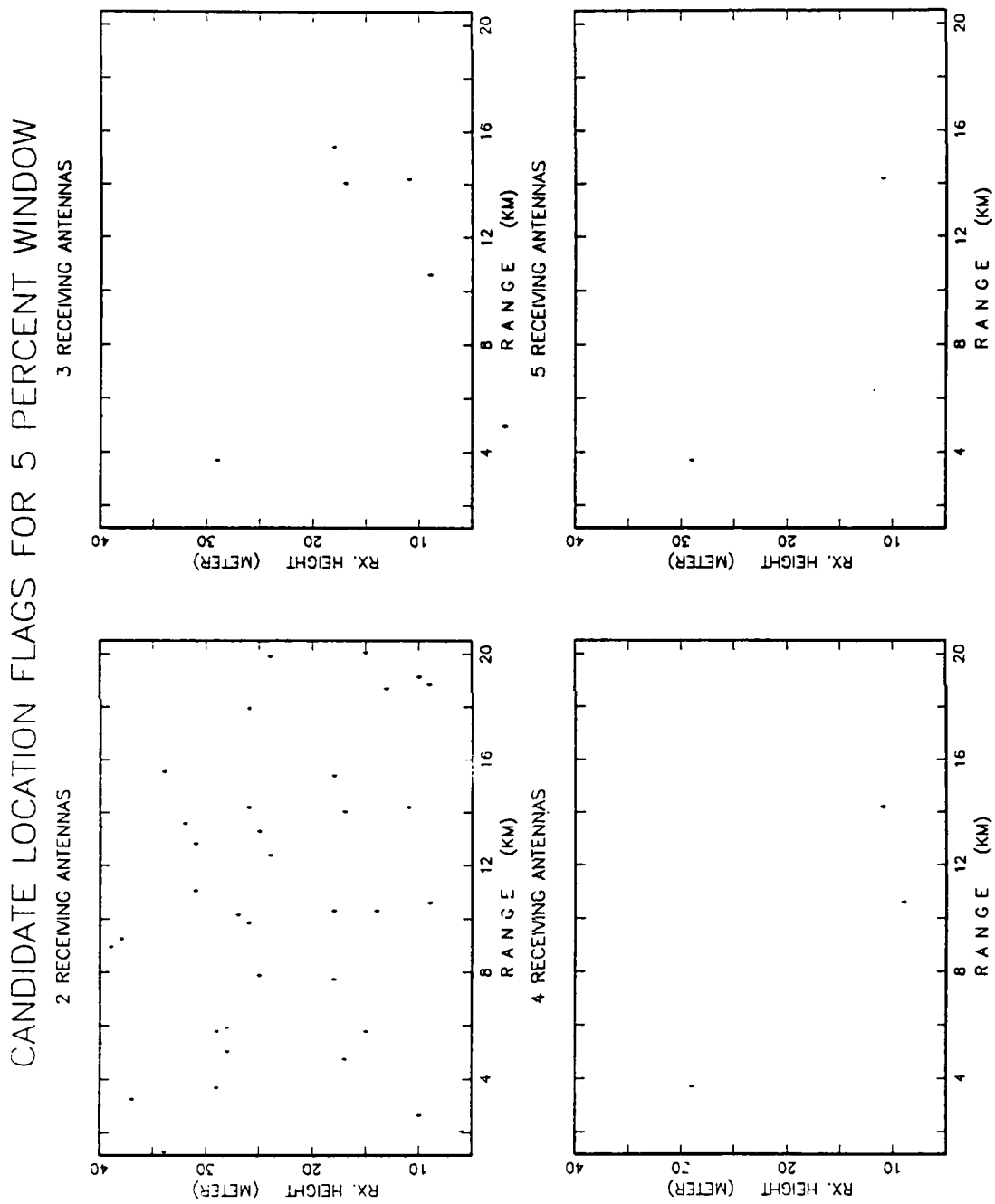


Figure 5.9: Ambiguity Level vs. Number of Receiving Antennas; Sea State 3 and 5% Window.

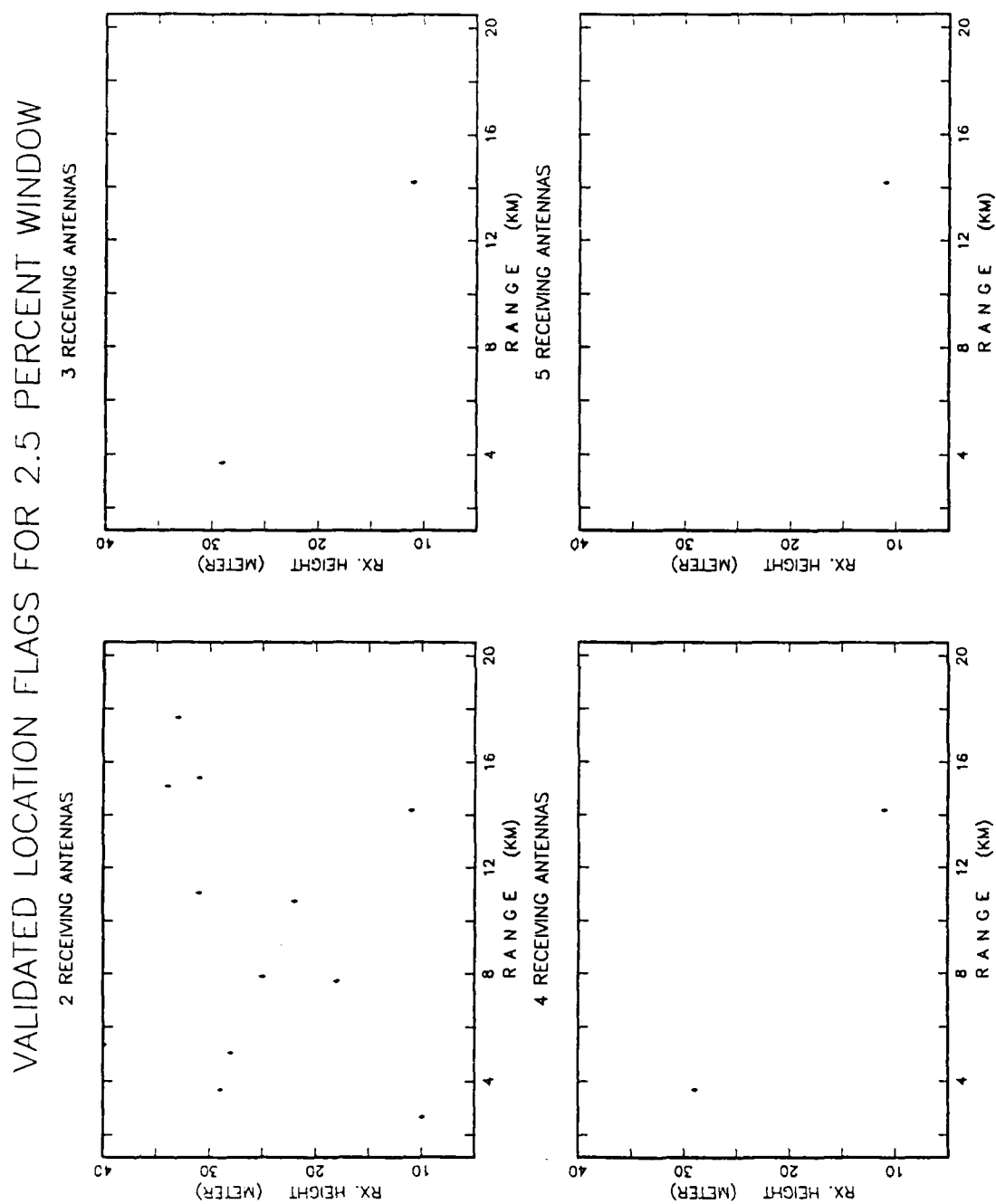


Figure 5.10: Ambiguity Level vs. Number of Receiving Antennas; Sea State 3 and 2.5% Window.

ESTIMATED VERSUS ACTUAL RANGE - SEA STATE 0

SOLID LINE - ACTUAL ; DOTS - ESTIMATED

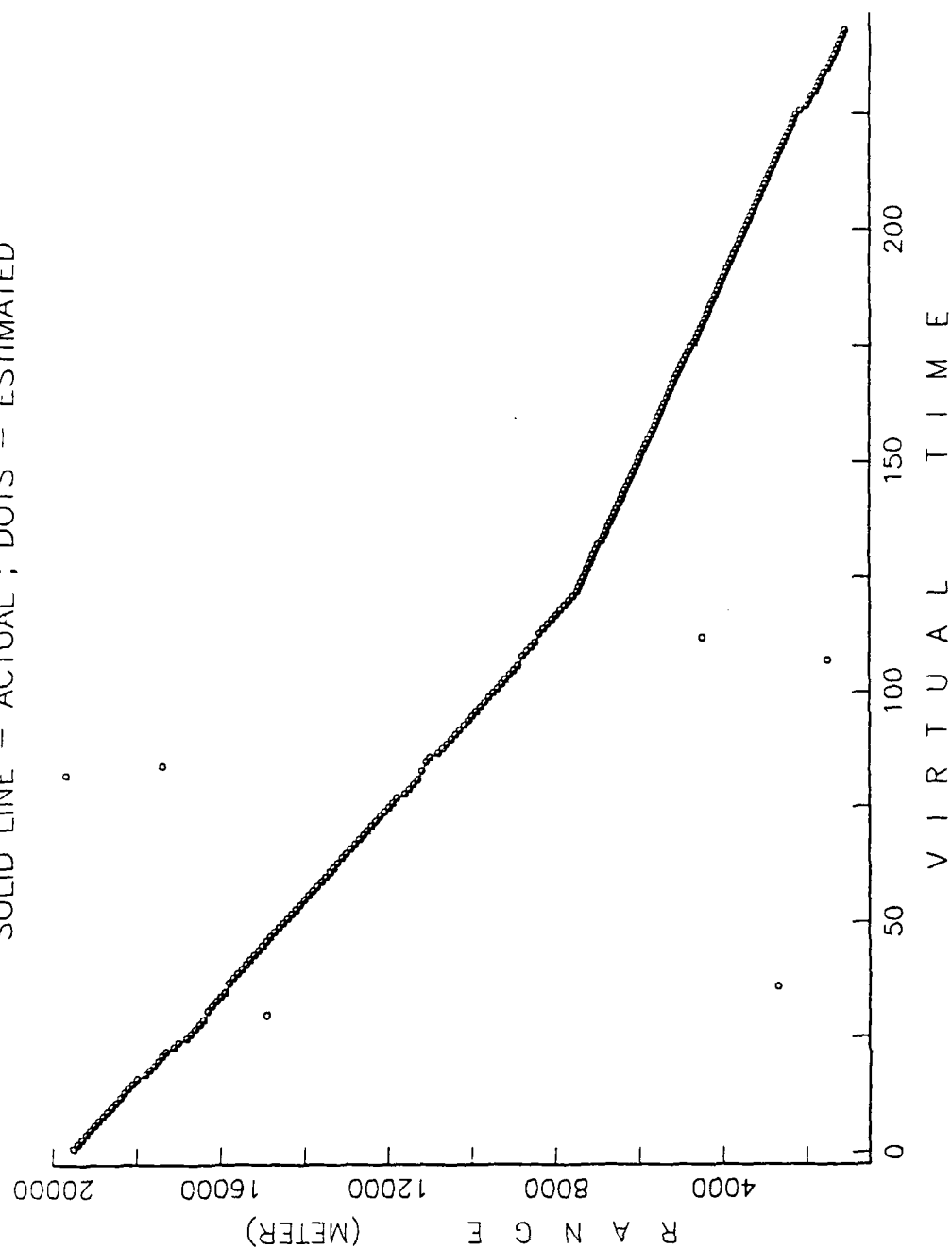


Figure 5.11: Estimated Results (Range); Sea State 0.

ESTIMATED VERSUS ACTUAL HEIGHT -- SEA STATE 0

SOLID LINE -- ACTUAL ; DOTS -- ESTIMATED

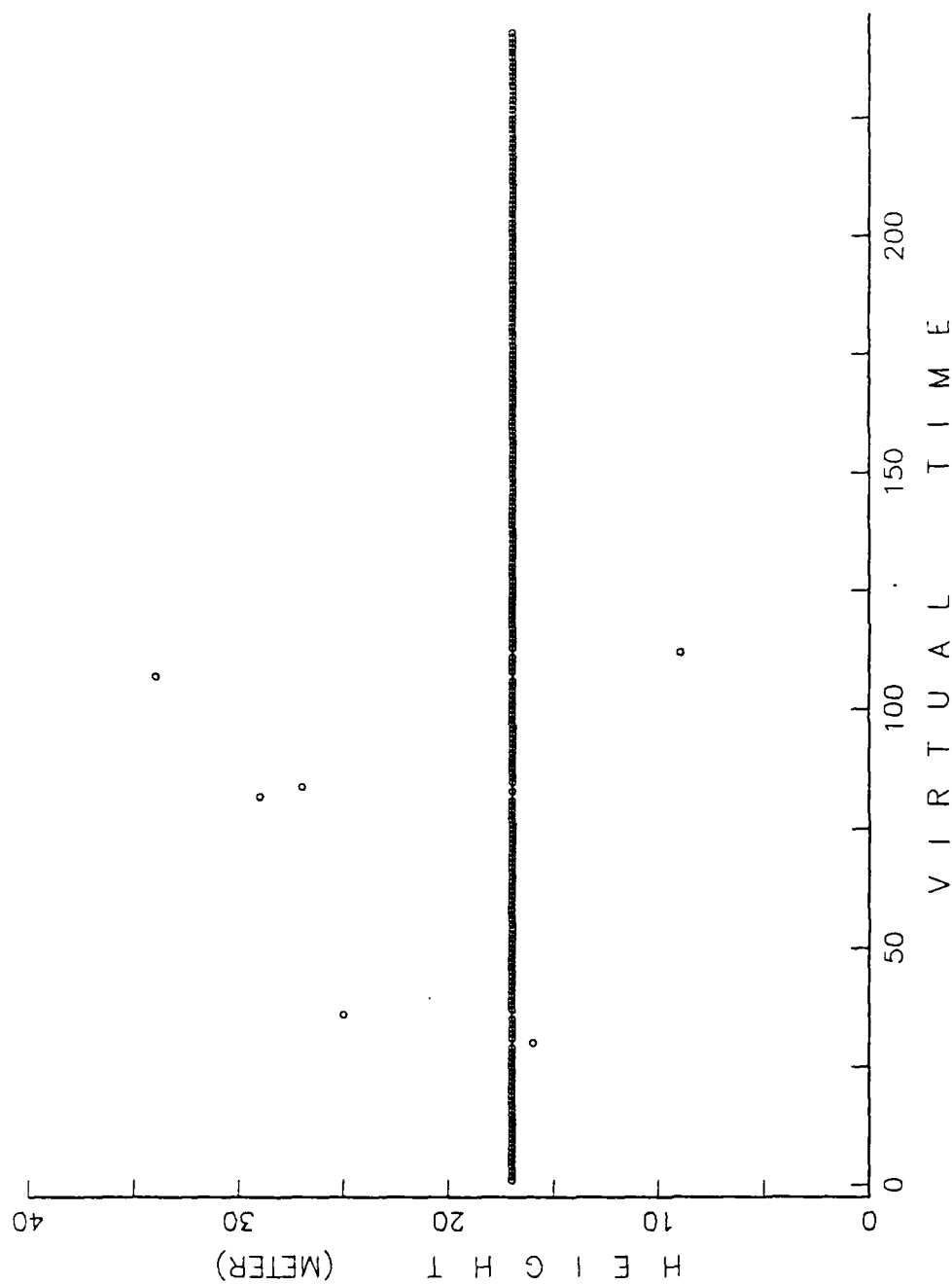


Figure 5.11 (continued): Estimated Results (Height); Sea State 0.

ESTIMATED VERSUS ACTUAL RANGE - SEA STATE 3

SOLID LINE - ACTUAL ; DOTS - ESTIMATED

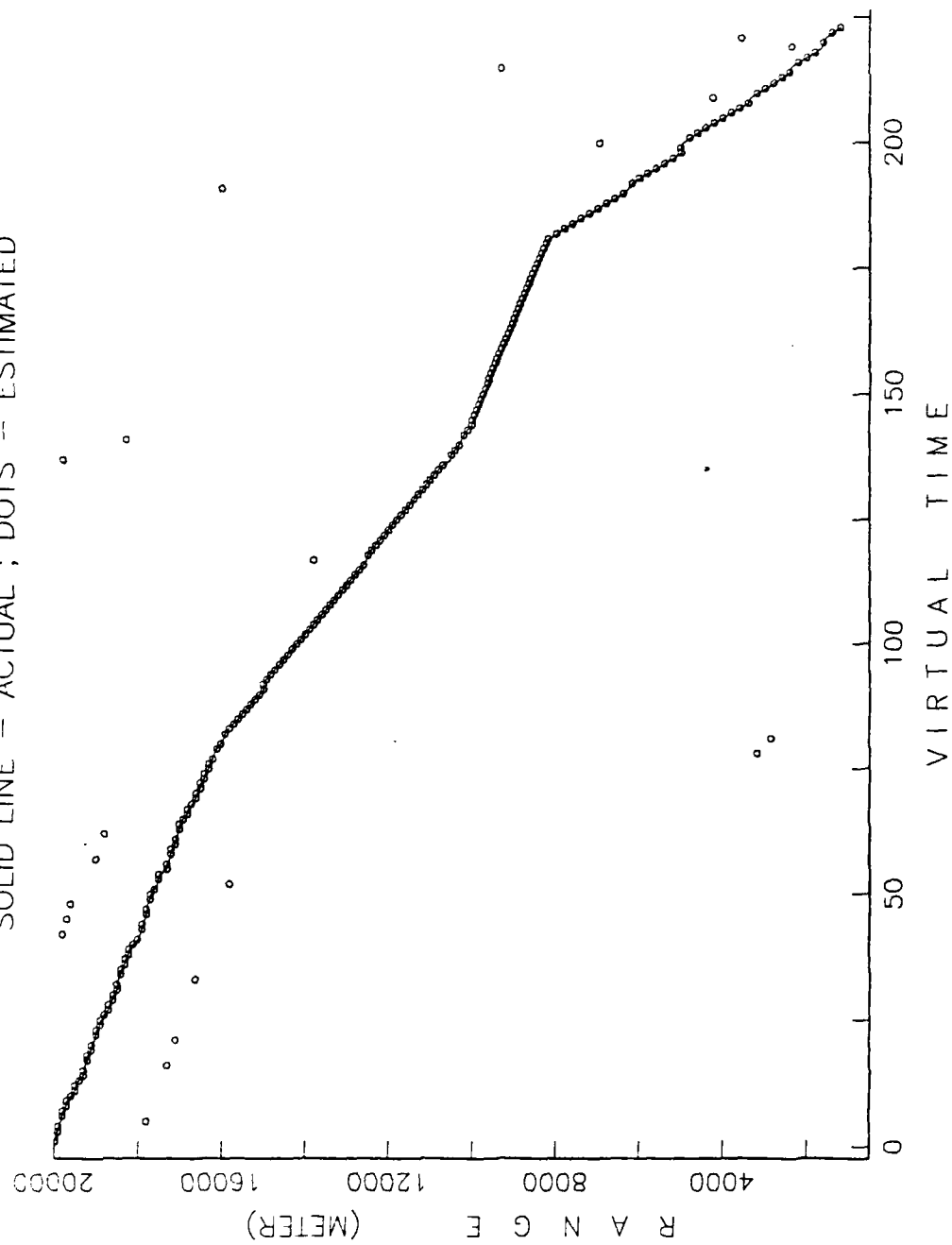


Figure 5.12: Estimated Results (Range); Sea State 3.

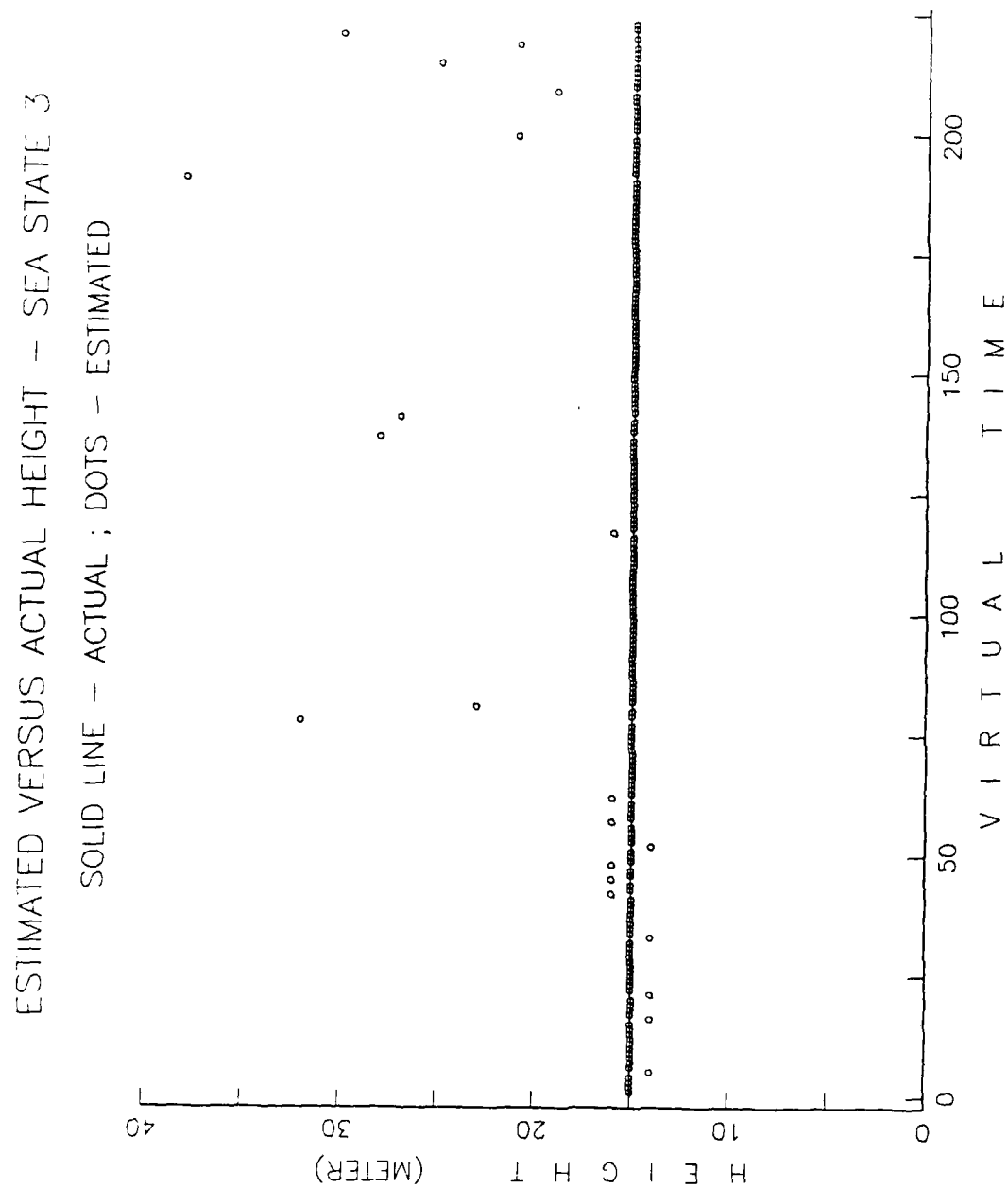


Figure 5.12 (continued): Estimated Results (Height); Sea State 3.

VI. ADDITIONAL PARAMETERS CONSIDERATION

This chapter deals with some parameters that have influence on the calculations and terms used for the estimation process. A few of them were mentioned but not discussed for all cases, and the others were not discussed previously.

A. VERTICAL POLARIZATION

So far we dealt with horizontal polarization, and all the calculations were done for this polarization. Vertical polarization complicates the problem a bit, since the reflection coefficient, ρ , changes significantly with the grazing angle, as shown in Figure 3.4.

Let us check some representative cases in order to see how much the reflection coefficient really changes due to vertical polarization.

Case 1: transmitter is located 10 Km apart from the receiver, at a height of 10 m, and it transmits with a frequency of 10 GHz. The receiver antennas are at heights of 12 m and 20 m. So, our case has the parameters:

$$R = 10 \text{ km},$$

$$h_t = 10 \text{ m},$$

$$f = 10 \text{ GHz } (\lambda = 3 \text{ cm}),$$

$$h_{r1} = 12 \text{ m, and,}$$

$$h_{r2} = 20 \text{ m.}$$

Using equations (5.4) to (5.12), we find that the grazing angles are equal to: $\psi_1 = 0.126^\circ$, and $\psi_2 = 0.172^\circ$, respectively for the receiving antenna heights.

Using the correct graph, (Figure 3.4), we find that the reflection coefficient due to the reflection, equals 0.98 for both grazing angles.

Case 2: in the second case the transmitter is higher, and the range between the receiver to the transmitter is reduced:

$$R = 4 \text{ km},$$

$$h_t = 40 \text{ m},$$

$$f = 10 \text{ GHz } (\lambda = 3 \text{ cm}),$$

$$h_{r1} = 12 \text{ m}, \text{ and},$$

$$h_{r2} = 20 \text{ m}.$$

Using the same method as in the first case, we find here, that the reflection coefficient for the lower receiving antenna is 0.82, while for the higher antenna it is 0.80.

Case 3: here we take an extreme case of very high transmitter, as well as receiver antennas:

$$R = 4 \text{ km},$$

$$h_t = 100 \text{ m},$$

$$f = 10 \text{ GHz } (\lambda = 3 \text{ cm}),$$

$$h_{r1} = 38 \text{ m}, \text{ and},$$

$$h_{r2} = 50 \text{ m}.$$

In this case, the reflection coefficients are 0.58 for the 38 m receiving antenna, and 0.55 for the 50 m antenna.

We can conclude that for low geometry (transmitter and receiver), and large ranges, the reflection coefficient can be assumed the same for all receiving antennas. For shorter ranges and larger heights, we should take into account the changes in the reflection coefficient for the different receiving antennas.

Practically, for the vertical polarization case, we need to modify the off line tables by the amount of the reflection coefficient changes. This can be done, since we know how to calculate it with the given parameters, and for the whole range and transmitter height field. The only parameter that has doubt is the kind of polarization. This verification must be done by another system, and provided as an input to the estimation process.

B. RECEIVER HEIGHT

As we saw in Chapter 4, the higher the receiver antenna is, the more complex the curve is. In our work we used a maximum receiving antenna height of 20 meters, since it is a reasonable height for a conventional missile boat. For a larger ship (such as a corvette or destroyer, for example), we shall need higher receiving antennas. The only influence, as mentioned before, is on the curves complexity. The solution for this is to use a greater resolution in the look up tables, to compensate for the higher ambiguity.

C. SHIP TILTING

For the ships of our interest (relatively small missile boats), the worst case rolling angle can be around 15° for cross wind cruising direction in sea state 3. For sea state 4, the extreme angle is about 20° for the same conditions. Since the tilt occurs for both sides, we can say that, to a first degree of approximation, the average tilt is 0° . Even though, let us check the worst case. The geometry of the problem is given in Figure 6.1. We will now check the tilt impact on the look up tables for two cases: the closest antennas (12 meters and 14 meters), and the extreme antennas (12 meters and 20 meters).

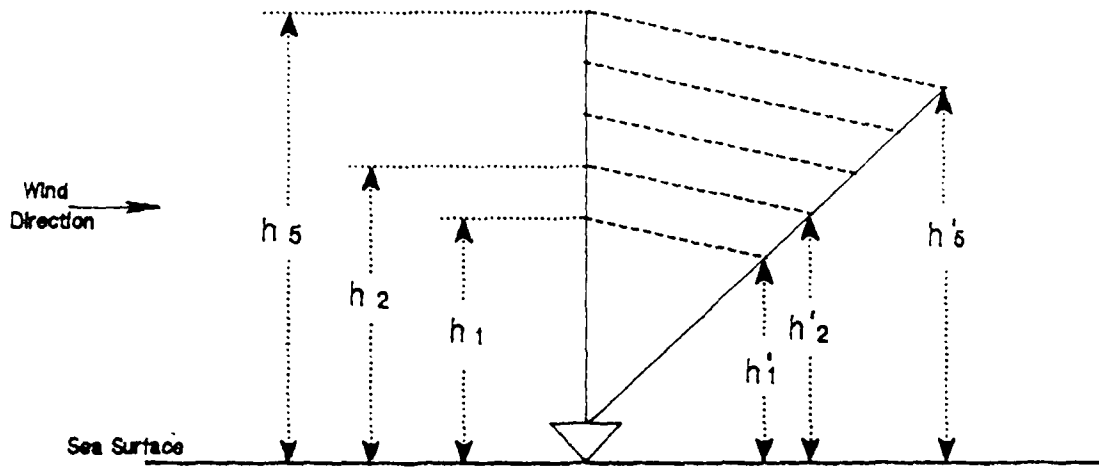


Figure 6.1: Tilted Ship Geometry.

Referring to Figure 6.1, in our case, $h_1 = 12$ m, $h_2 = 14$ m and $h_5 = 20$ m. The maximum tilt (roll) angle, α_{\max} , is taken as 15° for sea state 3, and 20° for sea state 4.

From Figure 6.1 we see that the actual height of each receiving antenna, after being tilted, is:

$$h'_i = h_i \cdot \cos \alpha \quad (i = 1, 2, \dots, 5). \quad (6.1)$$

For sea state 3 ($\alpha_{\max} = 15^\circ$), we obtain:

$$h'_1 = 12 \cdot \cos 15^\circ = 11.6 \text{ m} \quad (\text{where } h_1 = 12 \text{ m}), \quad (6.2)$$

and

$$h'_5 = 20 \cdot \cos 15^\circ = 19.3 \text{ m} \quad (\text{where } h_5 = 20 \text{ m}). \quad (6.3)$$

The actual distance between the antennas is 7.7 meters, instead of a theoretical value of 8 m. Figure 6.2 shows the ratio η_5^2/η_1^2 for receiving antennas located perpendicular to the sea level, in heights of 20 meter and 12 meter, respectively.

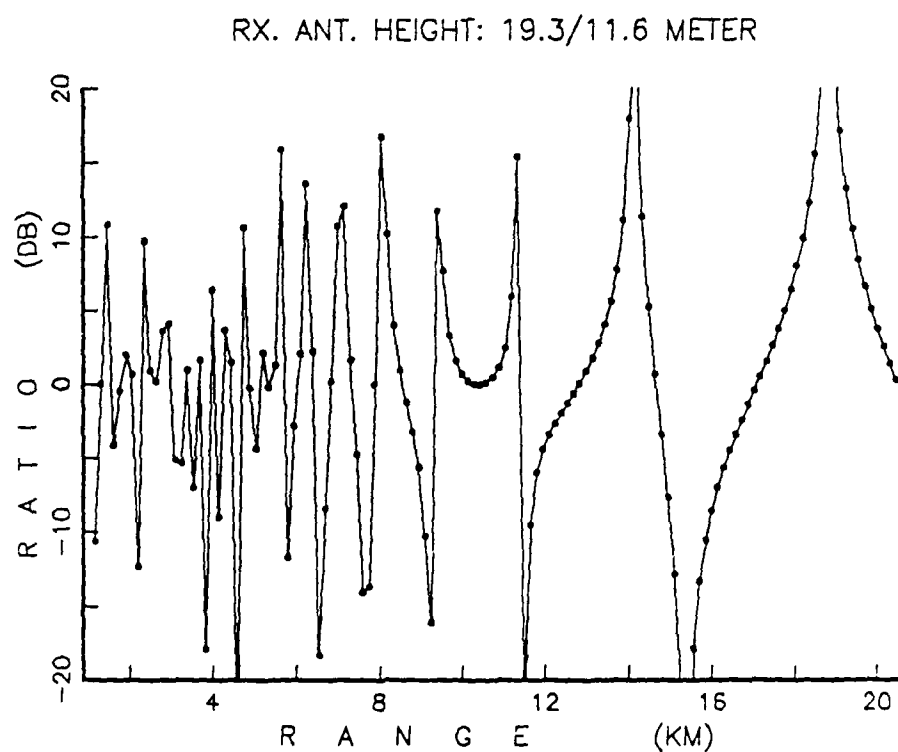
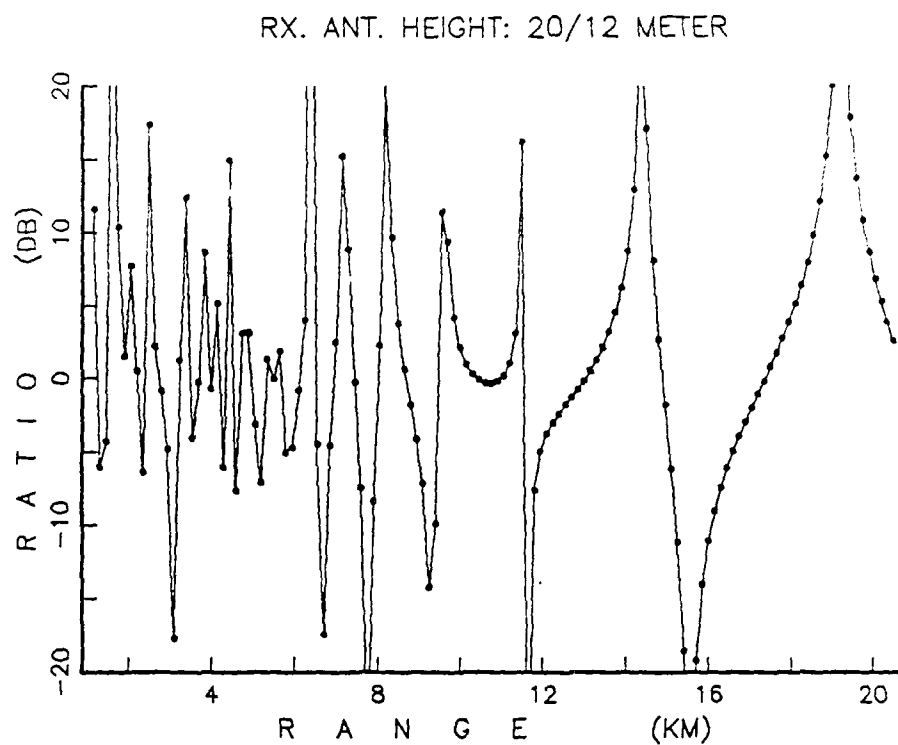


Figure 6.2: Ratio Between Attenuation Coefficients; Sea State 3, Receiving Antennas at 12 m and 20 m.

On the same figure we see also $(\eta_5^2/\eta_1^2)'/(\eta_1^2)'$ for the tilted case. Figure 6.3 shows the ratio between those ratios:

$$((\eta_5^2/\eta_1^2)|_{8m}) / ((\eta_5^2/\eta_1^2)|_{7.7m}).$$

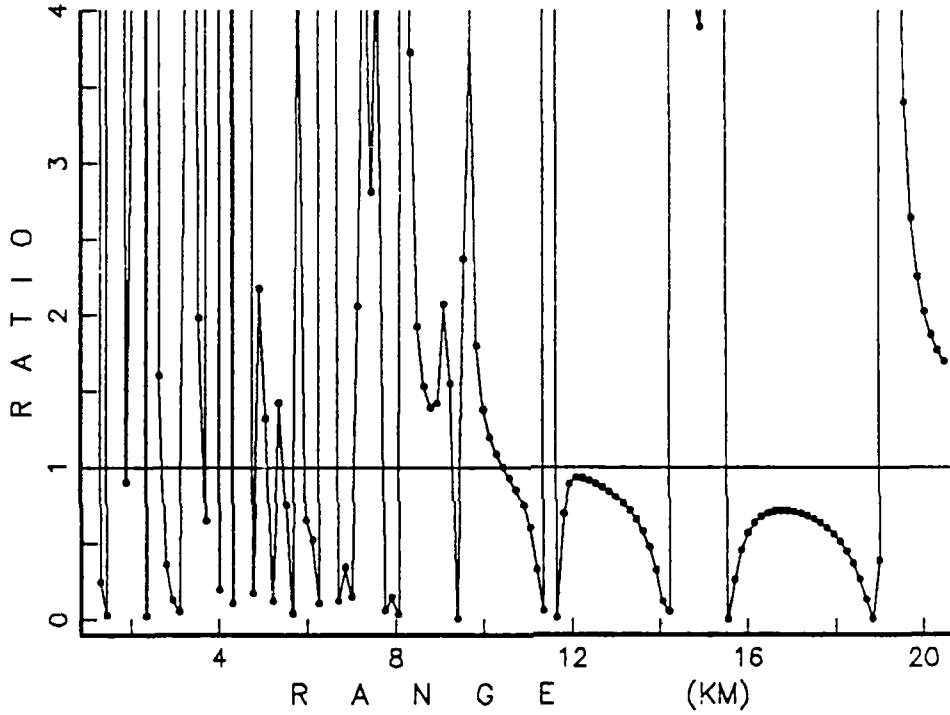


Figure 6.3: Ratio Between Ratios of Attenuation Coefficients; Sea State 3, Receiving Antennas at 12 m and 20 m.

Now we will repeat the calculations for receiving antennas at heights of 14 meters and 12 meters. Note that h'_1 remains the same (11.6 m), while h'_2 becomes:

$$h'_2 = 14 \cdot \cos 15^\circ = 13.5 \text{ m} \quad (\text{where } h_2 = 14 \text{ m}). \quad (6.4)$$

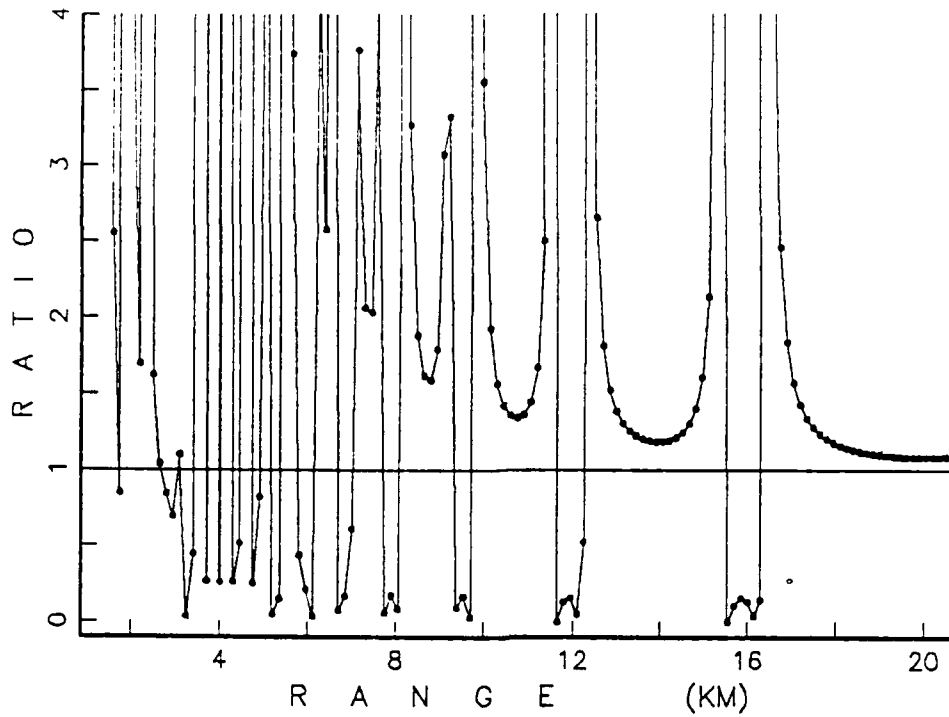


Figure 6.4: Ratio Between Ratios of Attenuation Coefficients; Sea State 3, Receiving Antennas at 12 m and 14 m.

The actual distance here is 1.9 meters, instead of 2 meters. Figure 6.4 shows the ratio between η_2^2/η_1^2 (perpendicular antennas), and $(\eta_2^2)'/(\eta_1^2)'$ (tilted antennas).

Repeating the same calculations for sea state 4 ($\alpha_{\max} = 20^\circ$), we obtain:

$$h_1' = 12 \cdot \cos 20^\circ = 11.3 \text{ m} \quad (\text{where } h_1 = 12 \text{ m}), \quad (6.5)$$

and

$$h_5' = 20 \cdot \cos 20^\circ = 18.8 \text{ m} \quad (\text{where } h_5 = 20 \text{ m}). \quad (6.6)$$

The actual distance between the antennas is 7.5 meters, instead of a theoretical value of 8 meters. Figure 6.5 shows both ratios of η_5^2/η_1^2 and $(\eta_5')^2/(\eta_1')^2$, while Figure 6.6 shows the ratio between those two ratios.

For the closest antennas we obtain:

$$h_2' = 14 \cdot \cos 20^\circ = 13.2 \text{ m} \quad (\text{where } h_2 = 14 \text{ m}), \quad (6.7)$$

while h_1' remains the same, 11.3 m. The actual difference is, therefore, 1.9 meters, instead of 2 meters. Figure 6.7 shows the ratio between η_2^2/η_1^2 (perpendicular antennas), and $(\eta_2')^2/(\eta_1')^2$ (tilted antennas).

To summarize these results, we see that the method is sensitive to ship tilting, since there is a difference between the tables for perpendicular and tilted configurations. The conclusion of these results is that the receiving antennas must be stabilized.

D. RECEIVER NOISE

In the case of our work, the received signal to noise ratio was assumed to be relatively high. The ranges of interest are less than 20 Km, while the missile ERP is in the order of 100 to 120 dBm. In addition, the transmitted signal propagates only one way. Therefore, any received signal is much larger than the receiver noise, and the signal to noise ratio is high enough, so we can disregard the noise.

E. ATMOSPHERIC ATTENUATION

The atmospheric attenuation can be treated in two ways: modify the look up tables with the attenuation data, since all the relevant parameters are known, or, more practically, to disregard it. Since we deal with ratios, the attenuation will have an influence only if the path difference is significant. As we already discussed

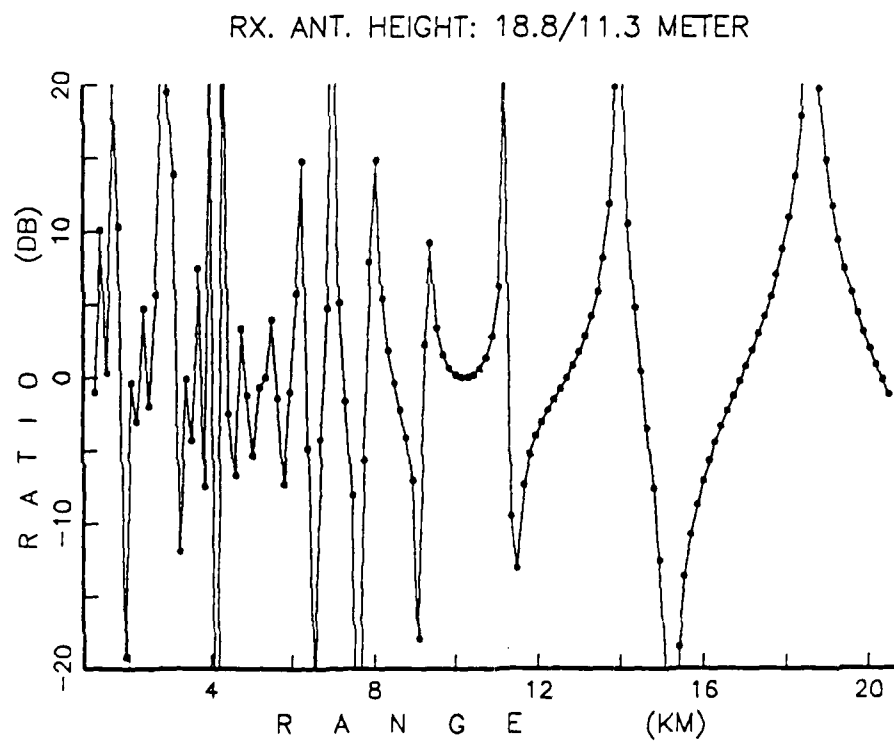
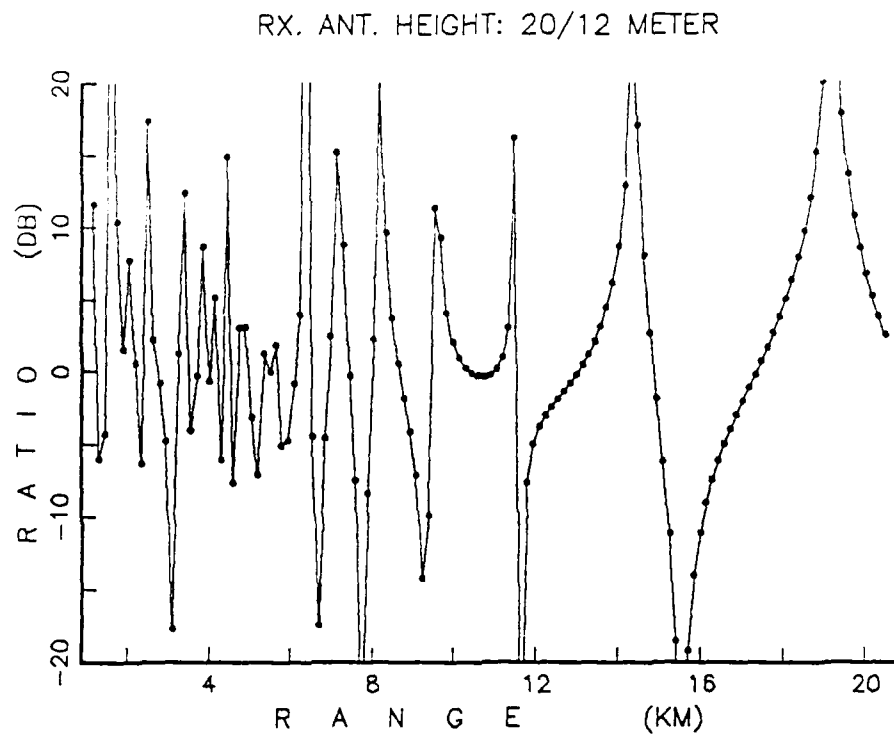


Figure 6.5: Ratio Between Attenuation Coefficients; Sea State 4, Receiving Antennas at 12 m and 20 m.

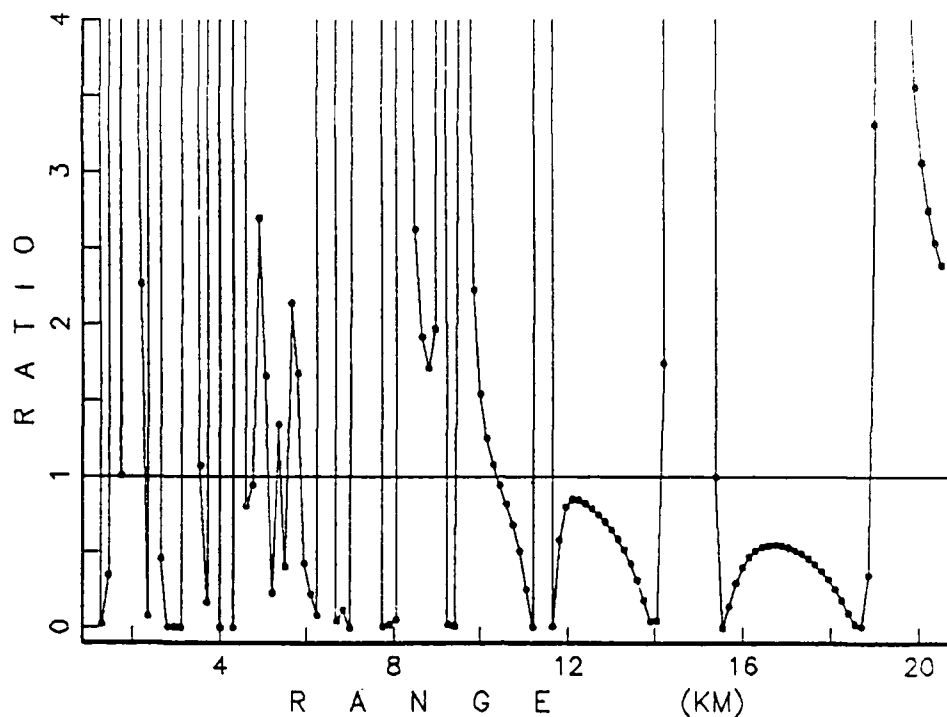


Figure 6.6: Ratio Between Ratios of Attenuation Coefficients; Sea State 4, Receiving Antennas at 12 m and 20 m.

in Chapter III, the path difference is negligible compared to the total path length. Therefore, the attenuation is practically the same for the direct and indirect path. so it has no influence on the problem, hence can be neglected.

F. OTHER MODELS

Appendix A gives other models for reflection coefficients, instead of the Ament model, that we used in this work. To use another model, the only thing that should be taken care of is modifying the model equation in the computer program. This point will be discussed in detail in the next chapter.

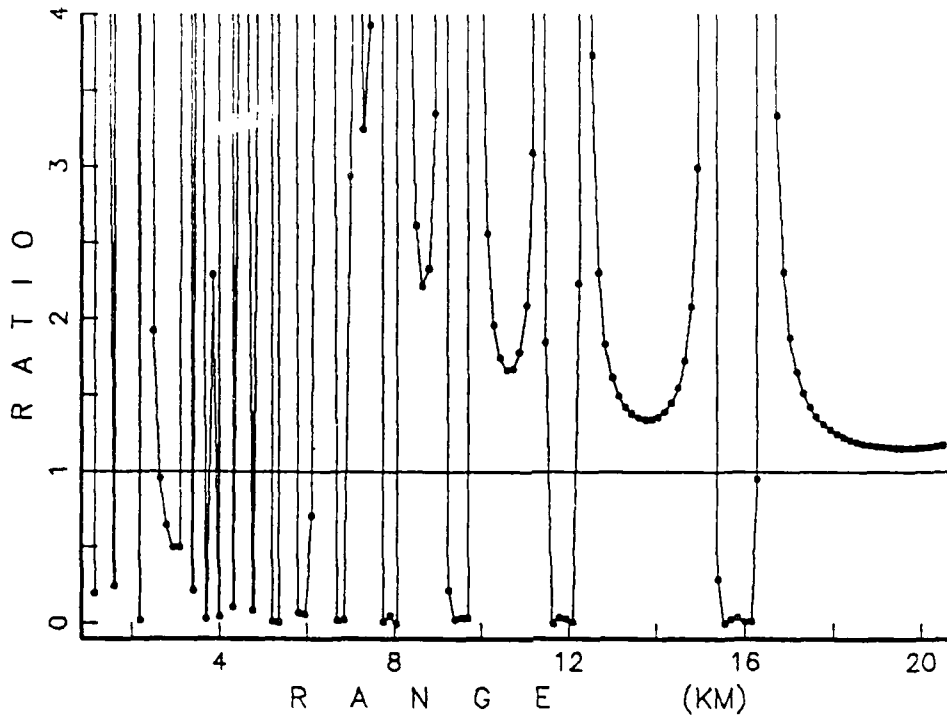


Figure 6.7: Ratio Between Attenuation Coefficients; Sea State 4, Receiving Antennas at 12 m and 14 m.

G. EARTH CURVATURE

In our work, we assumed a plane earth. In general, some geometries need to take account of the earth's curvature. Our particular geometry results in no influence from the earth curvature, as shown below. The extreme condition is for the lowest receiving antenna, and the lowest missile.

The maximum range that still allows plane earth assumption is calculated by using equation 6.8 [Ref. 7]. The problem geometry is shown in Figure 6.8.

$$R_{\max} = \sqrt{2a_e h_r + h_r^2} + \sqrt{2a_e h_t + h_t^2}, \quad (6.8)$$

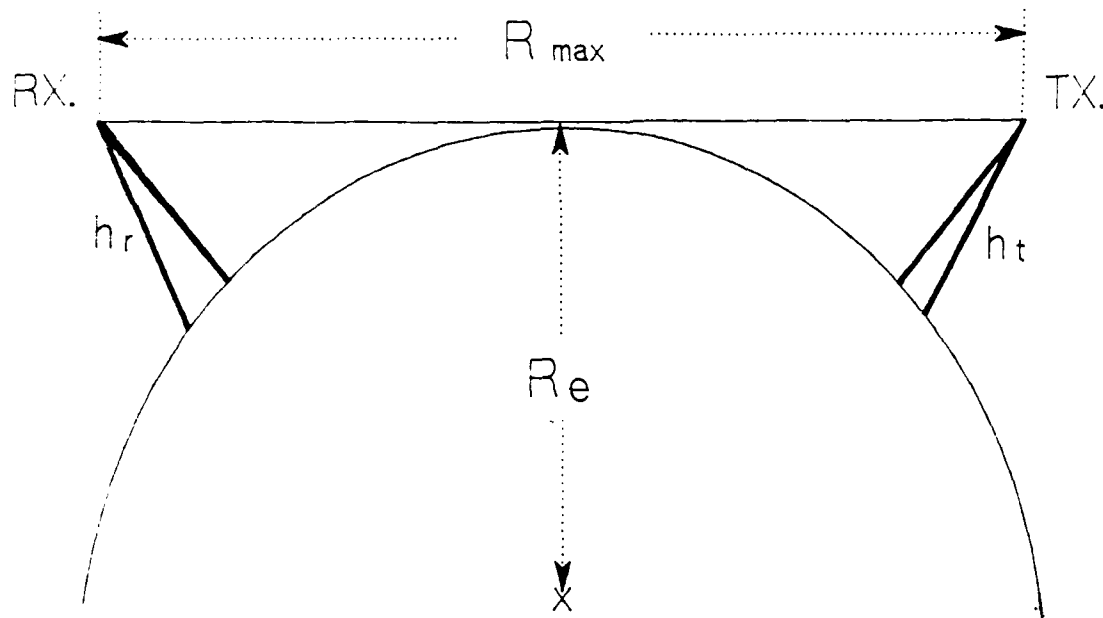


Figure 6.8: Plane Earth Assumption Geometry.

where:

a_e is the effective earth radius ($= 4/3 \times R_e$),

R_e is the earth radius ($= 6370$ Km),

h_r is the receiving antenna height, and,

h_t is the transmitter height.

For all practical purposes, the term of h^2 under the square root can be neglected.

Our extreme case is when the missile cruises in $h_t = 5$ m, and the lowest receiving antenna is located at height of $h_r = 12$ m. For this geometry we obtain a maximum range of:

$$R_{\max} = \sqrt{2 \cdot 8493 \cdot 10^3 \cdot 12} + \sqrt{2 \cdot 8493 \cdot 10^3 \cdot 5} = 23.5 \text{ Km.}$$

Since we deal with relative ranges of up to 20 Km, we can disregard the earth curvature.

VII. COMPUTER PROGRAM

The computer program in this work was written in APL. The listing is given in Appendix B and it includes all the necessary comments. This chapter presents an overview of the whole program, and then explains each function in greater detail.

The program consists of a few functions which call each other in sequence, and a main management function.

The sequence follows exactly after the one described in Chapter V, under "Detailed Discussion." All the inputs that must be given by external means, are inserted here by the user, as software parameters.

The program is started by typing RUN. The user is asked to enter sea state (0 to 7), and with this data, the RUN function calls the main function for receiving data, named DATAIN. This function automatically creates more needed parameters, in a random manner, between given limits. It is also possible for the user to dictate each one of these parameters, instead of creating them randomly by the program:

- frequency – between 2 to 18 GHz,
- ERP (Effective Radiated Power) – between 100 to 120 dBm (10^7 to 10^9 Watt),
- initial range for simulation (range where missile starts to radiate) – between 10 to 20 Kilometers, and,
- transmitter height – between 5 to 40 meters.

Other relevant parameters are programmed off-line as software parameters, and can be changed easily at any time. Those are:

- window width, as discussed in Chapter V,
- minimum transmitter height for the look up table,
- number of steps for the transmitter height for the table,
- resolution of transmitter height steps for the table,
- minimum range for simulation (if the missile passed this range without being intercepted, the simulation is failed and stops),
- range resolution for the look up table, both high resolution for short range, and regular resolution for longer range,
- number of range steps for each range resolution,
- resolution of simulation steps (range distance between each receiving), and,
- locations (heights) of receiving antennas.

The function then calculates the maximum range, and shows the major parameters on the screen (a full session is demonstrated later in this chapter.)

With all the necessary data, DATAIN returns to the management function, RUN. In the next step, RUN sends all the relevant parameters to the main function STARTPRO, and activates it.

STARTPRO is responsible for all the major calculations:

- creating off line tables which include also the attenuation coefficient, η^2 , and the reflection coefficient, ρ ,
- receiving five signals in the receiving antennas, and divide their powers to determine the ratios,
- comparing between the off line tables and the actual ratios,
- marking the correct (single) location, and finally,
- sending the location to the management function.

The signals for STARTPRO are created by the simulator SIM. This function is activated by STARTPRO, every time it needs a new set of receiving signals.

SIM receives the relevant parameters from DATAIN, and creates five signals due to those parameters and the geometry. The signal is calculated using equation 7.1.

$$S_i = ERP \cdot \eta^2 \cdot \rho \cdot \frac{1}{4\pi R^2}, \quad (7.1)$$

where:

ERP is the effective radiated power of the transmitter,

R is the relative range between the transmitter and the receiver,

η^2 is the attenuation coefficient, calculated by using Equation (3.5), and,

ρ is the reflection coefficient, calculated by using Equation (3.20).

After the management function RUN received the location of the transmitter from STARTPRO, it calls the translating function RHFIND in order to translate the coordinates of the table into range and height, and to type it.

A conceptual flow chart is given in Figure 7.1, and a simulation session is shown in Figure 7.2.

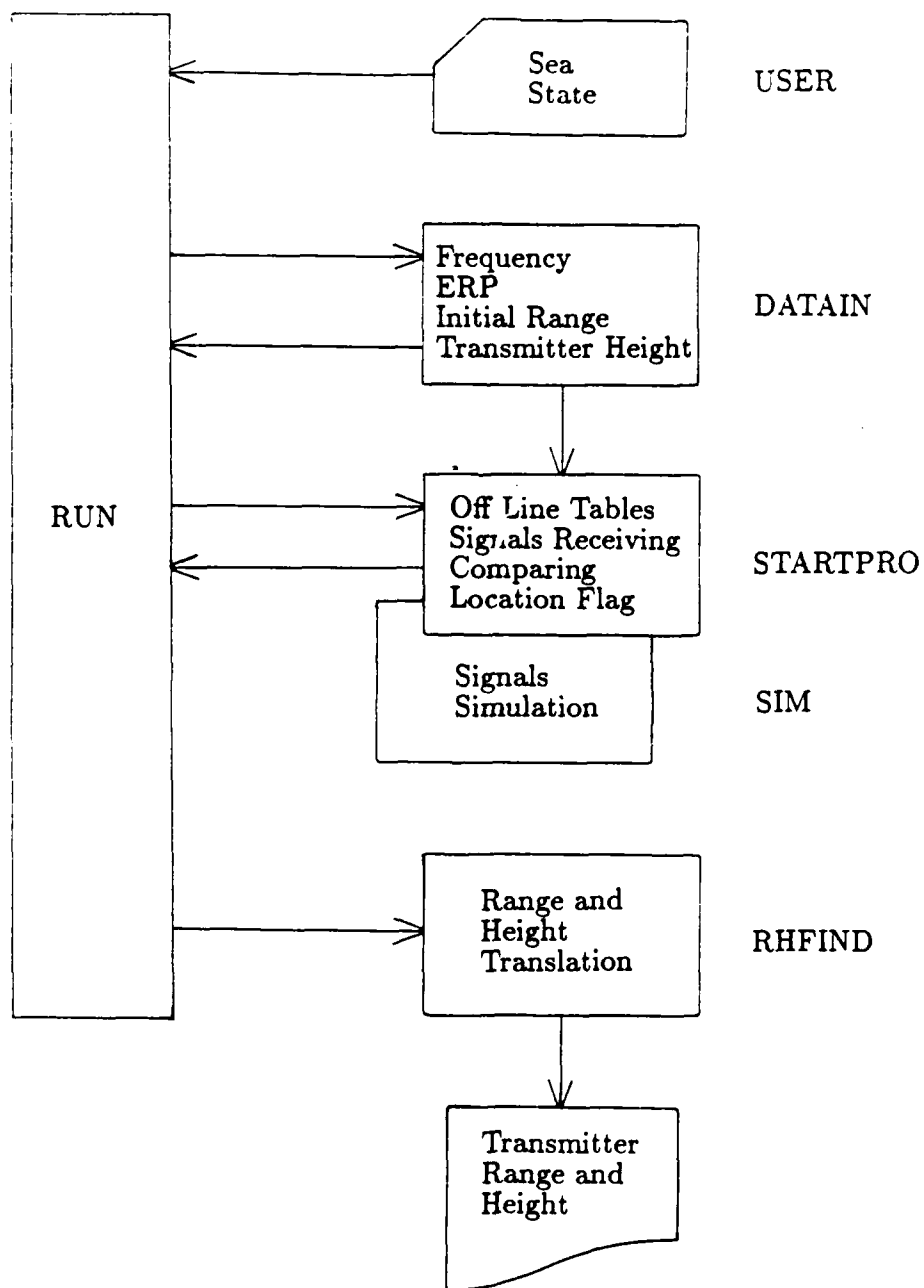


Figure 7.1: Estimation Process; Conceptual Flow Chart.

```

*RUN
ENTER SEA STATE:

0 - CALM      1 - SMOOTH    2 - SLIGHT
3 - MODERATE  4 - ROUGH     5 - VERY ROUGH
6 - HIGH      7 - VERY HIGH

*2 (for example)

RANGE INTERVAL FOR SIMULATION:
MINIMUM RANGE (IN METERS):      1000
MAXIMUM RANGE(IN METERS):      20000
SEA STATE:
2
FREQUENCY (IN GHZ):
8.85
INITIAL RANGE (IN KILOMETERS):
14.5
TRANSMITTER HEIGHT (IN METERS) - ACTUAL:
36
RECEIVER ANTENNAS HEIGHTS (IN METERS):
12   14   16   18   20

TRANSMITTER RANGE (IN KILOMETERS):
14.4
TRANSMITTER HEIGHT (IN METERS):
36

UPDATED ACTUAL RANGE (IN KILOMETERS):
14.4

```

Figure 7.2: Simulation Session Example. (Lines Starting with Asterisk (*) are Entered by the User.)

VIII. SUMMARY AND CONCLUSIONS

The work which had been done during this thesis research, together with the results obtained, show that the suggested method for passive range estimation using multipath effect can probably be used. The work developed the method theoretically, and proved its feasibility.

The accuracy of the estimated range and height depends upon many parameters, as well as receiving antennas configuration. A trade off should be done between number of receiving antennas, their heights, separation and window width, as described in Chapter V.

There is no analytical way for finding the optimum trade off, and only trial and error sessions can achieve a local optimum, as was done during this research.

Another question of interest is the accuracy of the rough sea model (Ament model in our case).

The answer to this question can only be obtained by sea trials. Those trials should answer the questions listed below:

- Is the theoretical analysis of the additional parameters in Chapter VI correct, or should we modify these parameters?
- What is the estimation accuracy if an incorrect sea state is entered, and is there a preferred direction for entering sea state (is it better to enter a higher sea state in case of uncertainty, or lower state)?
- How does the wind direction influence the accuracy, if at all, (upwind, downwind, and crosswind)?
- What is the practical feasibility of the suggested method, and with which limitations (such as sea state and wind direction)?

We should notice that the Ament model neglects the shadowing effect, although it deals with small grazing angles, where this effect does occur. It is questionable how far the shadowing effect changes the reality from the model.

A possible influence of the shadowing effect is the fact that the amplitude of the reflected wave will be lower, so that the signal minima will not be so sharp as is shown in Figure 4.2. A decrease in the amplitude of the specular reflection will also occur because of high sea state, and capillary waves. If sea trials show consistent errors, we can conclude that the Ament model is inadequate. In this case it will be necessary to develop another more accurate model.

It can be predicted that for sea state 0, the results will be more accurate than in any other case, while the more roughness, the less accurate the results.

In order to improve the estimation process, and to reach a lower rate of errors, we can modify the program. The modified program will consider also the past readings, and compare each present estimate with the previous ones. If the range becomes shorter by a reasonable increment, and the transmitter height remains almost the same, we can conclude that the estimate is correct. On the other hand, if the estimate does not meet this test, then another estimate should be made, and compared, and so on.

APPENDIX A: REFLECTION COEFFICIENT MODELS

In Chapter III we discussed the most popular model for reflection coefficient of a rough sea, the Ament model. There are several other models, which are given below. It should be noted that there are additional models which we will not cover here.

A. BULLINGTON MODEL

This model distinguishes between different surface profiles [Ref. 3,12]:

1. Sawtooth Profile

The wave height is distributed uniformly, but does not necessarily have uniform slope. The phase values have equal probability between $-\phi_m$ and $+\phi_m$, where

$$\phi_m = \frac{2\pi\sigma_h \sin \psi}{\lambda}, \quad (A.1)$$

and

σ_h is the RMS deviation of the waves height,

ψ is the grazing angle, and,

λ is the signal wavelength.

The reflection coefficient for the sawtooth profile is given by:

$$\rho = \frac{\sin \phi_m}{\phi_m} = \text{sinc} \phi_m, \quad (A.2)$$

and is shown in Figure A.1.

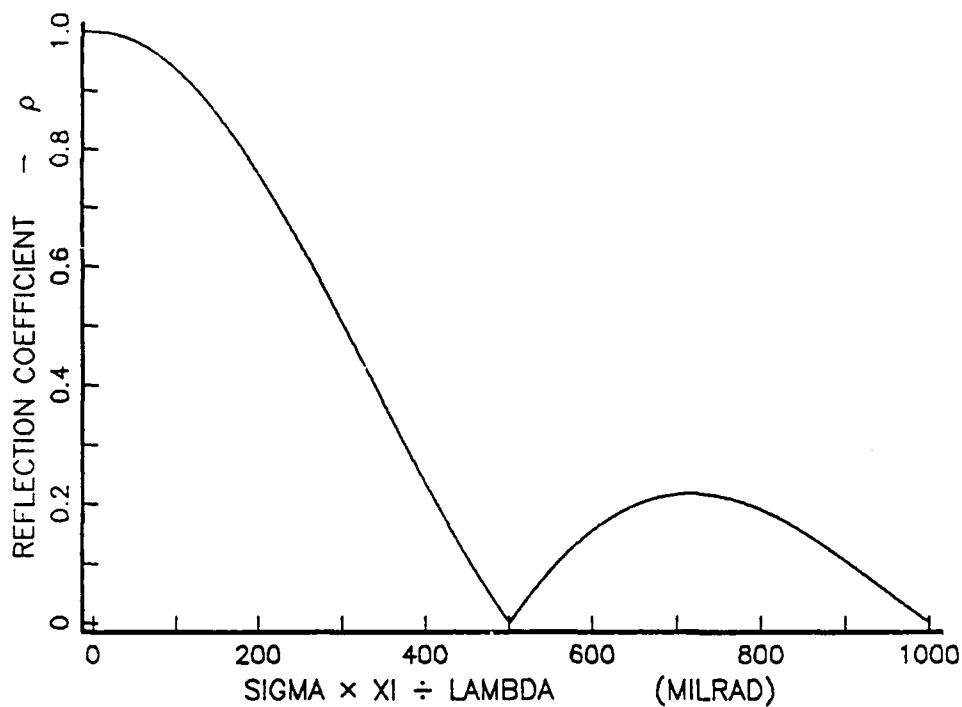


Figure A.1: Bullington Model – Sawtooth Profile.

2. Sinusoidal Profile

The reflection coefficient in this case is given by Equation (A.3), and is shown in Figure A.2.

$$\rho = J_0 \left(\frac{2\pi\sigma_h \sin \psi}{\lambda} \right), \quad (\text{A.3})$$

where J_0 is the Bessel function of the first kind and zero order.

3. Triangular Profile:

Here, the reflection coefficient is given by:

$$\rho = \left(\frac{\sin \phi_t}{\phi_t} \right)^2, \quad (\text{A.4})$$

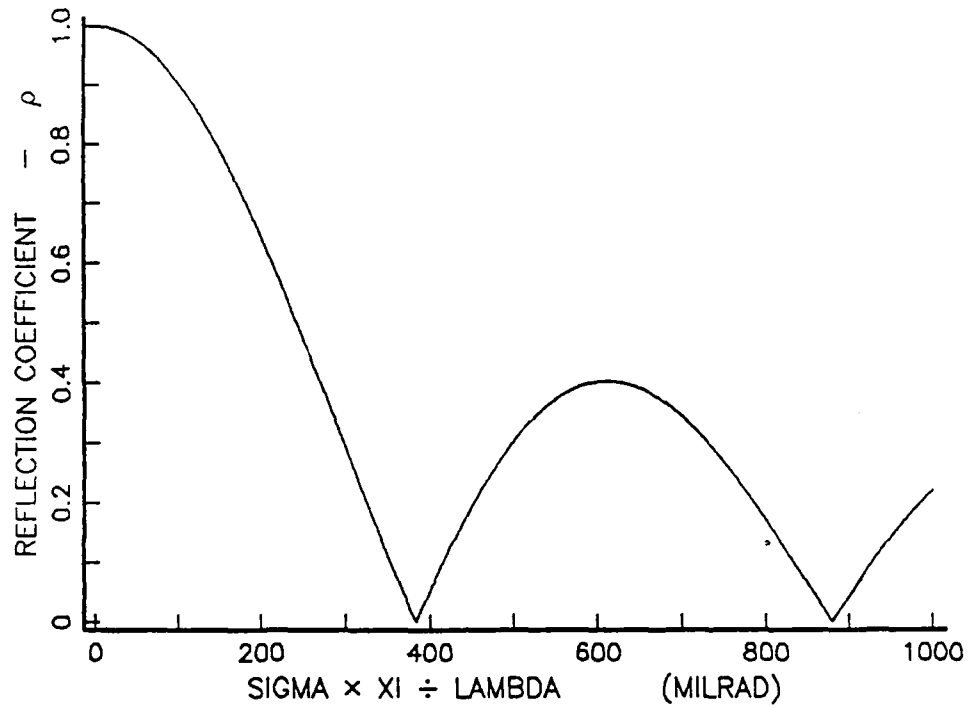


Figure A.2: Bullington Model – Sinusoidal Profile.

where the maximum phase is:

$$\phi_t = \frac{\pi \sigma_h \sin \psi}{\lambda}. \quad (A.5)$$

Figures A.3 and A.4 show the triangular profile reflection coefficient.

4. Sine Square Profile

The reflection coefficient is more complex in this model, and is given by Equation (A.6), and shown in Figure A.5.

$$\rho = \cos \phi_t \cdot J_0(\phi_t), \quad (A.6)$$

where ϕ_t is the same as given in Equation (A.5).

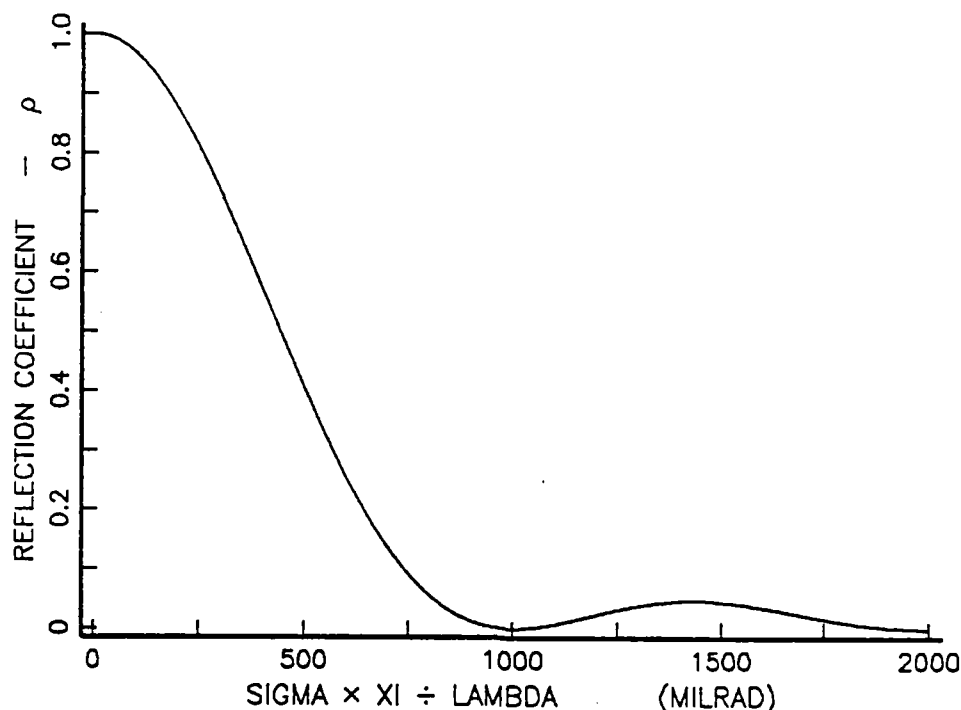


Figure A.3: Bullington Model - Triangular Profile.

B. DAVIES MODEL

The Davies model assumes that the surface has a random behavior, which yields a gaussian height distribution and correlation coefficient. This model neglects the shadowing effect, and is good for small to medium grazing angles ($\psi < 40^\circ$). In order to describe the surface, we introduce an arbitrary parameter, m/σ . Experiments above the sea surface show that a value of $m/\sigma = 50$ to 60, gives sufficient correlation between theoretical and experimental results. [Ref. 3].

The reflection coefficient for this model is given by:

$$\rho = \frac{m}{2\sigma} \cdot \sqrt{\sec \psi} \cdot \exp \left[- \left(\frac{m}{2\sigma} \right)^2 \tan^2 \psi \right]. \quad (A.7)$$

Figure A.6 shows the reflection coefficient. The value $m/2\sigma$ is 27 ($m/\sigma = 54$).

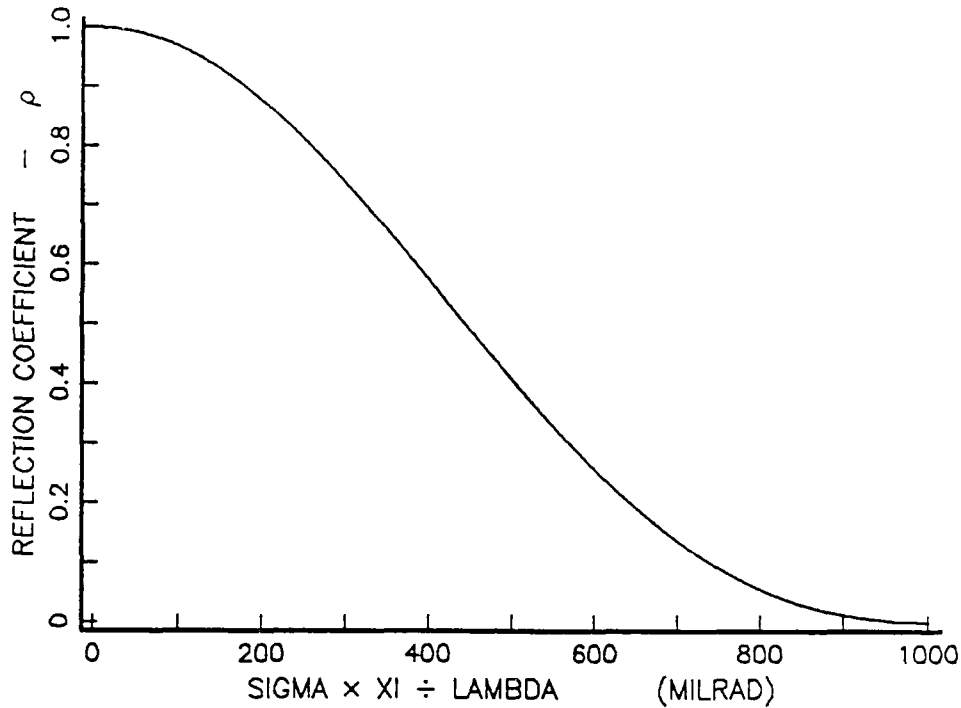


Figure A.4: Bullington Model - Triangular Profile (expanded).

C. ISAKOVICH MODEL

In this model we assume that the surface is irregular, isotropic in all directions, and has a normal height distribution. The parameter m/σ describes the surface (as in the Davies model). It is the only parameter which dictates the intensity of the scattering in a given direction. Changing the ratio will change the profile shape, as shown in Figure A.7 ($m/\sigma = 10$), and Figure A.8 ($m/\sigma = 20$). The shadowing effect is neglected and only far-field is calculated. The Isakovich model calculates the dispersion of waves for random surface [Ref. 3]:

$$\rho = \frac{m}{\sigma} \left[\frac{1 - \cos \psi \cos E_t \cos \theta + \sin \psi \sin E_t}{(\sin \psi + \sin E_t)^2} \right] \cdot \exp - \left[\frac{1}{8} \left(\frac{m}{\sigma} \right)^2 \frac{\cos^2 \psi + \cos^2 E_t - 2 \cos \psi \cos E_t \cos \theta}{(\sin \psi + \sin E_t)^2} \right]. \quad (A.8)$$

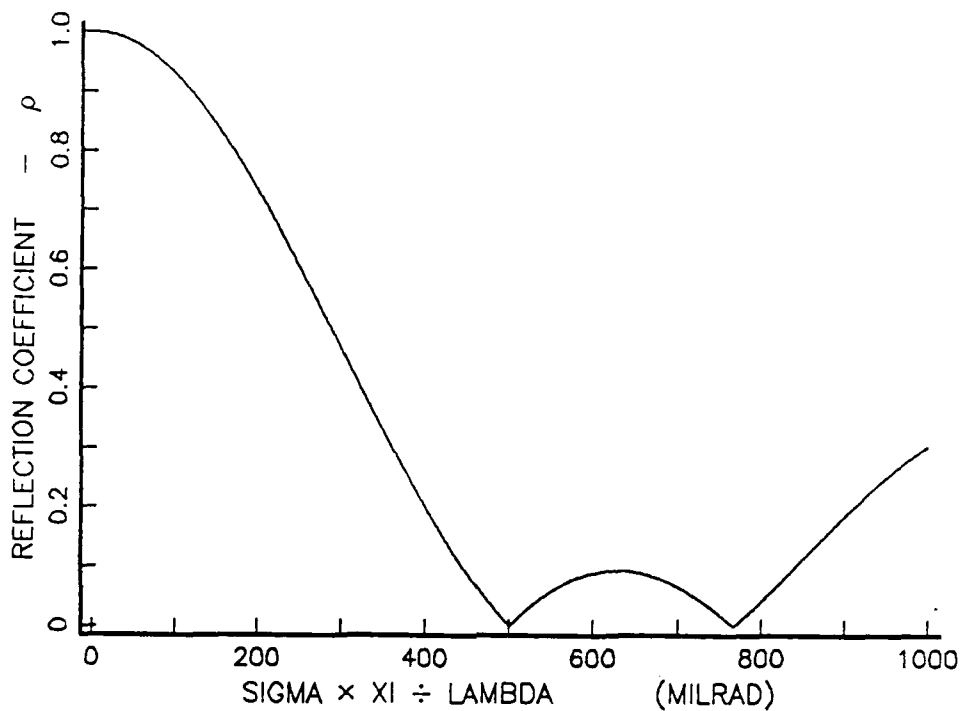


Figure A.5: Bullington Model – Sine Square Profile.

This model is much more complicated than the others, since it has two more parameters:

E_t is the observation angle, and,

θ is the azimuth angle.

In order to illustrate results comparable to those for the other modes, we assume that the azimuth angle is zero ($\theta = 0$). For simplicity, we calculate the reflection coefficient for two cases: zero observation angle, $E_t = 0^\circ$ (transmitter and receiver at the same level), and $E_t = -30^\circ$ (transmitter higher than the receiver).

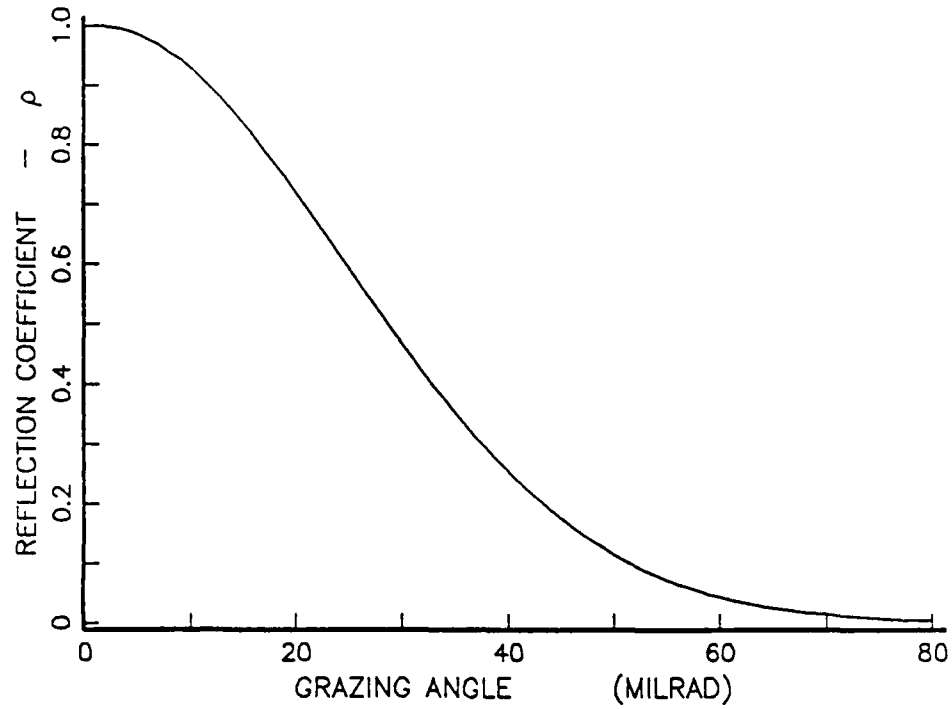


Figure A.6: Davies Model.

Using the assumption $\theta = 0$, we simplify Equation (A.8) to:

$$\rho_{\theta=0^\circ} = \frac{m}{\sigma} \left[\frac{1 - \cos \psi \cos E_t + \sin \psi \sin E_t}{(\sin \psi + \sin E_t)^2} \right] \cdot \exp - \left[\frac{1}{8} \left(\frac{m}{\sigma} \right)^2 \cdot \frac{\cos^2 \psi + \cos^2 E_t - 2 \cos \psi \cos E_t}{(\sin \psi + \sin E_t)^2} \right]. \quad (\text{A.9})$$

For the case of zero observation angle ($E_t = 0^\circ$), Equation (A.9) becomes even more simple:

$$\rho_{E_t=0^\circ} = \frac{m}{\sigma} \left(\frac{1 - \cos \psi}{\sin^2 \psi} \right) \cdot \exp - \left[\frac{1}{8} \left(\frac{m}{\sigma} \right)^2 \cdot \frac{\cos^2 \psi + 1 - 2 \cos \psi}{\sin^2 \psi} \right]. \quad (\text{A.10})$$

This case is illustrated in Figures A.7 and A.8 for two different values of m/σ . For -30° observation angle Equation (A.11) applies. The result is shown in Figure A.9.

$$\rho_{E_t = -30^\circ} = \frac{m}{\sigma} \cdot \left[\frac{2 - \sqrt{3} \cos \psi - \sin \psi}{2(\sin \psi - 0.5)^2} \right] \cdot \exp - \left[\frac{1}{8} \left(\frac{m}{\sigma} \right)^2 \cdot \frac{\cos^2 \psi + 0.75 - \sqrt{3} \cos \psi}{(\sin \psi - 0.5)^2} \right]. \quad (A.11)$$

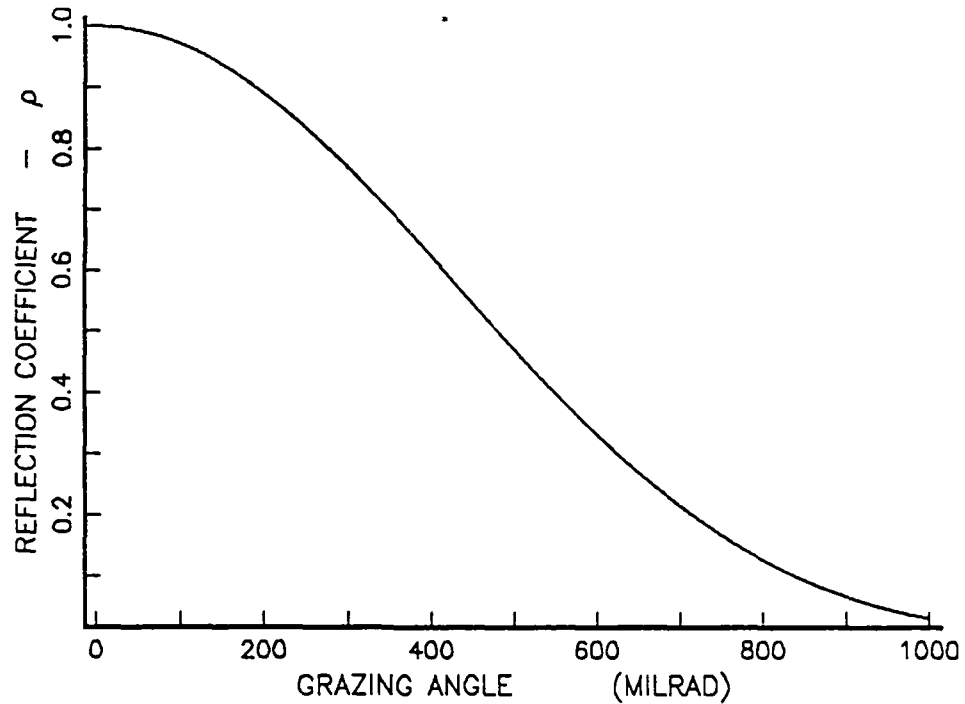


Figure A.7: Isakovich Model with Zero Observation Angle ($E_t = 0^\circ$), $m/\sigma = 10$.

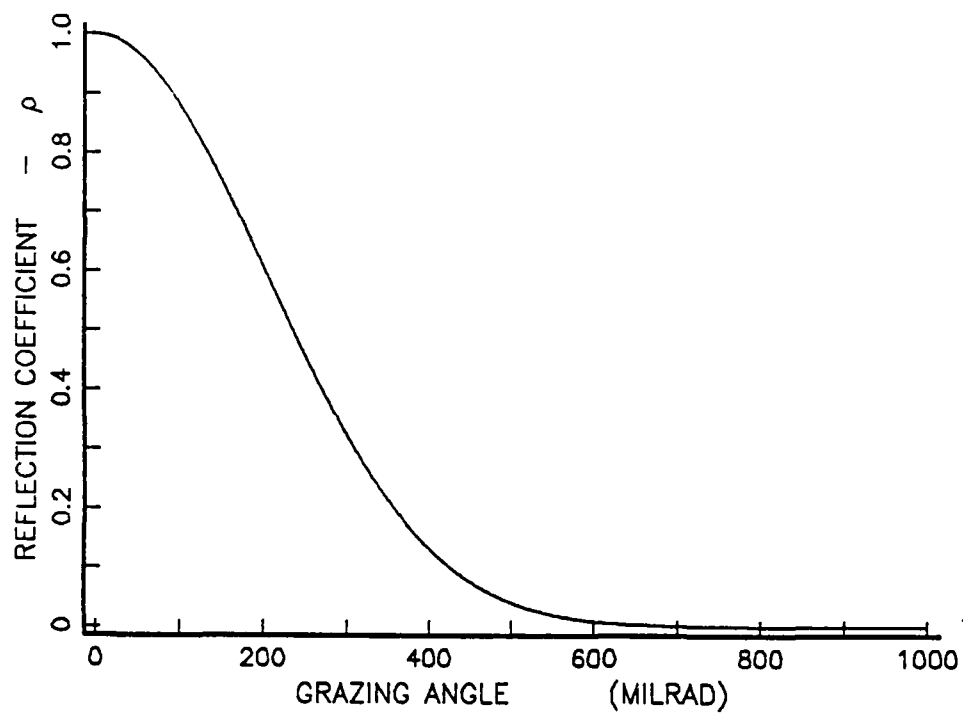


Figure A.8: Isakovich Model with Zero Observation Angle, ($E_t = 0^\circ$), $m/\sigma = 20$.

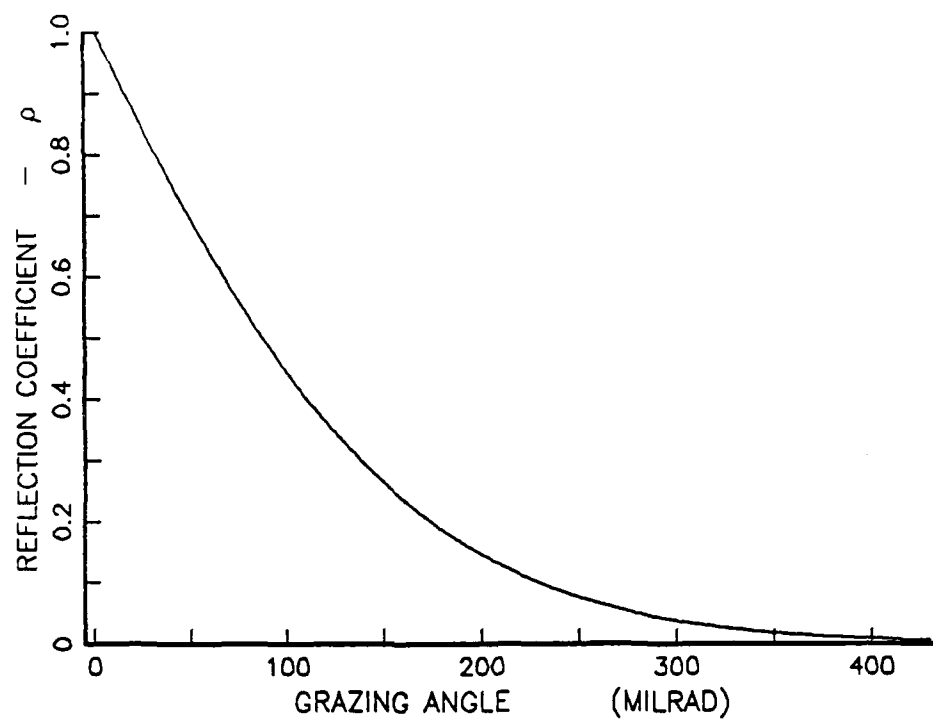


Figure A.9: Isakovich Model with Observation Angle of -30° , $m/\sigma = 20$.

APPENDIX B: COMPUTER PROGRAM LISTING

This appendix gives the listing of the computer program described in Chapter VII. RUN is the management function, which calls the other functions in order. DATAIN is the function responsible for the input data for further calculations. STARTPRO is the main function which does all the major calculations, as well as creating the look-up tables, and comparing the ratios of the actual received signals with the calculated ratios. SIM is the simulation function, which simulates the received signals from the missile. RHFIND is the function which translates the location of the missile in the table into a range and height.

```
**RUN
[0]  RUN
[1]  A  MANAGMENT FUNCTION
[2]  'ENTER SEA STATE:'
[3]  ' '
[4]  '0-CALM          1-SMOOTH          2-SLIGHT'
[5]  '3-MODERATE      4-ROUGH          5-VERY ROUGH'
[6]  '6-HIGH          7-VERY HIGH'
[7]  ' '
[8]  SEA←□
[9]  A  ENTERING ROUGHNESS PARAMETER
[10] ' '
[11] DATAIN
[12] A  INITIALIZATION
[13] RR:F STARTPRO HR3
[14] A  STARTING
→[15] →(FLAG=1)/STO
[16] A  END OF SESSION IF RANGE CANNOT BE FOUND
[17] RHFIND
[18] A  GO TO CHECK REAL RANGE AND HEIGHT
→[19] STO:→0
```

****DATAIN**

```

[0]  DATAIN
[1]  A  INITIALIZATION FUNCTION
[2]  A  □□□□□□□□
[3]  MINHEIGHT+4
[4]  A  'MINHEIGHT' IS THE MINIMUM TX. HEIGHT (LESS 1 METER)
[5]  A  □□□□□□□□
[6]  HEIGHTST+36
[7]  A  'HEIGHTST' IS THE NUMBER OF HEIGHT STEPS
[8]  A  □□□□□□□□
[9]  HEIGHTRES+1
[10] A  'HEIGHTRES' IS THE RESOLUTION OF HEIGHT STEPS
[11] A  □□□□□□□□
[12] C+0.975
[13] A  □□□□□□□□
[14] D+1.025
[15] A  'C','D' ARE LOWER AND UPPER LIMITS FOR OK (STARTPRO)
[16] A  □□□□□□□□
[17] RMIN+1000
[18] A  'RMIN' IS MINIMUM RANGE
[19] RMINS+RMIN
[20] A  'RMINS' IS MINIMUM RANGE FOR SIMULATION
[21] A  □□□□□□□□
[22] NSTEPS+125
[23] A  'NSTEPS' IS THE NUMBER OF RANGE STEPS
[24] A  □□□□□□□□
[25] RESO+100
[26] A  'RESO' IS THE RANGE STEPS RESOLUTION (LENGTH OF EACH STEP)
[27] A  □□□□□□□□
[28] HNSTEPS+130
[29] A  'HNSTEPS' IS THE NUMBER OF HIGH RESOLUTION RANGE STEPS
[30] A  □□□□□□□□
[31] HRESO+50
[32] A  'HRESO' IS THE RANGE STEPS (HIGH) RESOLUTION FOR SMALL
[33] A  RANGES
[34] A  □□□□□□□□
[35] SIMSTEP+50
[36] A  'SIMSTEP' IS THE RANGE STEPS RESOLUTION IN THE SIMULATION
[37] A  FUNCTION (VSIM)
[38] F+(1999+(?17001))+1000
[39] A  □□□□□□□□
[40] AF+9.35
[41] A  'F' IS FREQUENCY (IN GHZ); 2+18 GHZ
[42] ERP+100000000*?100
[43] A  □□□□□□□□
[44] AERP+1000000000
[45] A  'ERP' IS TRANSMITTER EFFECTIVE RADIATED POWER (IN WATTS);
[46] A  1E7+1E9 WATT (100+120 DBM)
[47] RI+20000*(500+1?300)+1000
[48] A  'RI' IS INITIAL RANGE (IN METERS); 10,000+16,000 METER
[49] A  □□□□□□□□

```

```

[50]  ARI+15400
[51]  HAT+4+?36
[52]  A          □□□□□□□□
[53]  A HAT+22
[54]  A 'HAT' IS TRANSMITTER HEIGHT (IN METERS);      5+40 METER
[55]  A HR3+14+5?16
[56]  A 'HR3' ARE RECEIVER'S ANTENNAS HEIGHTS (IN METERS)
[57]  A 'HR3' IS BETWEEN 15+30 METERS
[58]  A          □□□□□□□□
[59]  HR3+ 12 14 16 18 20
[60]  'RANGE INTERVAL FOR SIMULATION:'
[61]  'MINIMUM RANGE (IN METERS):'      ',RMIN
[62]  'MAXIMUM RANGE (IN METERS):'
[63]  ',RMIN+(NSTEPS*RESO)+(HNSTEPS*HRESO)
[64]  'SEA STATE:'
[65]  SEA
[66]  A 'SEA' IS ROUGHNESS PARAMETER
[67]  F
[68]  'INITIAL RANGE (IN KILOMETERS):'
[69]  RI+1000
[70]  'TRANSMITTER HEIGHT (IN METERS)-ACTUAL:'
[71]  HAT
[72]  'RECEIVER ANTENNAS HEIGHTS (IN METERS):'
[73]  HR3[ΔHR3]
[74]  A DISPLAING THE INITIAL SIMULATION DATA
+ [75]  →0

```

**STARTPRO

```

[0]      FO STARTPRO HR;IO;HA;R;LAMBDA;ET1;ET2;ET3;ET4;ET5;ET12;ET13;
          ET14;ET15;SI;SI12;SI13;SI14;SI15;R12;R13;R14;R15;OK12;
          OK13;OK14;OK15;TEMP;TEMP1;TEMP2;SH;RD1;RD2;RD3;RD4;
          RD5;DELTA1;DELTA2;DELTA3;DELTA4;DELTA5;TETA1;TETA2;
          TETA3;TETA4;TETA5;XI1;XI2;XI3;XI4;XI5;AJO1;RHO2;RHO3;
          RHO4;RHO5
[1]      A   MAIN CALCULATION AND COMPUTATION FUNCTION
[2]      IO+1
[3]      R+RMIN+(HRESO*HNSTEPS),(HRESO*HNSTEPS)+RESO*HNSTEPS
[4]      A   'R' IS RANGE VECTOR ('HNSTEPS' STEPS OF 'HRESO' METER
[5]      A   EACH, PLUS 'NSTEPS' STEPS OF 'RESO' METER EACH),
[6]      A   STARTING AT 'RMIN'
[7]      HA+MINHEIGT+HEIGTRES*HEIGTST
[8]      A   'HA' IS TRANSMITTER HEIGHT VECTOR ('HEIGTST' STEPS OF
[9]      A   'HEIGTRES' METER EACH)
[10]     GRH+(HEIGTST,(NSTEPS+HNSTEPS))p1
[11]     A   'GRH' IS MATRIX WHICH SHOWS ALL THE LOCATIONS OF
[12]     A   CANDIDATE RANGE AND HEIGHT COMBINATIONS
[13]     LAMBDA+0.3+FO
[14]     A
[15]     RD1+(((HA-HR[1])*2)*.+.R*2)*0.5
[16]     RD2+(((HA-HR[2])*2)*.+.R*2)*0.5
[17]     RD3+(((HA-HR[3])*2)*.+.R*2)*0.5
[18]     RD4+(((HA-HR[4])*2)*.+.R*2)*0.5
[19]     RD5+(((HA-HR[5])*2)*.+.R*2)*0.5
[20]     A   'RD' IS THE DIRECT DISTANCE BETWEEN TRANSMITTER
[21]     A   AND RECEIVING ANTENNAS (RESPECTIVELY)
[22]     DELTA1+(2*HA*HR[1])*+.R
[23]     DELTA2+(2*HA*HR[2])*+.R
[24]     DELTA3+(2*HA*HR[3])*+.R
[25]     DELTA4+(2*HA*HR[4])*+.R
[26]     DELTA5+(2*HA*HR[5])*+.R
[27]     A   'DELTA' IS THE DIFFERENCE BETWEEN THE DIRECT
[28]     A   PATH AND THE REFLECTED PATH FOR EACH RX.
[29]     A   ANTENNA (RESPECTIVELY)
[30]     TETA1+10*(Q(ΦpRD1)p|HR[1]-HA)+RD1
[31]     TETA2+10*(Q(ΦpRD2)p|HR[2]-HA)+RD2
[32]     TETA3+10*(Q(ΦpRD3)p|HR[3]-HA)+RD3
[33]     TETA4+10*(Q(ΦpRD4)p|HR[4]-HA)+RD4
[34]     TETA5+10*(Q(ΦpRD5)p|HR[5]-HA)+RD5
[35]     A   'TETA' IS THE OBSERVATION ANGLE BETWEEN THE RX.
[36]     A   ANTENNA AND THE TRANSMITTER (FROM THE LATEST
[37]     A   POINT OF VIEW)- FOR EACH RX. ANT. (RESPECTIVELY)
[38]     XI1+(Q(ΦpRD1)pHR[1]+HA)+RD1+DELTA1
[39]     XI2+(Q(ΦpRD2)pHR[2]+HA)+RD2+DELTA2
[40]     XI3+(Q(ΦpRD3)pHR[3]+HA)+RD3+DELTA3
[41]     XI4+(Q(ΦpRD4)pHR[4]+HA)+RD4+DELTA4
[42]     XI5+(Q(ΦpRD5)pHR[5]+HA)+RD5+DELTA5
[43]     A   'XI' IS THE SINE OF THE GRAZING ANGLE FOR EACH
[44]     A   RECEIVING ANTENNA (RESPECTIVELY)

```

```

+ [45]      + (SEA=0)/S0
+ [46]      + (SEA=1)/S1
+ [47]      + (SEA=2)/S2
+ [48]      + (SEA=3)/S3
+ [49]      + (SEA=4)/S4
+ [50]      + (SEA=5)/S5
+ [51]      + (SEA=6)/S6
+ [52]      + (SEA=7)/S7
[53]      A
[54]      S0:SH+SHL+SHH+0
+ [55]      +CONT
[56]      S1:SH+0.0325
[57]      SHL+0
[58]      SHH+0.065
+ [59]      +CONT
[60]      S2:SH+0.1375
[61]      SHL+0.065
[62]      SHH+0.21
+ [63]      +CONT
[64]      S3:SH+0.265
[65]      SHL+0.21
[66]      SHH+0.32
+ [67]      +CONT
[68]      S4:SH+0.43
[69]      SHL+0.32
[70]      SHH+0.54
+ [71]      +CONT
[72]      S5:SH+0.7
[73]      SHL+0.54
[74]      SHH+0.86
+ [75]      +CONT
[76]      S6:SH+1.08
[77]      SHL+0.86
[78]      SHH+1.3
+ [79]      +CONT
[80]      S7:SH+1.75
[81]      SHL+1.3
[82]      SHH+2.2
+ [83]      +CONT
[84]      A 'SHL' AND 'SHH' ARE THE LOWEST AND HIGHEST
[85]      A (RESPECTIVELY) RMS WAVES HEIGHT FOR EACH SEA STATE
[86]      CONT:
[87]      RHO1+*-2*((02)*SH*XI1+LAMBDA)*2
[88]      RHO2+*-2*((02)*SH*XI2+LAMBDA)*2
[89]      RHO3+*-2*((02)*SH*XI3+LAMBDA)*2
[90]      RHO4+*-2*((02)*SH*XI4+LAMBDA)*2
[91]      RHO5+*-2*((02)*SH*XI5+LAMBDA)*2
[92]      A 'RHO' IS THE REFLECTION COEFFICIENT FOR EACH
[93]      A RX. ANTENNA (RESPECTIVELY) - CALCULATED AFTER
[94]      A AMENT MODEL (SEE VSIM)

```

```

[95] ET1←RHO1×(10(((02)×((HA*2)+HR[1]×HA))0.÷(LAMBDA×R)))×2
[96] ET2←RHO2×(10(((02)×((HA*2)+HR[2]×HA))0.÷(LAMBDA×R)))×2
[97] ET3←RHO3×(10(((02)×((HA*2)+HR[3]×HA))0.÷(LAMBDA×R)))×2
[98] ET4←RHO4×(10(((02)×((HA*2)+HR[4]×HA))0.÷(LAMBDA×R)))×2
[99] ET5←RHO5×(10(((02)×((HA*2)+HR[5]×HA))0.÷(LAMBDA×R)))×2
[100] A 'ET1'+ 'ET5' ARE MULTIPATH ATTENUATION FACTORS FOR
[101] A EACH RECEIVING ANTENNA, RESPECTIVELY (MATRIX)
[102] ET12←ET1+ET2+1E-13
[103] ET13←ET1+ET3+1E-13
[104] ET14←ET1+ET4+1E-13
[105] ET15←ET1+ET5+1E-13
[106] A 'ET12'+ 'ET15' ARE RELATIONS BETWEEN THE MULTIPATH
[107] A FACTORS FOR EACH PAIR OF RX. ANTENNAS, RESPECTIVELY
[108] A (MATRIX)
[109] RCV:SI←SIM
[110] A 'SI' ARE RECEIVED SIGNAL LEVELS FOR ALL THE RECEIVING
[111] A ANTENNAS (VECTOR)
[112] REL:
[113] SI12←(ρGRH)ρSI[1]+SI[2]+1E-13
[114] SI13←(ρGRH)ρSI[1]+SI[3]+1E-13
[115] SI14←(ρGRH)ρSI[1]+SI[4]+1E-13
[116] SI15←(ρGRH)ρSI[1]+SI[5]+1E-13
[117] A 'SI12'+ 'SI15' ARE RELATIONS BETWEEN RECEIVED SIGNALS
[118] A PAIRS (MATRICES)
[119] COMP:
[120] R12←SI12+ET12+1E-13
[121] R13←SI13+ET13+1E-13
[122] R14←SI14+ET14+1E-13
[123] R15←SI15+ET15+1E-13
[124] A 'R12'+ 'R15' ARE RATIO MATRICES BETWEEN ACTUAL
[125] A AND THEORETICAL VALUES
[126] OK12←(R12≥C)^(R12≤D)
[127] OK13←(R13≥C)^(R13≤D)
[128] OK14←(R14≥C)^(R14≤D)
[129] OK15←(R15≥C)^(R15≤D)
[130] A 'OK12'+ 'OK15' ARE LOCATIONS OF RECEIVED SIGNALS
[131] A WHICH ARE EQUAL TO THE PRE-CALCULATED VALUES
[132] A (ACTUAL RELATIONS EQUAL TO THE THEORETICAL ONES)
[133] A (MATRICES)
[134] MATCOMP:
[135] GRH←OK12^OK13^OK14^OK15
[136] A 'GRH' ARE LOCATIONS WHICH ARE EQUAL ALSO BETWEEN
[137] A ANTENNAS PAIRS
→[138] →(1=+/,GRH)/RHFIN
[139] A CHECK IF THERE IS A SINGLE COMBINATION OF RANGE
[140] A AND HEIGHT
→[141] →(FLAG=1)/RHFIN
→[142] →RCV
[143] A IF MORE THAN ONE COMBINATION, GO TO ANOTHER RECEIVING
[144] A SESSION (AS LONG AS THE RANGE IS HIGHER THAN THE
[145] A MINIMUM RANGE). IN CASE OF A SINGLE COMBINATION GO TO
[146] A TRANSLATE INTO REAL READING (RANGE AND HEIGHT)
→[147] RHFIN→0

```

```

**SIM
[0]  A←SIM;LAMBDA;A1;A2;A3;A4;A5;SXI;SHR;SRHO
[1]  A RECEIVED SIGNAL AMPLITUDES SIMULATION (AT EACH
[2]  A RECEIVING ANTENNA), INCLUDING TRANSMITTER
[3]  A MOVEMENT INFLUENCE
[4]  LAMBDA←0.3÷F
[5]  FLAG←0
[6]  SXI←-30((|HR3-HAT)÷RI)
[7]  A 'SXI' IS THE GRAZING ANGLE
→[8]  →(SEA=0)/LAB1
[9]  SHR←SHL+(1?(SHH-SHL)×1000)+1000
[10] A 'SHR' IS THE RMS WAVES HEIGHT FOR SIMULATION
→[11] →LAB2
[12] LAB1:SHR←0
[13] LAB2:SRHO←*-2×(((02)×SHR×SXI+LAMBDA))*2
[14] A
[15] A THE SIMULATION USES AMENT MODEL FOR CALCULATING
[16] A THE REFLECTION COEFFICIENT (ρ):
[17] A
[18] A
[19] A ρ =EXP.(-2×(2×PI×H ×SIN.(XI)+LAMDA)*2)
[20] A S RMS
[21] A
[22] A
[23] A1+SRHO[1]×(ERP×4×(10(((02)×(HR3[1]+HAT)×HAT)+(LAMBDA×RI)))×2)÷(
04)×RI*2
[24] A2+SRHO[2]×(ERP×4×(10(((02)×(HR3[2]+HAT)×HAT)+(LAMBDA×RI)))×2)÷(
04)×RI*2
[25] A3+SRHO[3]×(ERP×4×(10(((02)×(HR3[3]+HAT)×HAT)+(LAMBDA×RI)))×2)÷(
04)×RI*2
[26] A4+SRHO[4]×(ERP×4×(10(((02)×(HR3[4]+HAT)×HAT)+(LAMBDA×RI)))×2)÷(
04)×RI*2
[27] A5+SRHO[5]×(ERP×4×(10(((02)×(HR3[5]+HAT)×HAT)+(LAMBDA×RI)))×2)÷(
04)×RI*2
[28] A 'SRHO' IS THE 'REFLECTION COEFFICIENT' (ρ) FOR
[29] A EACH RECEIVING ANTENNA (RESPECTIVELY)
[30] A←A1,A2,A3,A4,A5
[31] A 'A' IS A VECTOR OF RECEIVED AMPLITUDES (IN EACH
[32] A ANTENNA-RESPECTIVELY)
[33] RI←RI-SIMSTEP
[34] A UPDATING THE TRANSMITTER RANGE (IN 'SIMSTEP' METER STEPS)
→[35] →(RI≥RMINS)/RET
[36] ' '
[37] 'END OF SIMULATION SESSION!'
[38] FLAG←1
[39] A RANGE HAD NOT BEEN FOUND YET, BUT IS LFSS THAN THE
[40] A MINIMUM RANGE, OR END OF SIMULATION SESSION
→[41] RET:→0

```

**RHFIND

```

[0]  RHFIND;INDH;INDR;MATHR;INDVEC;LOC;VECGRH
[1]  A  FINDING AND DISPLAYING THE RANGE AND HEIGHT
[2]  A  OF THE TRANSMITTER
[3]  INDH←100000×MINHEIGHT+HEIGHTRES×\HEIGHTST
[4]  A  'INDH' IS AN HEIGHT INDEX
[5]  INDR←RMIN+(HRESO×\HNSTEPS),(HRESO×HNSTEPS)+(RESO×\NSTEPS)
[6]  A  'INDR' IS A RANGE INDEX
[7]  MATHR←INDH°.+INDR
[8]  A  'MATHR' IS A RANGE / HEIGHT INDEX MATRIX
[9]  INDEV←,MATHR
[10] FIND:
[11] VECGRH←,GRH
[12] A  CHANGING MATRICES INTO VECTORS
[13] LOC←VECGRH/INDEV
[14] A  SELECTING THE CORRECT LOCATION OF THE TRANSMITTER
[15] A  ('LOC' IS THE TX. LOCATION)
[16] R←100000|LOC
[17] H←\LOC+100000
[18] A  TRANSLATING INTO REAL RANGE ('R') AND HEIGHT ('H')
[19] ''
[20] ''
[21] 'TRANSMITTER RANGE (IN KILOMETERS):'
[22] R÷1000
[23] 'TRANSMITTER HEIGHT (IN METERS):'
[24] H
[25] ''
[26] ''
[27] 'UPDATED ACTUAL RANGE (IN KILOMETERS):'
[28] (SIMSTEP÷1000)+RI÷1000
→[29] →0

```


LIST OF REFERENCES

1. Naval Research Laboratories Report no. 8849, *Radar Echo Enhancement Using Surface Reflections*, by B. H. Cantrell, September 1984.
2. Bekmann, P. and Spizzichino, A., *The Scattering of Electromagnetic Waves from Rough Surfaces*, Vol. 4, Macmillan Company, 1963.
3. Bachynski, M. P., "Microwave Propagation Over Rough Surfaces," *RCA Review*, Vol. 20, no. 2, pp. 308-335, June 1959.
4. Evans, G. C., "Influence of Ground Reflection on Radar Target Tracking Accuracy," *Radar Resolution and Multipath Effects*, by D. K. Barton, pp. 27-35, Artech House, 1978.
5. Griesser, T. and Constantine, A. B., "Oceanic Low Angle Monopulse Radar Tracking Errors," *IEEE Journal of Oceanic Engineering*, Vol OE-12, no. 1, pp. 289-295, January 1987.
6. Long, M. V., *Radar Reflectivities of Land and Sea*, Lexington Books, 1975.
7. Blake, L. V., *Radar Range-Performance Analysis*, Artech House, 1986.
8. Kerr, D. E., *Propagation of Short Radio Waves*, McGraw-Hill Book Company, 1951.
9. Skolnik, M. I., *Introduction to Radar Systems*, 2nd Edition, McGraw-Hill Book Company, 1980.
10. Griffith Air Force Base, N. Y., Rome Air Force Development Center In-House Report no. RADC-TR-84-159, *The Use of the Glistening Surface Concept in Rough Surface Scattering*, by R. J. Papa, J. F. Lenon, and R. L. Taylor, July 1984.
11. Barton, D. K. and Ward, H. R., *Handbook of Radar Measurement*, Artech House, 1984.
12. Bullington, K., "Reflection Coefficient of Irregular Terrain," *Radar Resolution and Multipath Effects*, by D. K. Barton, pp. 107-114, Artech House, 1978.

13. International Conference on Radar, Publication no. 155, *Radar Multipath Theory and Experimental Data*, by D. K. Barton, pp. 308-312, 25-28 October 1977.
14. Barton, D. K., "Low Angle Radar Tracking," *Radar Resolution and Multipath Effects*, by D. K. Barton, pp. 349-366, Artech House, 1978.
15. Naval Research Laboratories Report no. 7747, *A Parametric Study of Multipath Effect on Radar Signal Amplitudes*, by G. H. Galloway, July 1974.

BIBLIOGRAPHY

Naval Research Laboratories Report no. 3301, *Detection Improvement in Multipath, Using Even and Odd Symmetric Antenna Patterns*, by B. H. Cantrell, May 1976.

Naval Underwater System Center, *A Comparison of multipath Arrival Structures Observed in the Presence of a Surface Duct with Predictions Obtained using Classical Ray Techniques and the Parabolic Equation Method*, by H. A. Freese, February 1985.

Naval Research Laboratories Memo. Report no. 3163, *Detection Ranges of Low Altitude Targets Over the Sea Surface*, by J. K. Hsiao, November 1975.

Huang, J. and Peake, W. H., *Electromagnetic Scattering From a Ship at Sea*, Columbus Electro-Science Lab, Ohio State University, September 1978.

Peyton, Z. P. and Goldman, L., "Radar Performance With Multipath, Using the Complex Angle," *Radar Resolution and Multipath Effects*, by D. K. Barton, pp. 195-202, Artech House, 1978.

Naval Research Laboratories Report no. 8369, *An Analytical Study of Radar Returns in the Presence of a Rough Sea Surface*, by H. R. Ralman, July 1972.

Naval Research Laboratories Report no. 7400, *Statistical Functions of Short Pulse Radar Sea Return*, by K. R. Schmidt, M. Thiebaud, and S. J. Weller, July 1972.

Sherman, S. M., "Complex Indicated Angles Applied to Unresolved Radar Targets and Multipath," *IEEE Transaction on Aerospace and Electronic Systems*, Vol. AES-7, no. 1, January 1971.

White, W. D., "Low Angle Tracking in the Presence of Multipath," *Radar Resolution and Multipath Effects*, by D. K. Barton, pp. 285-302, Artech House, 1978.

INITIAL DISTRIBUTION LIST

	No. of Copies
1. Defense Technical Information Center Cameron Station Alexandria, VA 22304-6145	2
2. Library, Code 0142 Naval Postgraduate School Monterey, CA 93943-5002	2
3. Chairman, Code 62 Department of Electrical and Computer Engineering Naval Postgraduate School Monterey, CA 93943-5000	1
4. Professor Jeffrey B. Knorr Code 62 Ko Naval Postgraduate School Monterey, CA 93943-5004	1
5. Professor Michael A. Morgan Code 62Mw Naval Postgraduate School Monterey, CA 93943-5002	1
6. Naval Attaché Embassy of Israel 3514 International Drive, N. W. Washington D. C. 20008	1
7. Commodore Ishai Haranati C/O Naval Attaché Embassy of Israel 3514 International Drive, N. W. Washington D. C. 20008	1

- | | |
|--|---|
| 8. Captain David Nitzan
C/O Naval Attaché
Embassy of Israel
3514 International Drive, N. W.
Washington D. C. 20008 | 1 |
| 9. Captain Meir Morag
C/O Naval Attaché
Embassy of Israel
3514 International Drive, N. W.
Washington D. C. 20008 | 1 |
| 10. Captain Amnon Shefi
C/O Naval Attaché
Embassy of Israel
3514 International Drive, N. W.
Washington D. C. 20008 | 1 |
| 11. Cdr. Moshe Marom
2101 Etna Place
Monterey, CA 93940 | 1 |
| 12. Cdr. Rami Sharon
C/O Naval Attaché
Embassy of Israel
3514 International Drive, N. W.
Washington D. C. 20008 | 1 |
| 13. Lcdr. Yuval Cohen
C/O Naval Attaché
Embassy of Israel
3514 International Drive, N. W.
Washington D. C. 20008 | 1 |
| 14. Dr. Amri Wandel
562 Kendall Ave. #19
Palo Alto, CA 94306 | 1 |
| 15. Lt. Avner Gal
C/O Naval Attaché
Embassy of Israel
3514 International Drive, N. W.
Washington D. C. 20008 | 5 |

- | | |
|--|---|
| 16. Space and Naval Warfare Systems Command
Code PWD 106
Washington D.C. 22202 | 1 |
| 17. Deputy Chief of Naval Operations
Code NOP-05
Washington D.C. 20350 | 1 |